SMART ORTHOPEDIC SPLINT FROM POLY(LACTIC ACID)-BASED COMPOSITES

WASANA NONKRATHOK

A Thesis Submitted in Partial Fulfillment of the Requirements for the
Degree of Master of Engineering in Materials Engineering
Suranaree University of Technology
Academic Year 2022

เฝือกอัจฉริยะจากพอลิแลกติกแอซิดคอมโพสิท

นางสาววาสนา นนกระโทก

วิทยานิพนธ์นี้เป็นส่วนหนึ่งของการศึกษาตามหลักสูตรปริญญาวิศวกรรมศาสตรมหาบัณฑิต
สาขาวิชาวิศวกรรมวัสดุ
มหาวิทยาลัยเทคโนโลยีสุรนารี
ปีการศึกษา 2565

SMART ORTHOPEDIC SPLINT FROM POLY (LACTIC ACID)-BASED COMPOSITES

Suranaree University of Technology has approved this thesis submitted in partial fulfillments of the requirement for a master's degree.

Thesis Examining Committee

(Assoc. Prof. Dr. Chaiwat Raksakulpiwat)
Chairperson

(Asst. Prof. Dr. Nitinat Suppakarn)
Member (Thesis Advisor)

(Asst. Prof. Dr. Tatiya Trongsatitkul)
Member (Thesis Co-advisor)

(Assoc. Prof. Dr. Pranee Chumsamrong)
Member

(Asst. Prof. Dr. Supagorn Rugmai)
Member

(Assoc. Prof. Dr Chatchai Jothityangkoon)
Vice Rector for Academic Affairs and Quality Assurance

(Assoc. Prof. Dr. Pornsiri Jongkol)
Dean of Institute of Engineering

วาสนา นนกระโทก : เฝือกอัจฉริยะจากพอลิแลกติกแอซิดคอมโพสิท (SMART ORTHOPEDIC SPLINT FROM POLY(LACTIC ACID)-BASED COMPOSITES). อาจารย์ที่ปรึกษา : ผู้ช่วยศาสตราจารย์ ดร. นิธินาถ ศุภกาญจน์, 118 หน้า.

คำสำคัญ : พอลิเมอร์จำรูป/พอลิแลกติกแอซิด/สารเพิ่มความเข้ากันได้/พอลิเอทิลีนไกลคอล/คอมโพสิท

จุดประสงค์ของการศึกษานี้ เพื่อปรับปรุงพฤติกรรมการจำรูป และสมบัติทางกลของพอลิเมอร์จำรูปพอลิแลกติกแอซิดและประเมินศักยภาพในการนำมาใช้ในการทำเฝือกอัจฉริยะ การใช้พอลิแลกติกแอซิด (PLA) มาเป็นพอลิเมอร์จำรูป ถูกจำกัด เนื่องจากความเปราะและอุณหภูมิการเปลี่ยนสภาพคล้ายแก้ว (T_g) ของมันค่อนข้างสูง เพื่อเอาชนะข้อจำกัดเหล่านี้ พอลิเอทิลีนไกลคอล (PEG) ที่ปริมาณต่างๆ (คิดเป็นร้อยละ 5, 10, 15, and 20 โดยน้ำหนัก) ถูกผสมเข้ากับ PLA โดยผล พบว่าการเติม PEG ที่ปริมาณ 10 เปอร์เซ็นต์โดยน้ำหนัก กับ PLA ลักษณะพฤติกรรมต่อแรงดึงของ 10PEG/PLA เปลี่ยนจากเปราะเป็นเหนียวมากขึ้นและค่า T_g ของ PLA ลดลง

อย่างไรก็ตามความไม่เข้ากันของการผสม PEG และ PLA ทำให้สมบัติการจำรูปของ 10PEG/PLA แย่ลง เพื่อปรับปรุงสมบัติการจำรูปของพอลิเมอร์ผสมนี้ จึงได้มีการใช้มาเลอิกแอนไฮไดรด์กราฟต์พอลิแลกติกแอซิด (PLA-g-MA) ที่ 0.45 เปอร์เซ็นต์การกราฟต์มาเลอิกแอนไฮไดรด์ มาเป็นสารเพิ่มความเข้ากันได้ ซึ่งเตรียมโดยใช้เครื่องอัดรีดชนิดสกรูคู่ โดยได้ตรวจสอบสมบัติทางความร้อน สมบัติทางกล สัณฐานวิทยา โครงสร้างจุลภาค และสมบัติการจำรูปของพอลิเมอร์ผสม 10PEG/PLA ที่เติม PLA-g-MA ที่ปริมาณ 2, 6, และ 10 เปอร์เซ็นต์โดยน้ำหนัก จากผลพบว่า พอลิเมอร์ผสม 10PEG/PLA ที่ปรับปรุงความเข้ากันได้ โดยเติม PLA-g-MA ที่ปริมาณ 2 เปอร์เซ็นต์โดยน้ำหนัก (2PMA/10PEG/PLA) มีค่ามอดูลัส ความต้านแรงดึง และความยืดสูงสุด ณ จุดขาด สูงกว่าพอลิเมอร์ผสม 10PEG/PLA ที่ไม่ได้ปรับปรุงความเข้ากันได้ นอกจากนี้พอลิเมอร์ผสม 2PMA/10PEG/PLA ยังมี T_g และปริมาณผลึกลดลง ซึ่งทำให้ประสิทธิภาพในการคงรูปและการคืนรูปดีขึ้น ส่วนค่าเปอร์เซ็นต์การคงรูปของ 2PMA/10PEG/PLA มีค่าเทียบเท่ากับ PLA แต่ 2PMA/10PEG/PLA สามารถเริ่มคืนรูปได้ที่อุณหภูมิต่ำลง

นอกจากนี้มอนต์มอริลโลไนต์ เคลย์ (montmorillonite clay, MMT) ที่ปรับปรุงด้วยสารลดแรงตึงผิว cetyltrimethylammonium bromide (CTAB) ซึ่งเรียกว่า OMMT ถูกเติมลงในพอลิเมอร์ผสม 2PMA/10PEG/PLA เพื่อเป็นการปรับปรุงสมบัติการจำรูปให้ดียิ่งขึ้น จึงได้ศึกษาผลของการเติม OMMT ที่ปริมาณ 1, 3, 5, and 7 ส่วนในร้อยส่วนของเรซิน (phr) ต่อสมบัติทางกล โครงสร้างจุลภาค และสมบัติการจำรูปของ OMMT/2PMA/10PEG/PLA คอมโพสิท จากผลพบว่า การเติม

OMMT ปริมาณ 1 phr ทำให้คอมโพสิทมีค่าความเค้นในช่วงการเสียรูปแบบพลาสติกสูงมากขึ้น ในขณะที่ค่าเปอร์เซ็นต์การดึงยืด ณ จุดขาดยังเท่าเดิม และยังพบว่า 1-OMMT/2PMA/10PEG/PLA มีอัตราการคืนรูปดีกว่า 2PMA/10PEG/PLA และยังสามารถทำการดึงและคืนรูปซ้ำได้หลายรอบที่การทดสอบการดึงที่ 50 เปอร์เซ็นต์ความเครียด

วิทยานิพนธ์นี้แสดงให้เห็นถึงความเป็นไปได้ในการปรับคุณสมบัติการจำรูปของ PLA เพื่อให้เหมาะสมเป็นไปตามข้อกำหนดของการใช้งานที่เกี่ยวข้องกับเฝือกอัจฉริยะ จากการศึกษาเกี่ยวกับการจำรูปของ PLA พบว่าทั้งแบบพอลิเมอร์ผสม และคอมโพสิท สามารถเอาชนะข้อเสียของ PLA ในการใช้งานในด้านการแพทย์ โดยพบว่าพอลิเมอร์จำรูปพอลิแลกติกแอซิด มี T_g ลดลง เข้าใกล้กับอุณหภูมิที่ร่างกายทนได้ และมีการปรับปรุงความเหนียวซึ่งเป็นจุดสำคัญในการใช้งานเป็นเฝือกให้ดีขึ้น นอกจากนี้การศึกษานี้ยังให้ความเข้าใจพื้นฐานเกี่ยวกับความสัมพันธ์ระหว่างโครงสร้าง คุณสมบัติของหน่วยความจำรูป และการประยุกต์ใช้ ซึ่งเปิดโอกาสสำหรับการพัฒนาวัสดุอัจฉริยะสำหรับสาขาการแพทย์ต่อไป

สาขาวิชาวิศวกรรมพอลิเมอร์
ปีการศึกษา 2565

ลายมือชื่อนักศึกษา.....
ลายมือชื่ออาจารย์ที่ปรึกษา.....
ลายมือชื่ออาจารย์ที่ปรึกษาร่วม .....

WASANA NONKRATHOK : SMART ORTHOPEDIC SPLINT FROM POLY(LACTIC ACID)-BASED COMPOSITES. THESIS ADVISOR : ASST. PROF. NITINAT SUPPAKARN, Ph.D., 118 PP.

Keyword : SHAPE MEMORY POLYMER/ POLY(LACTIC ACID)/ COMPATIBILIZER/ POLY(ETHYLENE GLYCOL)/ COMPOSITE

This study aims to improve shape memory behavior and mechanical properties of poly (lactic acid) (PLA) - based shape memory polymer (SMP) and to evaluate its potential use in smart orthopedic splint application. Utilization of PLA as SMP is limited due to its brittleness and relative high glass transition temperature (T_g). To overcome these limitations, poly (ethylene glycol) (PEG) at various content (5, 10, 15, and 20 wt%) was blended with PLA. Results showed that the addition of 10 wt% PEG to PLA enhanced tensile characteristics of 10PEG/PLA blend by altering PLA's brittleness into a tough behavior and reduced PLA's T_g.

However, the incompatibility between PEG and PLA blends diminished the shape memory characteristics of 10PEG/PLA blends. To enhance shape memory abilities of the blends, 0.45% maleic anhydride-grafted poly (lactic acid) (PLA-g-MA) was prepared by reactive blending using a twin screw extruder and used as a compatibilizer. Thermal and mechanical properties, morphologies, microstructures, and shape memory properties of the 10PEG/PLA blends containing 2, 6, and 10 wt% of PLA-g-MA were investigated. The results revealed that the compatibilized 10PEG/PLA blend containing 2 wt% PLA-g-MA (2PMA/10PEG/PLA) had superior tensile modulus, strength, and elongation at break to the uncompatibilized blend. Furthermore, it possessed a lower glass transition temperature and degree of crystallinity. The 2PMA/10PEG/PLA blend also achieved outstanding shape fixity and recovery performance. Its shape fixity ratio was equivalent to that of PLA while it can recover to the initial shape at a lower temperature.

In addition, montmorillonite clay (MMT) treated with cetyltrimethylammonium bromide (CTAB), called OMMT, was added to the 2PMA/10PEG/PLA blend, with the purpose of providing an alternative approach for enhancing its shape memory

properties. Effect of filler contents (1, 3, 5, and 7 phr) on mechanical, microstructure, and shape memory properties of the OMMT/2PMA/10PEG/PLA composite was examined. The results indicated that the composite containing 1 phr OMMT had a greater tensile stress in the plastic deformation zone than the 2PMA/10PEG/PLA blend, while its elongation at break remained unchanged. Moreover, the composite containing 1 phr OMMT had a greater recovery ratio than the 2PMA/10PEG/PLA blend, as well as superior repeatability of shape recoverability when programmed with 50% strain.

This thesis demonstrated the feasibility of optimizing the properties of shape-memory PLA to meet the requirements of applications involving smart orthopedic splints. The research of shape memory PLA, including PLA blends and composites, overcame the limitations of PLA in the medical industry. The resulting PLA-based SMP with a lowered T_g close to physiological temperature and an improved ductility were critically important that made the use of PLA-based SMP in orthopedic splints come to realization. This study also provided a fundamental understanding of the relationship between the structure, shape-memory properties, and application which open-up the possibility for further development of a smart material for medical field.

School of Polymer Engineering
Academic Year 2022

Student's Signature Hasana Nawarathne
Advisor's Signature Nitinat Suppakarn
Co-advisor's Signature T. Tungpaitool

ACKNOWLEDGEMENTS

I gratefully acknowledge Kitibandit Scholar from Suranaree University of Technology for their financial support. I would like to express my deep gratitude to my thesis advisor, Asst. Prof. Dr. Nitinat Suppakarn, for her invaluable support, guidance and constant encouragement throughout my educational life at Suranaree University of Technology. And I would like to thanks my thesis co-advisor, Asst. Prof. Dr. Tatiya Trongsatitkul, for her guidance, enthusiastic encouragement, and useful critiques of this research work. I am also grateful to Assoc. Prof. Dr. Wimonlak Sutapun, Asst. Prof. Dr. Pranee Chumsamrong, Asst. Prof. Dr. Supagorn Rugmai, and, Assoc. Prof. Dr. Chaiwat Raksakulpiwat for their valuable suggestion and guidance given as committee members. In addition, my grateful thanks are also extended to Dr. Siriwat Soontaranon and members of the Beamline 1.3W of Synchrotron Light Research Institute, Nakhon Ratchasima for their times, help and suggestion in the SAXS and WAXS techniques. I am grateful to Mr. Jiradet Sringam for his help. I also thank all faculty, staff members, and friends of School of Polymer Engineering for their encouragements and supports. Finally, I would like to especially thanks to my parents for their support and encouragement throughout my study at Suranaree University of Technology.

Wasana Nonkrathok

TABLE OF CONTENTS

Page

TABLE OF CONTENTS (Continued)

Page

TABLE OF CONTENTS (Continued)

Page

TABLE OF CONTENTS (Continued)

Page

LIST OF TABLES

Table **Page**

LIST OF FIGURES

Figure **Page**

LIST OF FIGURES (Continued)

Figure **Page**

LIST OF FIGURES (Continued)

Figure **Page**

CHAPTER 1
INTRODUCTION

1.1 Background

Smart material is a material whose one or more properties is significantly changed in response to different stimuli such as stress, temperature, moisture, pH, electric or magnetic fields. The material can create new and efficient products that ease to deal with customer needs and expectations. One typical example is shape memory polymers (SMPs). The special property of remembering their original shape after deformation leads to the development of innovative concepts as well as products.

Shape memory polymers (SMPs) have received an increasing attention over the past decade. This is not only because they can offer shape memory properties, but they are also light in weight, easy to fabricate, and some are biocompatible, as compared to other shape memory materials (i.e., ceramics and metal alloys). SMPs can be processed into temporary shapes, then rapidly restored to their original shapes under external stimuli such as heat, electromagnetism, solvent, light, and so on.

Thermally induced SMPs are the polymers that trigger by changing of temperature. A temporary shape of this SMP can be obtained by heating the polymer at temperature above their transition temperature (T_{trans}), deforming the polymer to form a desired shape and then cooling down to below the T_{trans} to fix the temporary form. When a thermally induced SMP is reheated to the T_{trans}, the elastic force, stored in the reversible phase, turns it back to the initial shape. These SMPs can be potentially used in medical applications such as orthopedic surgical devices, self-adjusting orthodontic wires, cardiovascular stents, and so on.

The emphasis of this study focuses on fabricating smart orthopedic splint, which is a medical device for immobilizing an injured bone, joint, limb or spine. The orthopedic splint materials used in the market are generally made from poly (lactic acid) (PLA) (Mehlhase, 2019), and thermoplastic poly (urethane) (TPU) (Green, 1984).

These splints can be easily formed by heating trigger to alter them to a temporary form that fits to a patient in situ. Thus, the splint is required to possess T_{trans} slightly above human body temperature (about 45°C) to ensure stable shape fixing in a minimally invasive configuration during medical treatment. The required mechanical properties of splint are Shore D hardness within a range of 65 to 80 (ASTM D2240), tensile strength within range of 42 to 62 MPa, and elongation at break of 5% (ASTM D638) (Joseph, 2015).

Poly (lactic acid) (PLA) is one of the most promising polymers for splint application. PLA not only has many excellent properties, *i.e.,* biocompatibility, biodegradability, ease processability, high mechanical strength, but also possesses excellent shape memory properties. The shape memory property of PLA is the result of its semi-crystalline nature (J. Xu & Song, 2015). The crystalline phase in PLA acts as the shape-fixing part that maintains dimensional stability during deformation and recovery. The amorphous phase acts as the shape-switching part, which could be thermally triggered to temperature above its glass transition temperature (T_g). Nonetheless, PLA still has some limitations due to its brittleness, and high T_g (about 60°C). These hinder its temporary shape programming and are possibly harmful to human tissue.

In order to use PLA as an orthopedic splint, its mechanical and thermal properties should be improved without deteriorating its shape-memory efficiency. Various approaches have been used to improve the performance of PLA based SMPs, including copolymerization or blending PLA with other polymers. Blending of a flexible polymer with PLA matrix can improve PLA's ductility and processability and is more practical and economical strategy as compared to copolymerization. There are several polymers that could provide flexibility for PLA such as poly (ethylene glycol) (PEG), poly (caprolactone) (PCL), and poly (propylene carbonate) (PPC). Among those, PEG is a common plasticizer used in PLA due to its biodegradable, non-toxic, and excellent chain flexible. Phanthong et al. (2018) have investigated the shape memory and physical properties of PEG/PLA blends. They found that blending PLA with PEG could yield the blend with excellent ductility. However, the shape recovery ratio of PEG/PLA

blends were decreased due to phase separation of PEG and PLA, which may lead to PLA embrittlement.

There are various approaches to reduce phase separation of PEG/PLA blend, e.g., copolymerization and addition of compatibilizer. In comparison to prepare copolymerization, the addition of a compatibilizer is less complicated. Hassouna et al. (2011) have reported that the addition of PLA-*g*-MA as a compatibilizer can improve tensile modulus, tensile strength, and elongation at break of the compatibilized PEG/PLA blend as compared to those without the compatibilizer. In addition, influence of compatibilizer on shape memory effect has been studied in a blend of high density polyethylene (HDPE) and nylon6 (PA6). Li and Tao (2010) have reported that the shape recovery rate of HDPE/PA6/POE-*g*-MAH blend (80/20/10) was capable of reaching 96.5% due to an improvement in the interfacial interaction of the HDPE/PA6 blends.

Additionally, incorporation of inorganic nano-additive is one of the effective strategies to increase the material's performance as an additional way to produce superior mechanical and shape memory performance (J. Liu et al., 2015). Fu and coworkers studied the effect of clay content on the shape memory capabilities of a polylactic acid/citric acid-clay composite. They reported that clay provided strong restrictions on PLA chains, which contributed to the anisotropic driving force for shape recovery (Fu et al., 2018).

This research work aims to enhance mechanical and shape memory properties of PLA based shape memory material. In this system, PEG and PLA-*g*-MA were respectively used as a plasticizer and a compatibilizer, while montmorillonite clay (MMT) was surface modified with Cetrimonium bromide (CTAB) and used as a filler.

1.2 Research objectives

The aims of this research are as follows:

(i) To investigate effect of PEG content on shape memory and physical properties of PEG/PLA blends.

(ii) To investigate effect of PLA-*g*-MA content on shape memory and physical properties of compatibilized PEG/PLA blends (PLA-*g*-MA/PEG/PLA).

(iii) To investigate effects of montmorillonite clay content on shape memory and physical properties of PLA-*g*-MA/PEG/PLA composites.

1.3 Scope and limitation of the study

Blends of Poly (lactic acid) (PLA) and poly (ethylene glycol) (PEG) were investigated. PEG with molecular weight of 4,000 g/mol was used at various contents, i.e., 5, 10, 15, and 20 wt%. All blends were prepared using a co-rotating intermeshing twin screw extruder and test specimens were made using a compression molding machine. Effect of PEG content on shape memory and physical properties of PEG/PLA blends was studied. The PEG/PLA blend with optimal mechanical and thermal properties was selected for further study on the effect of compatibilizer content.

Poly (lactic acid) grafted with maleic anhydride (PLA-*g*-MA) was prepared by using a co-rotating intermeshing twin screw extruder with 5 phr maleic anhydride (MA) and 1 phr dicumyl peroxide (DCP). The prepared PLA-*g*-MA was characterized before using as a compatibilizer for PEG/PLA blends. Effect of compatibilizer content on shape memory and physical properties of compatibilized PEG/PLA blends was studied. PLA-*g*-MA contents used in this study were 2, 6, and 10 wt%. The compatibilized PEG/PLA blend with the optimal properties was selected to further study.

Montmorillonite clay (MMT) was surface modified with Cetrimonium bromide (CTAB), called OMMT, used as a filler for compatibilized PEG/PLA blend. The OMMT content was varied, i.e., 1, 3, 5, and 7phr. Effects of OMMT content on shape memory properties and physical properties of compatibilized PEG/PLA composites was investigated.

CHAPTER 2

LITERATURE REVIEWS

2.1 Shape memory polymers (SMPs)

Shape Memory Polymers (SMPs) is a kind of smart material that are capable of memorizing temporary shape and recovering their original shape upon external stimulus i.e., heat, light, electromagnetism, solvent, and so on. In generally, SMPs are comprise of two phases. One is the fixity phase or netpoints to memorize the original shape of polymer while the another one is the switching phase that allows forming the temporary shape and enables recovering to the original shape under its transition temperature (T_{trans}) (Peponi, Navarro-Baena, & Kenny, 2014). The netpoints can be achieved by chemically cross-linked (covalent bonds) or physically cross-linked (intermolecular interactions). The chemically cross-linked SMPs are referred to as thermosets and physically cross-linked ones are referred to as thermoplastics. The switching segment is either crystalline, or amorphous and therefore the transition temperature (T_{trans}) is either a melting temperature (T_m), or a glass transition temperature (T_g) (Jinsong, Lan, Liu, & Du, 2011).

Among SMPs, thermally induced SMPs which their shape memory behavior is triggered by changes in temperature are received increasing attention in potential medical applications such as orthopedic surgical devices, self-adjusting orthodontic wires, cardiovascular stents, and so on. The molecular mechanism of thermally induced shape memory polymer can be summarized and shown in Figure 2.1. Upon heating above T_{trans} of the switching phase (blue or red frizzy line), this phase becomes flexible and easily deformed, while the fixity phase (black dot points) can prevent the chain slipping over intermolecular bond. When the polymer is cooled down under the stress, the switching phase fix the chains keeping the temporary shape and it can release the stress. Eventually, the temperature is raised above T_{trans}, the chains can release strain to gain entropy, and return to their original maximum entropy state, corresponding to the relaxed macroscopic shape (Oliver, Seddon, & Trask, 2016).

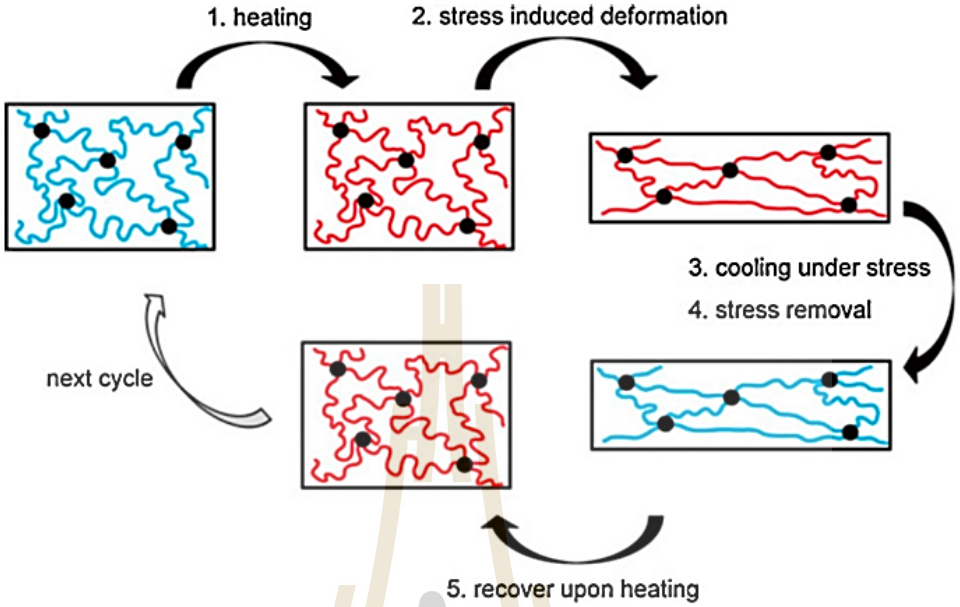

Figure 2.1 The molecular mechanism of a shape memory polymer throughout a thermal cycle. (Oliver et al., 2016)

To study the shape memory performance of SMPs, the quantification of the shape memory effect is generally realized through mechanical tests with specific procedures and parameters. The stress–strain test is most commonly used to develop quantitative mechanical analysis techniques of SMPs. In addition, many research works have been analyzed the shape memory effect using a dynamic mechanical analyzer (DMA), which is designed as a thermo-mechanical cyclic test. The data can be represented the relationship of stress and strain in a two-axis system at fixed temperature, or more variable represents in a three-axis by adding the temperature axis to allow observing the curve behavior of shape memory effect as shown in Figure 2.2 and it can be classified into four steps; (Peponi et al., 2014)

- The first step, the sample test is heated to a temperature above T_{trans} of polymer without applied stress.
- The second step, the sample is applied a stress to produce deformed material (ε_m).

- The stress is held while the material is cooled to a temperature below the T_{trans}. Once the temporary shape is fixed (ε_m), the stress is removed (ε_u).
- Finally, the sample is reheated above its T_{trans} and in this way the polymer recovers its original shape (ε_p).

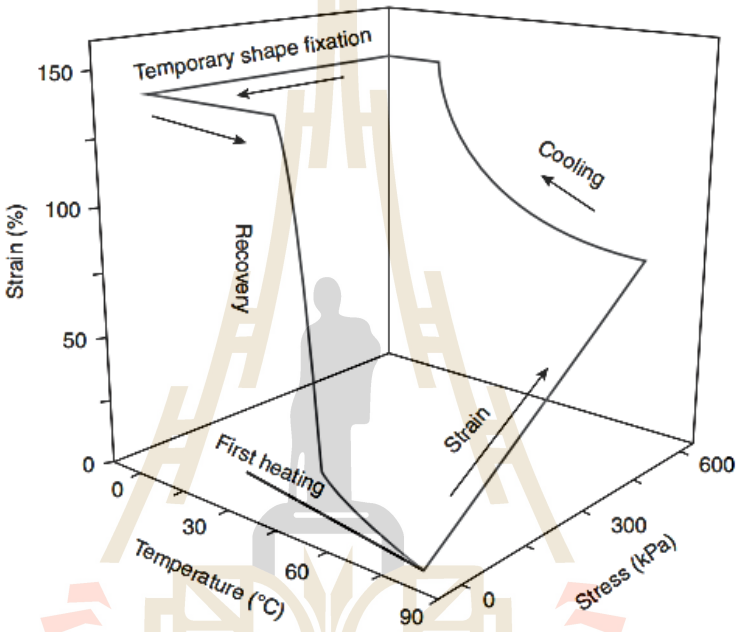

Figure 2.2 Cyclic stress–strain test. (Peponi et al., 2014)

In order to quantify the shape memory efficiency, the main parameters are:

- Shape recovery ratio, R_r, is the ability of the material to return to its original shape. The shape recovery ratio has also been called %recovery, strain recovery, normalized strain recovery.

$$R_r = \frac{\varepsilon_m - \varepsilon_p}{\varepsilon_m} \times 100\%$$

- Shape fixity ratio, R_f, describes as how well the shape holds its temporary shape during storage and is given by this equation,

$$R_f = \frac{\varepsilon_u}{\varepsilon_m} \times 100\%$$

Other parameter, shape recovery time (t) is the time that it takes for an SMP to reach its recoverable strain at T_{trans}. It can determine how fast an SMP responds to the stimulus. This parameter is mostly reported by studies that video-record real-time shape changes.

This study emphasizes on fabricating smart orthopedic splint, which is a medical device for immobilizing an injured bone, joint, limb or spine. This splint can be easily deformed and recovered by heating trigger to alter it to a temporary form and to respectively turn to its original form that fits to a patient in situ. Thus, the shape fixity performance of this splint should be close to 100% to ensure stable shape fixing in a minimally invasive configuration during surgical delivery. In addition, high repeatability and shape recovery are also needed for splint application.

2.2 Studies of shape memory polymers

The important shape memory quantities of SMPs are the shape recovery ratio (R_r) and the shape fixity ratio (R_f). For an ideal SMPs, both R_r and R_f values should be near to 100%, with a sharp transition temperature, resulting in a complete shape fixing and fast recovery. An improve SMPs with high R_r can be obtained by increase either the crosslinking density of a thermoset SMP or the degree of physical crosslinking in a thermoplastic SMP. An alternative way to improve the R_r of SMPs is by the incorporation of fillers into the SMPs. With the intention of improving the R_f of SMPs, several methods have been used. Adjusting the composition of the co-monomers and/or introducing cross-linkers into the SMPs are for examples. It could be also done by inducing the crystallinity segment of polymer to hinder the relaxation of chain mobility (Jianwen Xu & Song, 2011).

This study will emphasize on thermoplastic shape memory polymer because its ease of fabricate and is capable of reprocess. Several strategies have been used to improve the shape memory properties of different thermoplastic SMPs. The details are described as followed polyurethanes, block copolymers, polymer blends, and polymer composites.

2.2.1 Polyurethane based SMPs

Wang et al. (2010) investigated the molecular morphology of poly (ester urethane) (PEU) shape-memory polymer during the cold drawing programming in the shape memory cycle. Poly (ester urethane) consisted of poly(**ε**-caprolactone) (PCL) as the soft segment and 2,4-toluene diisocyanate (TDI)-ethylene glycol (EG) as urethane hard segment. The melting temperature of the PCL soft segment was 55°C. It was reported that the cold drawing processes were divided into three stages. In the first stage (up to about 100% strain) of the cold drawing programming, amorphous PCL chains oriented, whereas the crystalline PCL and hard segment maintained their origin state. In second stage (~100 to 250% strain), the hard segments and the crystalline PCL chains started to align with the stretching direction and quickly reached a high degree of orientation while amorphous PCL chains underwent stress induction. In this stage, the temporary shape was fixed. In the third stage (above 250%), the orientation functions of the crystalline PCL and the hard segment level off at their respective maximum. For recovery process was studied at 36°C. When the temperature was increased, the SMP started to recover to its permanent shape. In this stage, the hard segments restored first because of the strengthening of hydrogen bonds and the amorphous PCL chains restored to their original state serving as the physical cross-links. Eventually the crystalline PCL chains lose their alignment and partially recover to their original state with some residual orientation, which probably was due to irreversible deformation of the lamellae in the drawing process. After it returned to its original shape, it was the ready for the next cycle of the shape-memory process.

2.2.2 Block copolymer based SMPs

Zhu et al. (2018) investigated shape memory effect of a multiblock polyesters that composed of poly (***ε***-decalactone) (PDL) and poly (cyclohexene phthalate) (PCHPE). This material was processed using a combination of switchable polymerization catalyst of epoxide, anhydride, and lactone, which linked aliphatic and semiaromatic block polyesters. The polymer was formed as triblock polyester, which firstly produced using ring-opening copolymerization (ROCOP) of epoxide and anhydride, subsequently using ring-opening polymerization (ROP) of lactone to form PLA segment. Consequently, 4,4′-methylenediphenyl diisocyanate (MDI) as a chain

extender was used to increase molar mass and formed the desired structure of multiblock polyesters (PLA–PDL–PLA triblock). In this study, PCHPE content was varied as 26, 42, 49, and 59 wt%. The resulting multiblock polyesters are amorphous, and the blocks are phase separated; glass transition temperatures are ∼−45 and 100 °C. Shape memory test of sample was performed by stretched to 300% strain at ambient temperature (18 °C) and allowed to relax quiescently for 30 min, during which time only a slight retraction occurred, and the fixed strain stabilized at ∼280% for all samples. The result reported that high strain fixation needed for shape memory materials was only achieved for addition of 59 wt% PCHPE content (MBPE-59), which contained the highest content of rigid block. It was because sufficient rigid block content (PCHPE) was required to enable shape fixation by percolation of the rigid block across the network under shear.

Koosomsuan, Yamaguchi, Phinyocheep, and Sirisinha (2019) studied shape memory properties of two thermoplastic multiblock copolymers composed of poly (lactic acid) (PLA) and poly (ethylene glycol) (PEG) having different PEG-segment lengths of 6,000 and 11,000 g/mol. The multiblock copolymers with different PEG segment lengths both containing 18.9 wt% PEG, 75.4 wt% PLA, and 4.7 wt% HDI, were prepared via transesterification reaction followed by chain extension reaction. This system consisted of PEG-plasticized PLA domains (soft phase) as switching segment and PLA-rich domains combined with hexamethylene diisocyanate (HDI) units capable of forming hydrogen bonds as hard segment. They reported that the multiblock copolymer composed of longer PEG segment length (11,000 g/mol) exhibited better shape memory performance under all pre-strain conditions due to its more defined phase separated morphology. By optimizing the programming temperature to 40 °C, the most balance between shape fixity ratio of 97% and shape recovery ratio of 76%.

2.2.3 Polymer blend based SMPs

Li and Tao (2010) studied the effect of reactive compatibilizer on shape memory properties of high-density polyethylene (HDPE)/nylon6 (PA6) blends. Ethylene–octane copolymer graft maleic anhydride (POE-*g*-MAH) was used as a reactive compatibilizer for immiscible HDPE/PA6 blend. The POE-*g*-MAH content was varied as 3, 5, 8, and 10 phr. In this polymer, the crystalline region of PA6 was dispersed in HDPE

matrix acting as the physical crosslinking structure, while flexible HDPE chains offered ability of a reversible large deformation. Shape recovery properties of HDPE/PA6/POE-*g*-MAH (80/20/10) blend was examined by using universal testing machine with heating chamber. The stretching force mode was applied to the dumbbell specimen. The impact of transition temperature was observed at various temperature i.e., 120, 125, 130, 135, and 140°C. The recovery time of sample was recorded when the deformed sample maximally recovered to their original shape. Shape recovery rate of sample was determined from the ratio of the difference between distance of temporary sample and recovered sample to the difference between distance of temporary sample and initial sample. The results indicated that the shape recovery rate and recovery speed of the blends increased with the increasing of POE-*g*-MAH content. This because the POE-*g*-MAH may improve the interfacial interaction of the HDPE/PA6 blends and the shape recovery rate was capable of reaching 96.5%. The optimal shape response temperature of HDPE/PA6/POE-g-MAH (80/20/10) blend was 135°C, which was slightly higher than the melt point of HDPE (130°C).

Lai, Li, Kao, and Liu (2019) studied shape memory properties of physical blends of olefin block copolymer (OBC) and ethylene-vinyl acetate copolymer (EVA), with and without modification of one or two of the components. The modified blends, based on maleic anhydride modified OBC (OBC-*g*-MA) and/or vinyltriethoxysilane (VTEOS) modified EVA (EVA-*g*-VTEOS), included OBC/EVA-*g*-VTEOS, OBC-*g*-MA/EVA, and OBC-*g*-MA/EVA-*g*-VTEOS blends. The shape memory properties of modified blends were compared with those of the unmodified OBC/EVA blend. They reported that shape fixity ratio of neat OBC was only 35% and shape recovery ratio was 95%, whereas neat EVA didn't exhibit any shape memory effect at 90°C, the temperature being above EVA's melting temperature. The result of unmodified OBC/EVA blend also behaved like the neat EVA. After VTEOS grafting on EVA, the OBC/EVA-*g*-VTEOS blend significantly increased in both shape fixity ratio and shape recovery ratio, being 81% and 95%, respectively. The shape memory performance was still high for the modified blends of one or two of the modified components. In order to understand the factors of the increase of shape fixity ratio, they suggested that it was because the interactions between maleic anhydride and vinyl acetate could avoid the disrupted crystalline

domains or disentangled molecular chains increased. For the shape recovery ratio, they reported the elastic behaviors of the silane crosslinked EVA and the crystalline OBC regions, as chemical and physical crosslinks, respectively. In addition, the high stored internal strain energy from the molecular orientation fixed in the temporary shape was responsible for the high shape recovery ratio.

2.2.4 Polymer composite based SMPs

Y. Liu, Li, Yang, Zheng, and Zhou (2015) investigated mechanical and shape-memory properties of polymer nanocomposite network by chemically cross-linking cellulose nanocrystals (CNCs) with polycaprolactone (PCL) and polyethylene glycol (PEG). The cross-linking reaction was prepared from aqueous dispersion process by using 4,4-Diphenylmethane diisocyanate (MDI) as a crosslinker. Three different compositions of the PEG/PCL/CNC nanocomposites were prepared as 50/50/10, 60/40/10, and 70/30/10, the PEG and PCL were in unit of wt% and CNC indicates as phr. The mechanical properties showed the tensile stress increased, whereas the elongation to break clearly decreased with increasing PEG content. This was because of the high crystallinity of the nanocomposites with a high PEG component. The PEG/PCL/CNC (60/40/10) nanocomposite achieved the best mechanical properties. The important key to achieve a high mechanical strength for low molecular weight polymers was not only because they contained chemical cross-link in their structures, but they also contained well dispersion of CNC fillers in PCL–PEG matrix, giving the covalent bonds between CNC and polymer chains. In addition, the storage modulus was increased while the $\tan\delta$ was slightly decreased with increasing PEG. Lower $\tan\delta$ was contributed to the good shape-memory property. The thermoresponsive was performed on a DMA instrument using the controlled force mode to determine shape-memory fixity ratio (R_f) and recovery ratio (R_r). For the water-responsive shape-memory effect was investigated the angle of the folded specimen using a video camera. Firstly, the samples were folded by deforming sample at 60°C then cooling sample to -10°C under constant stress to fix the temporary shape. The recovered shape was conducted in water at 37°C. The result presented that the PEG/PCL/CNC (60/40/10) nanocomposite exhibited excellent thermo-induced and water-induced shape-memory effects in water at 37 °C. While the nanocomposite with containing 50 and 70

wt% of PEG had the Rf and the Rr, respectively, these were lower than both R_f and R_r of 60 wt% of PEG ($R_f \approx 100\%$, $R_r \approx 90\%$). This was because adding 50 wt% of PEG, lowered crystallinity of their nanocomposite whereas adding 70 wt% of PEG lowered cross-linking degree of their nanocomposite.

Qi, Jing, et al. (2016) investigated shape memory properties of poly (propylene carbonate) (PPC)/microfibrillated cellulose (MFC) composite by using heat and water stimuluses. Where PPC acted as the switching phase due to its good elasticity and expected that good interaction of PPC and MFC could be formed the physical cross-links acting as the fixing phase. In this work, MFC was modified by a one-step mechanical–chemical approach involving ball milling and an esterification reaction to improve its dispersion in PPC matrix and interaction with PPC chain. They studied the effects of modification of MFC and MFC content (5-10 wt%) on shape memory properties of their composites. The thermally induced shape memory properties of PPC composites were evaluated on a dynamic mechanical analyzer (DMA). It was reported that with addition of MFC, the shape fixity (R_f) increased but the shape recovery (R_r) remained almost constant. With adding 5 wt% or 10 wt% modified-MFC, both R_f and R_r increased to 95%. The possible explanation was that MFC in composites could be disturbed the chain motion of PPC by its aggregation. After the modification of MFC, modified-MFC had good dispersion in PPC and it reacted more to PPC molecules, which generated enough interfacial interactions as physical cross-linking points. This crosslink in SMPs provided less relaxed networks which induced high retraction force and good shape recovery. In order to observe the water-induced shape memory properties of PPC composites, sample was processed as followed; Firstly, the straight (original shape) specimens were bent into “U” like shape (temporary shape) at 60°C and retained this shape with external load during cooling back to room temperature (25°C). After that, the deformed sample was immersed in water at 30°C and the shape recovery was recorded using a digital camera at different time. The results showed that the deformed PPC/modified-MFC strips could be recovered at 30°C when it was immersed in water because the great hydrophilic nature of modified-MFC, which its surface contained an abundance of surface hydroxyl and carbonyl groups. When it was immersed in water, forming a hydrogen bond of weak water and

modified-MFC to replace the strong interactions of PPC and modified-MFC, leading to the decrease of T_g. Thus, the shape recovery of PPC/modified-MFC composites could be also actuated by water.

The property-owning requirements of orthopedic splint are Shore D hardness within a range of 65 to 80 according to ASTM D2240, tensile strength within range of 42 to 62 MPa, elongation at break of 5% according to ASTM D638, and flexural modulus within range of 1,862 to 2,344 MPa according to ASTM D5023 (Joseph, 2015). Previously, splint materials were made from plaster, but splint made from such materials are heavy, sensitive to water, take time too long in surgery (Green, 1984). Nowadays, the orthopedic splint materials used in the market are generally made from thermoplastic materials, such as poly (lactic acid) (PLA), and thermoplastic poly (urethane) (TPU). This is because they easily to provide formable orthopedic splints materials in the form of sheets and to preform fitting shape for application to the human body to form a splint.

In addition, biodegradable shape memory polymers (SMPs) have attracted great attention in the recent year. Poly (lactic acid) (PLA) is one of the most promising polymers for fabricating splint. PLA not only has many excellent properties, i.e., biomedical fields, biocompatibility, biodegradability, non-toxicity, and high mechanical strength but also possesses excellent shape memory properties.

Shape memory behaviors of PLA are presented from both physical entanglement and the crystallization of PLA that can act as the net-points or fixity phase, while the long chains between the fixing part is the switching phase. Nonetheless, shape memory effect of PLA is limited to small strain deformation (<10%) during the temporary shape programming and relatively high T_g. This limits its use in many applications especially in medical field which has small operating temperature window of a few degrees above baseline body temperature.

2.3 Strategies to overcome limitations of PLA

In order to overcome these limitations, addition of second polymer or some plasticizer can be added to improve the toughness of PLA and to modify its T_g without deteriorating shape-memory efficiency of PLA. Moreover, incorporation of proper filler

into PLA matrix has been reported to capable of improving the shape memory performance of shape memory PLA.

2.3.1 Plasticized PLA and PLA blends

Navarro-Baena et al. (2016) studied mechanical and shape memory properties of poly (lactic acid) (PLA) and poly (**ε**-caprolactone) (PCL) blends. The blends of PLA/PCL, with weight ratio of 100/0, 70/30, 50/50, 30/70, and 0/100, were prepared by using co-rotating extrusion. With the increasing PCL content, the elastic modulus and maximum stress were decreased. Elongation at break of PLA/PCL (50/50) showed the lowest value, which involved its morphology. To be specific, a co-continuous structure was observed which was due to phase separation and poor adhesion between PLA and PCL. Shape memory properties was investigated only for the blend of 30 wt% PCL and reported that the shape fixity (R_f) for two cycles was higher than 96%. The shape recovery (R_r) was 83% in the first cycle, whereas decreased to 77% after the second cycle. It was found that the shape memory parameters were quite high for the two thermomechanical cycles.

Qi, Dong, Liu, Liu, and Fu (2016) studied a rapid electroactive ternary shape memory polymer (SMP) composite of poly (propylene carbonate) (PPC) and poly (lactic acid) (PLA) containing multiwalled carbon nanotubes (MWCNTs). In binary polymer blends, the PLA contents varied from 0 wt% to 100 wt%, where PPC acted as the switching domain and PLA acted as the fixing domain. Mechanical properties, thermal property, phase morphology, and shape memory properties of the PPC/PLA blends were investigated. It was found that the tensile strength of the blends increased with the increasing PLA content, which was from the relatively high strength of pure PLA. When the PLA contents were above 30 wt%, the strain at break of the blends decreased dramatically to 90%. For the thermal property, the T_g of both PPC and PLA shifted significantly towards each other in the blend, suggesting that PPC and PLA were partially compatible. Shape memory properties of the PPC/PLA blends were evaluated on a dynamic mechanical analyzer (DMA Q800, TA Instruments) using the switching temperature at 50°C. It showed that the PPC90/PLA10 had good shape recovery ratio (R_r) of near 80% but poor shape fixity ratio (R_f). These were because PLA could only form the small droplet phase and its vitrification could not completely fix the

deformed shape, therefore the R_f was quite low (62%). The PPC70/PLA30 and PPC50/PLA50 both showed R_r of near 80% and R_f above 90%. They explained that the PLA phase of 30 wt% and 50 wt% were formed as continuous phase in the PPC matrix, which contributed to the good shape fixing performance. With the addition of PLA above 50 wt%, showed poor R_r but good R_f of near 100%. The SEM images of this blend suggested that PPC formed island-like domains in PLA matrix, which PPC was less interconnected.

Phanthong et al. (2018) studied the effect of poly (ethylene glycol) (PEG, Mw = 2,000 g/mol) as a plasticizer on the shape memory, thermal, mechanical properties of plasticized PLA with PEG. PLA and PEG were blended, and the plasticizer PEG content varied as 0, 5, 10, 15, 20, 30, and 40 wt% using solution casting method. The results found that the glass transition temperature of PEG/PLA blend decreased with an increasing of PEG content. When the content of PEG increased to above 20 wt%, phase separation was be observed from the DSC curves. The dynamic mechanical properties of the PLA/PEG blends showed that both the slope of storage modulus-temperature curves and the peaks of loss modulus-temperature curves were shifted significantly to a lower temperature with increased the PEG content. They explained that the plasticization effect of PEG can effectively enhanced the motion capacity of the molecular chains of PLA/PEG blends and resulted in increasing the elongation at break. The shape memory properties, neat PLA had a good shape memory effect but its brittleness and relatively low elongation at break limited its applications as SMP. When addition of PEG into PEG/PLA blends showed that the shape recovery ratio decreased while shape fixity ratio was still high. Because the increase of PEG content led to the phase separation which had negative effects on shape memory properties of the blends.

2.3.2 Compatibilized PLA blends

Shen, Lu, Zhou, and Liang (2012) investigated thermomechanical and shape memory properties of shape memory biodegradable blends from poly (lactic acid) (PLA) and poly (ethylene glycol) (PEG) (M_n = 20,000 g/mol) in the presence of ethyl cellosolve-blocked polyisocyanate (EC-bp) as a cross-linker. The blends were prepared by solution casting method. The PEG content was fixed at 10 wt% while the

EC-bp contents were varied as 1, 2, and 5 wt%. With the addition EC-bp to blend systems, it was found that the thermomechanical properties of the cross-linked specimen were more sensitive to temperature change and possessed higher elasticity ratio of the glass state modulus to its the rubbery modulus. These properties were beneficial for good shape memory properties. The results were found that all EC-bp cross-linked samples showed good results in both shape fixity (R_f) and shape recovery (R_r) values of more than 98%. This was because the cross-linking effect of EC-bp led to the larger fixing and recovery force. Moreover, they studied the effect of PEG with different contents (10, 20, and 30 wt%) on the shape memory behaviors. It was found that the R_f was decreased, and R_r was increased with an increase of PEG content. This was due to the flexibility of PEG, which resulted in easier molecular chain motion.

Qin, Yu, Chen, Zhou, and Zhao (2018) studied the shape memory properties of poly (lactic acid) (PLA)/poly (propylene carbonate) (PPC) blends (70/30) with added dicumyl peroxide (DCP) used as a crosslinker at different amounts (0.5, 1, 1.5, and 2.0 wt%). The characterization of test samples was carried out to study the effect of DCP on PLA/PPC/DCP blends on tensile properties and shape memory behaviors. For the tensile properties, all the samples exhibited ductile behavior with yield strength above 45 MPa. Adding of 1wt% DCP, the elongation at break increased from 40% (PLA/PPC 70/30) to 107% (PLA/PPC/DCP 70/30/1) and dropped when the content of DCP was above 1 wt%. The result demonstrated that up to 1 wt% of the DCP content could improve the compatibility of PLA and PPC. The decrease of elongation at break when DCP content > 1 wt% caused by excessive crosslinking leading to a decrease in chain mobility. The effect of the cross-linking on the shape memory performance was measured at different recovery temperature i.e., 40, 45, 50, 55, and 60 °C. The result showed that shape recovery ratio (R_r) decreased with decreasing recovery temperature. When the recovery temperature was 60 and 55 °C, the R_r was almost 100% for all the samples. While the recovery temperature was set as 45 °C, the R_r increased with increasing the DCP content. It could be seen that the driving force for the shape recovery at low temperature (45°C) was related to the crosslinking structure.

Kim, Jang, and Kim (2019) studied the effect of compatibilizer on mechanical and shape memory properties of poly (lactic acid) (PLA) and poly (methyl methacrylate-block-n-butyl acrylate-block-methyl methacrylate) (Poly (MnBM)) (80/20) blend. Styrene–acrylonitrile-maleic anhydride (SAN-MAH) copolymer was expected to act as a fine compatibilizer, consequently enhanced the ductile property of PLA/Poly (MnBM) blend. The SAN-MAH contained 18.0 wt% MAH group and was added in the blend at the amount of 1.0, 3.0, 5.0, and 7.0 wt%. In the mechanical test, tensile and flexural strengths of the blends with 1 wt% of SAN-MAH showed highest value. When the SAN-MAH content was greater than 1 wt%, the tensile and flexural strengths gradually decreased as the SAN-MAH content increased up to 7 wt%. This was due to an excess amount of the SAN-MAH. In addition, impact strength of the blend increased with the increase of SAN-MAH up to 7 wt%. This was because of that the PLA/Poly (MnBM) blend became more ductile, when the SAN-MAH was presented. The tensile energy of the PLA/Poly (MnBM) blend with 1 wt% of SANMAH was greater than that of the blend without SAN-MAH. Shape memory behavior of the PLA/Poly (MnBM) blend with 1 wt% of SANMAH was measured at 90°C by cyclic stretch and recovery process. The recovery ratio of tensile energy was measured from the tensile energy of the blend elongated to 100%. The result reported that the recovery ratio of tensile energy between first and second stretch were 83% for PLA/Poly (MnBM) blend with SAN-MAH and 56% for the blend without SAN-MAH. This was because the increased compatibility between the PLA and Poly (MnBM) with adding SAN-MAH and probably led to better energy dissipation than the blend without SAN-MAH. Thus, the brittleness of PLA was decreased and become ductile, and shape memory behavior was also improved.

2.3.3 PLA composites

Qi, Dong, Liu, Liu, and Fu (2016) studied a rapid electroactive ternary shape memory polymer (SMP) composite of poly (propylene carbonate) (PPC) and poly (lactic acid) (PLA) containing multiwalled carbon nanotubes (MWCNTs). The appropriate binary blends were PPC70/PLA30 and PPC50/PLA50, which was chosen to future mix with MWCNTs at different amounts (1, 2, and 3 phr). Electrical conductivity and electroactive shape memory property of the composites were examined. The results show that electrical conductivity of the PPC70/PLA30/CNTs composites

increased when the MWCNTs content was increased from 0 to 3 phr. To observe the temperature of sample during applied voltage, the surface temperature of the sample was monitored using a digital temperature recorder. It was reported that the surface temperature of PPC70/PLA30/CNT3 increased to 80 °C within 30 s with a voltage of 30 V, whereas the surface temperature of PPC70/PLA30/CNT1 could not reach its switching temperature with a voltage of 30 V. Thus, high electrical conductivity allowed fast activation of shape recovery by applying a constant voltage.

Sessini et al. (2018) investigated the thermally activated shape memory response of biodegradable nanocomposites based on poly (lactic acid) (PLA) and poly (**ε**-caprolactone) (PCL) blend in 70/30 proportion reinforced with 1 wt% of different type of cellulose nanocrystals (CNC). In order to study how the different functionalization can affect the final properties of the nanocomposites. The difference of CNC means that they were functionalized by grafting of both PLA and PCL using the -OH groups onto the CNC surface as initiators for the reaction. The polymer nanocomposites were prepared by co-rotating extruder and compression molding. The result revealed that the compatibilization of the PLA/PCL blend was affected by the addition of the different functionalized-CNC. The incorporation of CNC-g-PLA into the blend presented better affinity of polymer matrix and CNC, which related to the mechanical properties that all the parameters were increased. This could be due to the localization of the nanofiller mainly in the PLA/PCL blend interface. For the shape memory properties, all the samples presented excellent values for both shape fixity (R_f) and shape recovery (R_r) higher than 98% and 80%, respectively. And the shape memory behavior of nanocomposites was not affected by addition of CNC nanofillers.

Raghunath, Kumar, Samal, Mohanty, and Nayak (2018) studied the effect of nanofiller on shape memory properties of polylactic acid (PLA) and epoxidized soybean oil (ESO) nanocomposite. The shape memory polymer (SMP) nanocomposite films of optimized PLA/ESO blend (80:20) were prepared using at three different loadings (*i.e.*1, 3, and 5 wt%) of acid functionalized multiwalled carbon nanotubes (COOH-MWCNT) as nanofiller. The PLA + 20wt%ESO + 3wt%COOH-MWCNT was chosen to future test shape memory performance. Shape memory test of sample consisted of two methods, the first method was thermal shape recovery test and the second

one was electroactive shape recovery performance test. In the thermally induced shape recovery of sample was performed by bending test at temperature about 45°C resulting that recovery ratio of sample was 88.88% which could be considered as good percentage of recovery by thermal actuation. In the electroactive shape recovery performance of sample was carried out by deforming to bent shape and then recovered to its flat permanent shape under a constant DC voltage of 40 V as a stimulus. The sample could recover to its permanent shape with 92% recovery ratio within 75 s. The presence of COOH-MWCNT, which encouraged electrically conductive fillers and caused the recovery ratio to increase when triggered by an electric source, could be the cause of the recovery response.

Chow, Tham, and Seow (2012) studied the effect of maleic anhydride grafted poly(lactic acid) (PLA-g-MAH) on the mechanical and thermal properties of PLA/ halloysite clay (HNC) composites. PLA-g-MAH with difference content (i.e., 4, 6, 8, 10 phr) was added into the composite system of 97 wt% PLA and 3 wt% HNC. They reported that the addition of PLA-g-MAH increased the flexural modulus and strength of PLA/HNC composites substantially. This was due to the incorporation of PLA-g-MAH, which improved interfacial bonding between HNC and PLA. Furthermore, the addition of HNC and PLA-g-MAH had no effect on the T_m and T_g of PLA, but increased the degree of crystallinity of PLA/HNC in the presence of PLA-g-MAH.

Tanoue, Hasook, Iemoto, and Unryu (2006) investigated the properties of PLA/PEG/ organoclay composites. Two kinds of organoclay, Clay A (2 theta = 5 degree) and Clay B (2 theta = 3.8 degree) and two kinds of PEG plasticizer having different molecular weights (M_w of 2,000 and 300,000-500,000, named as PEG2k and PEG500k, respectively) were studied. According to the XRD diffraction results and TEM images, the size of clay agglomerations in PLA/PEG/organoclay nanocomposites is larger than that of PLA/organoclay in the same organoclay using case, and is almost independent of molecular weight of PEG. These results imply that addition of PEG to PLA/organoclay nanocomposites during melt compounding will not be useful for the preparation of a PLA/organoclay having fully exfoliated clay platelets. For the PLA/Clay A composite, the interlayer of clay A decreased with adding both PEG, while the interlayer of clay B in the PLA/Clay B composite increased after adding PEG. According

to their findings, PEG2k is a good plasticizer for PLA/Clay B nanocomposites manufactured by melt compounding because it increases the tensile strength and elongation at break of PLA/Clay B nanocomposites.

CHAPTER 3

EXPERIMENTAL

3.1. Materials

Materials used in this study and their functions are presented in Table 3.1

Table 3.1 Materials, their chemical formulae, and functions.

Material	Chemical formulae	Company	Function
Poly (lactic acid) (PLA, Grade: 4043D, 4% D-isomer)	$C_3H_4O_2$	Nature Works Co. (Minnetonka, Minnesota, USA)	Polymer matrix based-SMPs
Poly (lactic acid) (PLA, Grade: Luminy® LX975, 12% D-isomer)	$C_3H_4O_2$	Total Corbion	Polymer matrix based-SMPs
Poly (ethylene glycol) (PEG, Mw: 4,000 g/mol)	$C_{2n}H_{4n+2}O_{n+1}$	Dow Chemical Company -	Plasticizer
Maleic anhydride (MA)	$C_4H_2O_3$	Loba Chemie PVT. LTD	Compatibilizer
Dicumyl peroxide (DCP)	$C_{18}H_{22}O_2$	Sigma-Aldrich Co., LLC	Initiator
Chloroform	$CHCl_3$	RCI Labscan	Solvent
Methanol	CH_3OH	RCI Labscan	Precipitated solvent
Phenolphthalein	$C_{20}H_{14}O_4$	Sigma-Aldrich Co., LLC	Indicator
Potassium hydroxide	KOH	QREC	Titrant

Table 3.1 Materials, their chemical formulae, and functions. (Continued)

Material	Chemical formulae	Company	Function
Sodium montmorillonite clay with cation exchange capacity (CEC) value of 80 meq/100g	Na^+-MMT	Thai Nippon Co., Ltd.	Filler
Cetyltrimethylammonium bromide (CTAB)	$C_{19}H_{42}BrN$	RCI Labscan	Surfactant

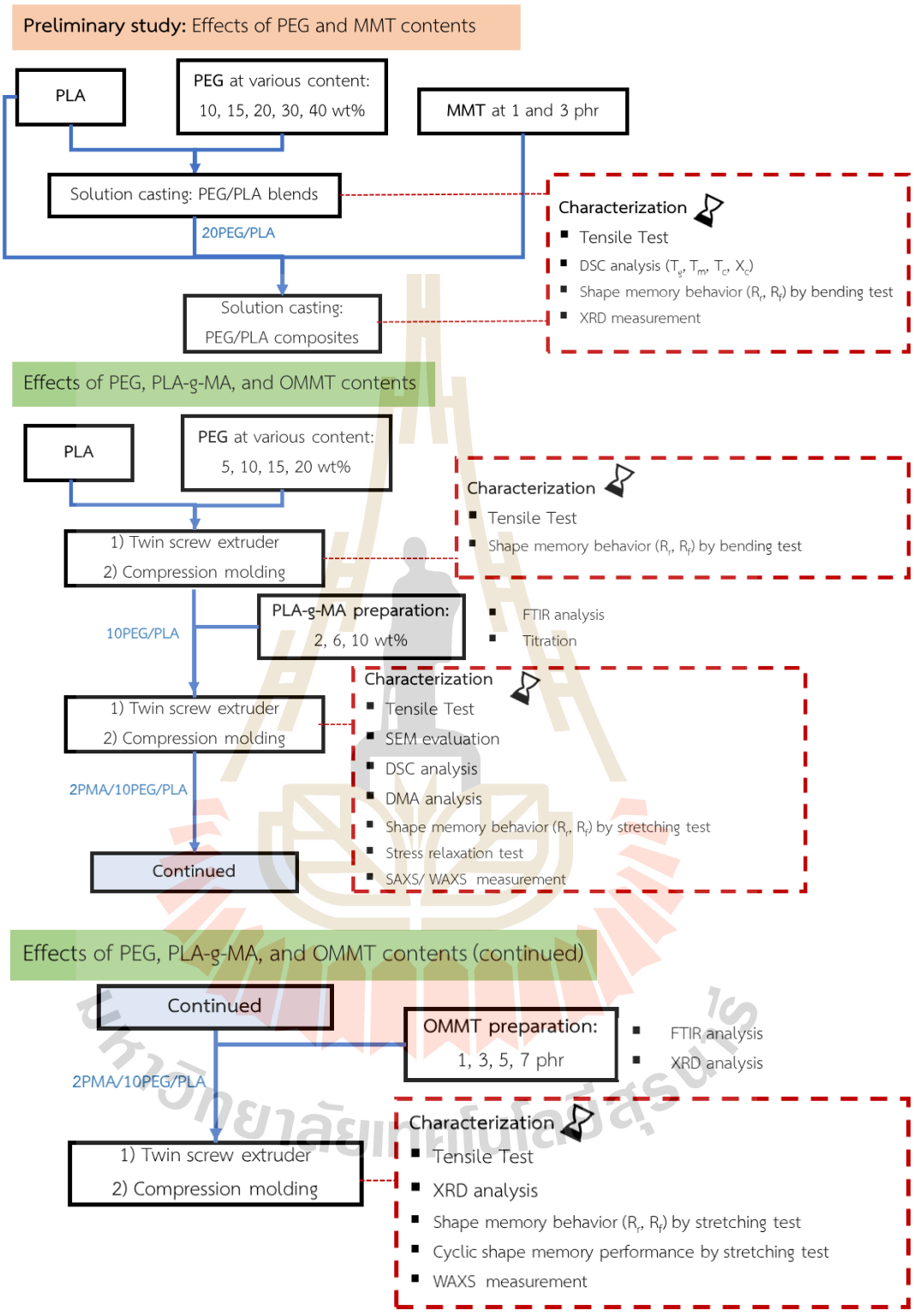

Figure 3.1. Schematic diagram of the research.

3.2 Effects of PEG and MMT contents on properties of PLA prepared via solution casting method.

3.2.1 Sample preparation by the solution casting method

PLA, PEG and MMT were dried under vacuum at 50°C for 24 h prior to use. Solvent casting was utilized in making SMPs films from PLA. 8 g of PLA was mixed with 100 ml of DCM in an enclosed bottle. At least four hours later, the mixture was stirred at a constant speed of 350 rpm at room temperature with a magnetic stirrer until a clear or homogeneous solution was obtained. After carefully pouring the solution into a Petri dish glass, it was allowed to dry at ambient temperature for 24 hours before being dried for 4 hours at 60°C to ensure total DCM removal.

The same procedure as described previously was used to prepare the PEG/PLA blends and nanocomposites. Solutions of PLA or PEG/PLA were produced with a constant solids content of 8% w/v. The PEG content of PLA/PEG blend films was altered at 10%, 15%, 20%, 30%, and 40% wt. To synthesize plasticized PLA nanocomposites with MMT concentrations of 1 and 3 phr, MMT was dispersed in DCM and sonicated for 30 minutes prior to mixing with the PEG/PLA blend solution to ensure uniform dispersion. Each sample had a film thickness of about 150 μm. The samples were named according to the amount of PEG in the PEG/PLA blends and the amount of MMT present. For example, a PLA blend containing 20% PEG is referred to as 20PEG/PLA. The blend of 20PEG/PLA containing 1 phr MMT was named 1MMT/20PEG/PLA. 3MMT/PLA is a PLA that has not been plasticized and contains 3 phr MMT.

3.2.2 Characterization of the sample

The solution cast sample was subjected to a preliminary examination to determine the effect of PEG content and MMT as a filler on the properties of the PLA blend and composite, which included the following characterization procedures.

3.2.2.1 Tensile properties

Tensile testing was conducted at room temperature using a 1 kN load cell and a 50 mm/min cross head speed on a Universal Testing Machine (UTM) (5565 Model, Instron, UK) in accordance with ASTM D882. Rectangular specimens measuring 100 mm in length and 10 mm in width were formed.

3.2.2.2 Differential scanning calorimetry (DSC)

Thermal properties of PLA and plasticized-PLA films were measured with a DSC (TGA/DSC 1 Instruments SDT 2960, USA). Under a nitrogen atmosphere, the tests were carried out at temperatures ranging from 35 to 200°C at a heating rate of 10°C/min.

3.2.2.3 X-ray diffraction (XRD)

The interlayer spacing and peak position angle of MMT were determined by XRD performed on D8-Advance Bruker AXS model with CuKα radiation having a λ = 1.542 angstrom. The samples were characterized using a scanning range of 2θ from 3 to 25°, with a constant scanning speed 0.2°/min.

3.2.2.4 Shape memory properties by bending test

Shape memory performance of samples were evaluated by shape recovery test. The size of sample was 60 mm x 5 mm x 0.20 mm. To test shape recovery, the samples were formed into spiral shape at 65°C followed by rapid cooling in cold water (10°C) to obtain a temporary shape as shown in Figure 3.2. To evaluate shape recovery performance, the sample was reheated in a water bath at 65 °C for 2 minutes to relax residual stresses and allow the sample to recover its initial shape. The sample recovery rate was determined using a digital camera, and the shape recovery ratios (R_r) were derived using the following equation:

$$R_r = \frac{\theta_r}{\theta_i} \times 100\% \quad (3.1)$$

where R_r is shape recovery ratio, θ_i is initial angle, and θ_r is recovered angle.

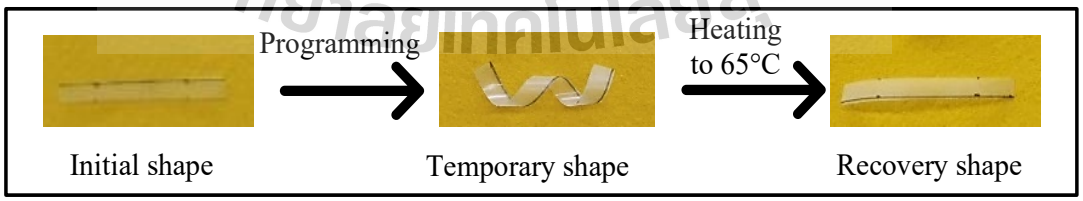

Figure 3.2. A schematic representation of shape memory testing.

3.3 Effects of PEG and PLA-*g*-MA contents on mechanical and shape memory properties of PLA prepared via melt blending method.

3.3.1 Preparation of maleic anhydride grafted poly (lactic acid) (PLA-*g*-MA)

In order to graft maleic anhydride (MA) onto poly (lactic acid), PLA (100 phr), MA (5 phr), and DCP (1 phr) were pre-mixed together before being fed into a twin-screw extruder (Model: CTE-D16L32, Thailand) (L/D=32). The extruder temperature profile, from the feed throat to the die, was 50/160/180/180/180/180/175°C with a screw speed of 80 rpm. The grafting reaction was carried out for 1.30 min in the extruder. The amount of DCP and MA used in this study are according to the work of Hwang and coworkers (Hwang et al., 2012), which revealed that the maximum MA grafting on PLA could be obtained by 1 phr DCP and 5 phr MA. Before using as a compatibilizer, the prepared PLA-g-MA was dried at 100°C in a vacuum for 4 hours to eliminate any unreacted MA.

3.3.2 Preparation of PLA blends using melt blending method

To prepare plasticized PLA, PLA and PEG were dried in a vacuum oven at 50°C for 24 h prior to the blending process. PEG was melted at 60°C, premixed with PLA pellets, and allowed to cool before being fed through a twin-screw extruder (Model: CTE-D16L32, Thailand) (L/D=32). The temperature profile from hopper to the die was 50/160/180/180/180/180/175°C. while the screw speed was 60 rpm. The PEG content was varied, i.e., 5, 10, 15, and 20 wt%. The plasticized PLA was denoted according to the amount of PEG content, *i.e.*,5PEG/PLA, 10PEG/PLA, 15PEG/PLA, and 20PEG/PLA, respectively. After mixing, the extrudate from the exit die was cooled with an air blower and pelletized. Compound pellets were formed using a compression molding machine (LabTech, LP20-B) to create test specimens It was heated at 170°C without pressure for 5 minutes and then compressed under pressure of 100 MPa for 3 minutes.

The same process as described previously was used to prepare compatible PEG/PLA blends. Prior to compounding, PLA, PEG, and PLA-g-MA were hot-premixed. The PLA-g-MA was employed in a variety of concentrations, including 2, 6,

and 10 phr. Compression molding machines were used to create the test specimens, which were then examined according to the procedures specified in the following section.

3.3.3 Characterization of PLA-*g*-MA

FTIR analysis and the titration method were used to confirm the PLA molecules grafted with maleic anhydride.

3.3.3.1 Functional group analysis

Functional groups of PLA, MA, and PLA-g-MA will be evaluated by a Fourier transform infrared (FT-IR) (Bruker Tensor 27, USA) spectroscopy with an attenuated total reflection (ATR) accessory. Spectrum of a sample will be recorded in a wavenumber range of 4000 to 400 cm^{-1} with a number of scans of 64.

3.3.3.2 Grafting content of maleic anhydride

Maleic anhydride grafting content of the prepared PLA-*g*-MA will be determined by a titration method according to method described by (Hwang et al., 2012). In order to purify the sample, the prepared PLA-*g*-MA will be firstly dried in a vacuum oven at 80°C for 4 h to remove unreacted MA. Then, the grafted PLA of 2 g was dissolved in 20 mL chloroform. After that, it was precipitated with excess content of methanol followed by drying at 80°C until the weight become constant. Then, the purified sample of 1 g was completely dissolved in 20 mL of chloroform and titrated with 0.02 M methanolic potassium hydroxide (KOH) by using phenolphthalein as an indicator. The content of MA grafting will be calculated using the following equation (3.2).

$$\%\ \mathrm{MA} = \frac{N_{KOH} V_{KOH} \times 98.06 \times 100}{2W_{sample}} \qquad (3.2)$$

where N_{KOH} is the normality of KOH (mol/equivalent); V_{KOH}, the volume of KOH (liters); W_{sample}, the weight of sample (grams); and the molecular weight of maleic anhydride is 98.06 g/mol.

3.3.4 Characterization of PLA blends

The properties of the compound prepared by melt blending method were determined. This section examines the characterization in full.

3.3.4.1 Tensile properties

Tensile properties of PLA and PLA blends were measured using a universal testing machine (UTM) (Instron 5565 Model, UK) with a load cell of 5 kN and a cross head speed of 10 mm/min at room temperature. Test specimen was prepared according to ASTM D638 standard (Type V). In each condition, at least five samples were tested, and averaged values were reported.

3.3.4.2 Thermal properties

Thermal characteristics i.e., glass transition temperature (T_g), crystallization temperature (T_c), cold crystallization temperature (T_{cc}), melting temperature (T_m), and crystallinity (X_c) of specimens, before and after stretching, were determined using a differential scanning calorimeter (DSC) (Perkin Elmer-PYRIS Diamond-DSC). Experiments were conducted in a single heating step between 25 and 200°C at a rate of 10°C/min in a nitrogen environment to compare the exact thermal characteristics of unstretched and stretched samples. The crystallinity (X_c) of sample was estimated using the following equation:

$$X_c = \frac{\Delta H_m - \Delta H_{cc}}{\omega \Delta H_m^o} \times 100\% \qquad (3.3)$$

where ΔH_m and ΔH_{cc} are the enthalpies of melting and cold crystallization, respectively. ω is the weight fraction of PLA and $\Delta H_m{}^0$ is melting enthalpy of 100% crystalline PLA (93.7 J/g).

3.3.4.3 Thermomechanical properties

The storage modulus and loss factor ($\tan\delta$) values were determined in tension mode using a DMA Instruments. After cooling to -40°C and equilibration for 5 minutes, each sample was loaded with a dynamic strain amplitude of 0.03% at a frequency of 1 Hz. During the measurement, the temperature was raised from -40 to 100°C at a rate of 2 °C/min.

3.3.4.4 Shape memory properties by bending test

Bending test was used to investigate the shape memory properties of the PEG/PLA blend sample. The sample was 60 mm x 10 mm x 2 mm in dimension. The sample was heated in a water bath to 60 °C, then bent into a U shape

and then cooled with an ice pack to produce a temporary shape. The shape recovery ratio was determined by immersing the sample into the hot water (60 °C) for 1 min to relax residual stresses and allow the sample to recover its initial shape. The shape change of each sample over time was recorded by digital camera and the recovery ratio of the sample was calculated using equation 3.4. The shape memory testing of the specimen is depicted in Figure 3.3.

$$R_r = \frac{\theta_r}{180} \times 100\% \tag{3.4}$$

where R_r is shape recovery ratio and θ_r is recovered angle

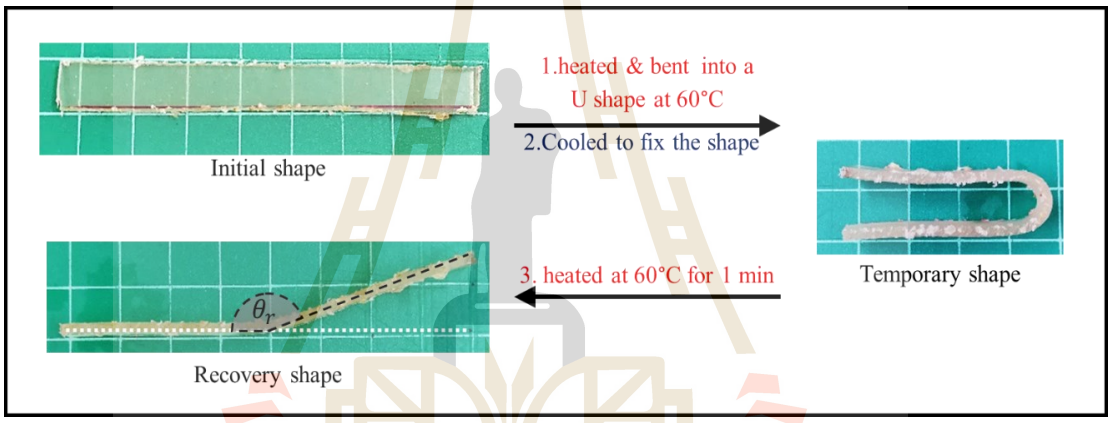

Figure 3.3. A schematic representation of shape memory bending test.

3.3.4.5 Shape memory properties by stretching test

Shape memory tests were performed using a UTM (Instron 5569 Model, UK) equipped with a heating chamber. Shape recovery ratio (R_r) and shape fixity ratio (R_f) of the specimens were determined. The programming temperature (T_p) is 45°C in this study because the T_g of the PEG/PLA blend is less than 45°C, as indicated by the sample's DSC thermogram. The following steps were performed, (1) The specimen with an initial length of L_0 was heated to 45°C for 5 minutes and then stretched to 100% strain at a constant strain rate of 10 mm/min (L_1). (2) The specimen was maintained at a constant 100% strain while being quenched with an ice pack. (3) After removing the sample from the test equipment, it was maintained at room temperature for 24 hours (L_2). (4) The stretched specimens were immersed in a water bath at different temperature of 40, 50, and 60°C to observe recoverability of the specimen

(L_3). Figure 3.4 illustrates the test piece obtained at each stage of the shape memory test. At least five specimens were tested in each condition. R_r and R_f values were determined as follows:

$$R_f = (\frac{L_2}{L_1}) \times 100\% \quad (3.5)$$

$$R_r = (\frac{L_2 - L_3}{L_2 - L_0}) \times 100\% \quad (3.6)$$

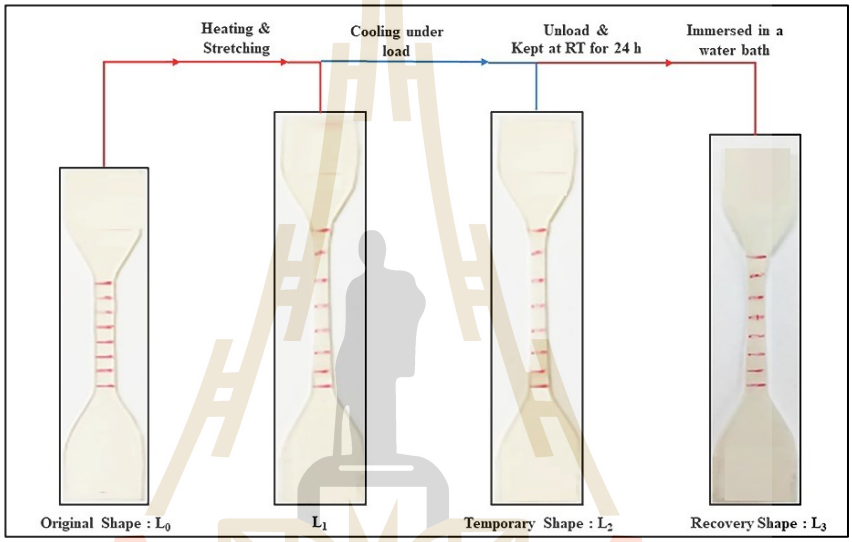

Figure 3.4. Diagram of shape memory test.

3.3.4.6 Stress relaxation

The stress relaxation test was conducted with the assistance of a DMA Instruments. Each sample was heated from 25 to 45°C for 5 minutes. Following that, the sample was stretched to 100% strain at a rate of 10 mm/min. During whole experiment, the tension was maintained, and the decrease in stress was recorded versus time. The dimensions of the test specimens were 10 mm x 4 mm x 1.0 mm.

3.3.4.7 Morphology

Morphologies of the blends were analyzed by using a scanning electron microscope (SEM) (JEOL JSM-6010LV, USA) at a voltage of 5 kV. Samples were cryo-fractured in liquid nitrogen and coated with gold for 3 min to ensure suitable electrical conductivity.

3.3.4.8 Microstructure evaluation

In situ Small-angle X-ray scattering and wide-angle X-ray scattering (SAXS/WAXS) measurements using BL1.3W beamline of Synchrotron Light, was applied to study micro-structure evolution of specimens during shape memory test including the initial state, after heating, after stretching, and after recovery. X-ray energy of 9 keV (λ = 1.38 Å) was applied with the exposure duration of 60 s. q-range for SAXS measurement was 0.04–0.7 nm^{-1}. The specimen-to-detector distances for WAXS and SAXS measurements were 0.24 and 5.18 m, respectively. WAXS and SAXS scattering data were processed by using the SAXSIT4.41 software.

3.4 Effect of organoclay on mechanical, thermal and shape memory properties of 10PEG/PLA composites prepared via melt blending method

3.4.1 Preparation of organoclay

MMT was dried and ground prior to being modified. CTAB was added at 1.0 CEC of MMT, as calculated by equation 3.7.

$$\text{Weight of surfactant}(g) = n\ x\ CEC\ (\frac{meq}{g})x\ A(g)\ x\ B(\frac{g}{mol}) \qquad (3.7)$$

where A is weight of clay (g), B is molecular weight of surfactant (g/mol).

CTAB was dissolved in 3000 ml of hot deionized water (70 °C), with vigorous stirring. Then, 100 g of MMT was added to the hot CTAB solution and vigorously stirred for 3 hours. Following that, the suspension was washed several times with deionized water until water conductivity was close to 54 µS (MMT's conductivity in deionized water was determined to be close to 54 µS). The modified MMT, known as organoclay, was vacuum filtered before being dried in an oven at 70 °C and crushed to powder. Organoclay particle size is controlled using a Sieve shaker with a mesh number of 270 (53 micron).

3.4.2 Preparation of compatibilized 10PEG/PLA composites using melt blending method

The concentration of organoclay was varied at 1, 3, 5 and 7 phr. To ensure uniform dispersion of organoclay in the PLA matrix, a solution cast masterbatch of organoclay/PLA was prepared. PLA: organoclay: chloroform had a weight ratio of 10:3:180. To start, organoclay and chloroform were sonicated for 30 minutes, followed by the addition of PLA to the organoclay suspension and continuous stirring at room temperature for 4 hours using a magnetic stirrer. Following that, it was placed into a Petri dish glass and left to dry for 24 hours at room temperature before being dried at 60°C for 4 hours. Before mixing with PLA, PEG, and/or PLA-g-MA, the masterbatch compound was chopped into small pieces. The composite compound and test specimen were produced in the same method as stated in Section 3.3.2.

3.4.3 Characterization

3.4.3.1 Functional groups analysis

MMT and organoclay functional groups were identified using FTIR (Bruker Tensor 27, USA) spectroscopy in conjunction with the KBr pellet technique. A sample's spectrum was measured in the wavenumber range 4000 to 400 cm^{-1} with a total of 64 scans.

3.4.3.2 Structure of MMT and organoclay

The interlayer spacing and peak position angle of MMT and organoclay structures were characterized using an X-ray diffraction spectrometer (XRD) performed on D8-Advance Bruker, model AXS with a Cu-Kα radiation source (λ = 1.542 Å). The device was operated at a voltage of 40 kV and a scan speed of 0.2 s /step with a step size of 0.01 °. The MMT, organoclay, and the compatibilized PEL/PLA composites were characterized using a scanning range of 2θ = 3 - 25°.

3.4.3.3 Tensile properties

Tensile properties of PLA and PLA blends were measured using a universal testing machine (UTM) (Instron 5565 Model, UK) with a load cell of 5 kN and a cross head speed of 10 mm/min at room temperature. Test specimen was

prepared according to ASTM D638 standard (Type V). In each condition, at least five samples were tested, and averaged values were reported.

3.4.3.4 Shape memory performance

Shape memory performance of the specimen were performed using a UTM (Instron 5569 Model, UK) equipped with a heating chamber. Shape recovery ratio (R_r) and shape fixity ratio (R_f) of the specimens were determined. The programming temperature (T_p) is 45°C similar to previous section. The following steps were performed, (1) The specimen with an initial length of L_0 was heated to 45°C for 5 minutes and then stretched to 100% strain at a constant strain rate of 10 mm/min (L_1). (2) The specimen was maintained at a constant 100% strain while being quenched with an ice pack. (3) After removing the sample from the test equipment, it was maintained at room temperature for 24 hours (L_2). (4) The stretched specimens were immersed in a water bath at different temperature of 40, 50, and 60°C to observe recoverability of the specimen (L_3). At least five specimens were tested in each condition. R_f and R_r values were determined as follows equation 3.5 and 3.6, respectively.

Additionally, Shape memory behavior under cyclic stretch and recovery process of the specimen was investigated. The specimens were heated to 45 °C, stretched to 50 or 100 %strain, and then allowed to recover at 60 °C. After then, the initial recovered specimens were stretched and recovered a second and third time. In this part, the R_r values of each cycle were compared to evaluate the repeatability of the specimen's shape memory performance. In addition, the tensile energy of the specimen was measured at each period of stretching to determine the recovery ratio of tensile energy. According to Kim and coworkers (Kim et al., 2019), the recovery ratio of tensile energy was measured from the tensile energy of the specimen for the second stretch divided by the first stretch of the specimen compare to that of the third stretch divided by the second stretch of the specimen, could be indicative of the shape memory performance of the specimen.

3.4.3.5 Microstructure evaluation

The microstructure and crystallinity of the specimen during cyclic stretch and recovery process were analyzed by synchrotron wide-angle X-ray

scattering (WAXS) technique. X-ray energy of 9 keV (λ = 1.38 Å) was applied with the exposure duration of 60 s. The specimen-to-detector distances for WAXS measurements were 0.24 m. WAXS scattering raw data were processed by using the SAXSIT4.41 software. The microstructure investigation of a specimen can be divided into seven parts: original, first stretching, after first recovery, second stretching, after second recovery, third stretching, and after third recovery. The specimen was heated during the stretch procedure at 45 °C and recovered at 60 °C.

CHAPTER 4
RESULTS AND DISCUSSION

4.1 Effects of PEG and MMT contents on properties of PLA prepared via solution casting method.

4.1.1 XRD measurement

The change in the basal space of a MMT was investigated using XRD. The peak position in the MMT XRD spectrum shifts proportionally to MMT interlayer spacing, which can expand or contract. The interlayer spacing of MMT can then be calculated using the XRD peak position using Bragg's law equation:

$$d = \lambda / (2\sin\theta) \quad (4.1)$$

where d is the interlayer spacing of clay, λ is the X-ray wavelength of CuKα equal to 1.5418 Å, and θ is the incident angle of X-ray.

Figure 4.1 depicts the XRD patterns of MMT, PLA, 3MMT/PLA, 20PEG/PLA, and 3MMT/20PEG/PLA. According to Bragg's law (equation 4.1), the characteristic peak of MMT was observed at 2θ equal to 6.12°, which corresponded to a basal spacing of 1.44 nm. For semi-crystalline polymer, crystalline phase of PLA shows peaks appears at 2θ equal to 16.5° and 19° corresponding to (200/110) and (203) planes of α-form PLA crystallites along with the nearby broaden peak of amorphous phase (Koosomsuan et al., 2019). When 3 phr MMT was added to the PLA matrix, the XRD pattern of the 3MMT/PLA nanocomposite showed that the MMT peak (at 6.12°) remained unchanged, while the PLA peak position at 16.5° was slightly shifted to the lower 2θ, and the intensity was also significantly increased as compared to those of neat PLA. These indicated that polymer chains could not penetrated between MMT layers, the structure of MMT remained unaltered. Moreover, the MMT layers may be increased the nucleation density of the PLA led to its crystalline phase was increased.

When adding 3 phr MMT into 20PEG/PLA blend, the XRD peak of MMT was not clearly observed as compared to that of 3MMT/PLA. This may be because the small segmental mobility of PEG facilitated the PLA chain's penetration into MMT particles.

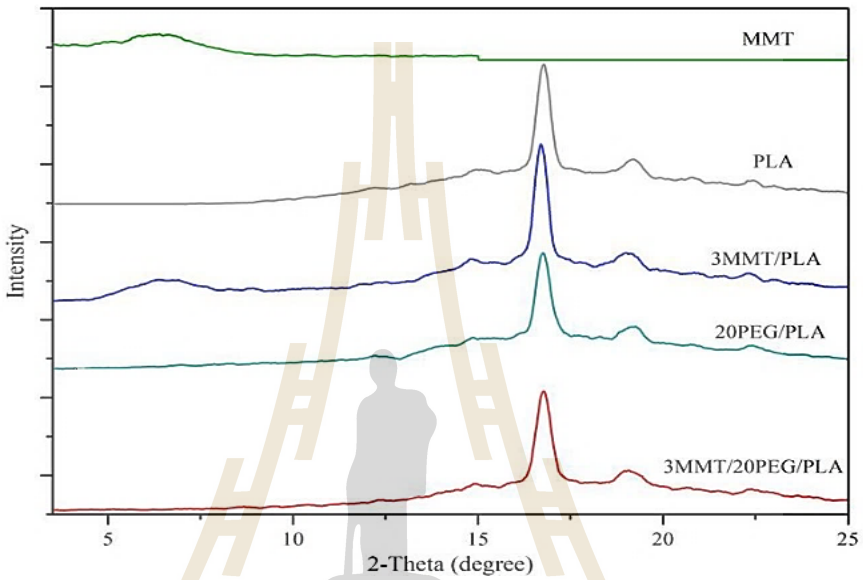

Figure 4.1. XRD patterns of MMT, PLA, 3MMT/PLA, 20PEG/PLA, and 3MMT/20PEG/PLA.

4.1.2 Tensile properties

Table 4.1 summarizes the tensile properties of PLA, PEG/PLA blends, and MMT/PEG/PLA nanocomposites, including tensile strength at yield, tensile stress at break, tensile modulus, and elongation at break. PLA had the highest modulus (approximately 1.67 GPa) and the lowest elongation at break (approximately 4.65 percent). The addition of PEG to the PLA matrix significantly improved the ductility of plasticized PLA, as evidenced by a 20-fold increase in elongation at break compared to PLA. Tensile strength at yield, tensile stress at break, and tensile modulus all decreased significantly as PEG content increased. This was because the presence of PEG in the PLA matrix increased the chain mobility of the PLA matrix.

When 3 phr of MMT was added to PLA composite with MMT as a filler, the tensile properties of 3MMT/PLA nanocomposite decreased when compared to

those of neat PLA. This could be due to the presence of unexfoliated MMT in PLA, as corroborated by the XRD results reported above. The addition of 1 and 3 phr of MMT into plasticized 20PEG/PLA nanocomposites increased the tensile moduli to 1.19 and 1.49 GPa, respectively, for 1MMT/20PEG/PLA and 3MMT/20PEG/PLA nanocomposites. Nonetheless, their elongation at break was less than that of the 20PEG/PLA blend. This could be due to the incorporation of MMT particles, which reduced the chain mobility of PLA.

Table 4.1. Tensile properties of PLA, PEG/PLA blends, and MMT/PEG/PLA nanocomposite films

Sample	Strength at yield (MPa)	Stress at break (MPa)	Modulus (GPa)	Elongation at break (%)
PLA	-	43.76 ± 1.36	1.67 ± 0.26	4.65 ± 0.30
10PEG/PLA	21.64 ± 1.02	16.87 ± 0.91	1.03 ± 0.09	86.56 ± 4.03
15PEG/PLA	24.83 ± 1.47	18.70 ± 0.76	1.12 ± 0.16	86.71 ± 6.08
20PEG/PLA	24.43 ± 1.34	15.72 ± 0.98	1.10 ± 0.11	51.78 ± 5.02
30PEG/PLA	16.01 ± 1.13	11.09 ± 1.07	0.72 ± 0.11	47.74 ± 4.43
40PEG/PLA	12.89 ± 0.44	10.77 ± 1.36	0.24 ± 0.17	56.24 ± 10.23
1MMT/20PEG/PLA	16.41 ± 1.58	13.04 ± 1.79	1.19 ± 0.12	14.07 ± 5.48
3MMT/20PEG/PLA	19.15 ± 1.87	15.61 ± 1.85	1.49 ± 0.22	23.01 ± 7.08
3MMT/PLA	-	37.78 ± 1.48	1.16 ± 0.57	3.13 ± 1.27

4.1.3 Thermal analysis

Thermally induced shape recovery of PLA commonly happens at its T_g (55°C). The addition of the plasticizer PEG and the nanofiller MMT is known to impact the mobility of polymer chains, hence affecting T_g. Thus, it is crucial to explore the T_g value as a function of PEG content and MMT incorporation in order to know the onset switching temperature of PLA blends and PLA nanocomposites, respectively. The DSC thermogram and thermal properties of the PLA blends and composites are shown in

Figure 4.2 and Table 4.2, respectively. The T_g of PLA was determined to be 55°C using the DSC curve. PEG concentrations of 15, 20 and 30 wt% in PLA resulted in a drop in the T_g of PLA to 50°C, 47°C, and 42°C, respectively. These results imply that the polymer chains can readily slip past one another due to the plasticizing effect of PEG, requiring less energy for the phase transition process. This effect was also well agreed with the tensile properties result in which the increase of flexibility in plasticized PLA was observed. However, cold crystallization temperature (T_{cc}) of the blend with 30% PEG obvious observed at 98 °C. This could be the result of phase separation between PEG and PLA. This could be due to PEG's plasticizing effect, which increases polymer chain mobility and thus facilitates PLA crystallization. The addition of plasticizer reduced the melting temperature (T_m) of PLA. However, as the PEG content of the blend increased up to 40% by weight, the T_g of PLA could not be determined. This was due to the fact that the melting point of PEG at 52°C overshadowed the T_g of PLA.

Based on these findings, the 20PEG/PLA blend with the lowest T_g of 47°C, which should be beneficial for medical applications, was chosen for further investigation. PLA and 20PEG/PLA nanocomposites with MMT contents of 1 and 3 phr were formed. According to Figure 4.2, the presence of 3 wt % MMT in PLA had little to no effect on PLA's T_g but had a significant effect on its T_m. The melting point of PLA shifted to a higher temperature, possibly due to the MMT acting as a nucleating agent. This results in more nuclei with smaller PLA crystals, requiring more energy to destroy the crystalline structure. This was supported by the XRD result of 3MMT/PLA, which showed that the intensity of the PLA crystalline peak was increased when compared to that of neat PLA.

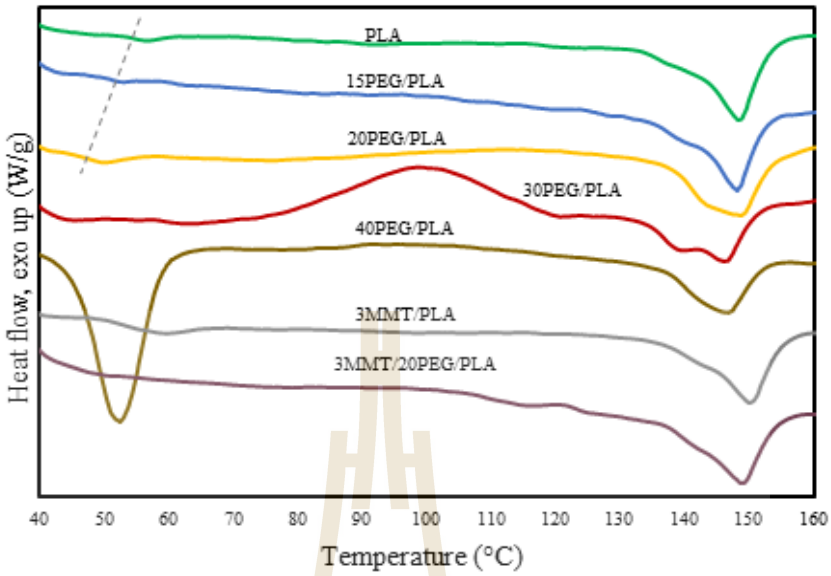

Figure 4.2. DSC thermograms of PLA, PEG/PLA blends and MMT/PEG/PLA nanocomposites.

Table 4.2. Summarized thermal properties of the samples.

Sample	T_g (°C)	T_m (°C)
PLA	55	150
15PEG/PLA	50	149
20PEG/PLA	47	150
30PEG/PLA	42	148
40PEG/PLA	-	149
3MMT/PLA	41.6	152
3MMT/20PEG/PLA	41.8	150

4.1.4 Shape memory performance

As shown in the DSC data, the T_g of all samples is between 47 and 55°C. As a result, thermal recovery studies on PLA, PEG/PLA, and MMT/20PEG/PLA films at specified T_{trans} of 65°C were carried out. The recovery ratio of the sample was calculated using equation 3.1 and is stated in Table 4.3, and images of the shape recovery behaviors are displayed in Figure 4.3.

PLA film had the highest shape recovery ratio of 98.2%. As PEG was added, the shape recovery ratio of plasticized PLA films reduced considerably as compared to that of neat PLA. It is obvious from the data that the presence of PEG reduced the tensile modulus of plasticized PLA. The modulus has been related to the shape fixation phase of SMPs. As a result, if the modulus lowers, shape memory performance may suffer. On the other hand, the form recovery ratio of 20PEG/PLA was the highest of all PEG/PLA blends. This suggested that the low T_g of 20PEG/PLA increased polymer chain relaxation in the amorphous phases of PLA, providing a driving force for the polymer chains to return to their initial shape and return faster than neat PLA, as illustrated in Figure 4.3. The shape recovery ratio of 20PEG/PLA with MMT was larger than that of 20PEG/PLA without MMT. This is because the exfoliated MMT acts as a physical crosslink between PLA chains, increasing the shape recovery ratio from 93.3% of 20PEG/PLA to 98% of 1MMT/20PEG/PLA.

Table 4.3. Shape recovery tests of PLA, PEG/PLA blends and MMT/PEG/PLA nanocomposites

Sample	Recovery ratio (%)
PLA	98.2
10PEG/PLA	56.1
15PEG/PLA	81.7
20PEG/PLA	93.3
30PEG/PLA	88.9
40PEG/PLA	87.2
1MMT/20PEG/PLA	98.0
3MMT/20PEG/PLA	97.2

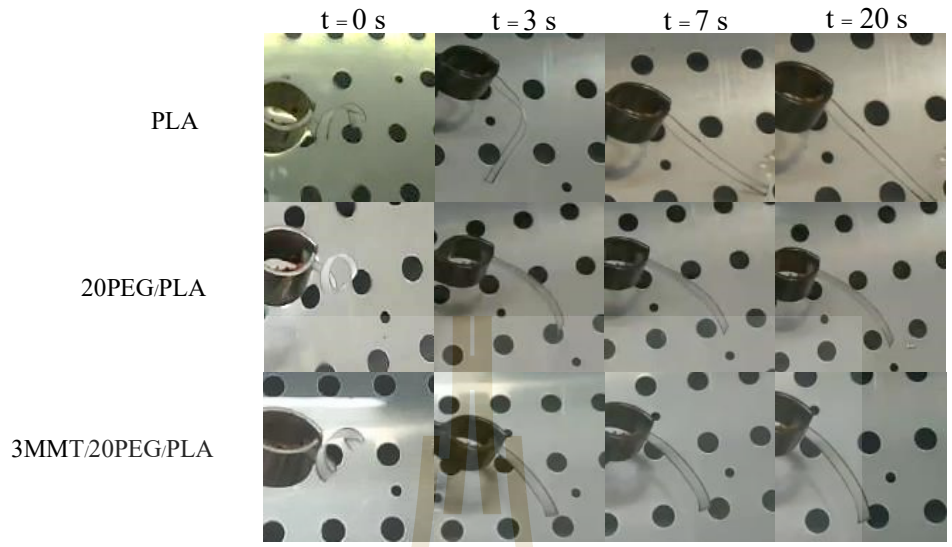

Figure 4.3. Photographs of the shape recovery behaviors of PLA, 20PEG/PLA, and 3MMT/20PEG/PLA films in a water bath at 65 °C.

In this chapter, shape memory films made of PLA, its blends, and nanocomposites made of PLA were explored. To summarize, adding PEG to PLA benefited in reducing the material's brittleness and high T_g. When PEG in concentrations of 10 and 15 wt% was added in PLA blends, the elongation at break increases nearly 20 times. Among the blend, the T_g of plasticized PLA with 20 wt% PEG had the lowest temperature (47°C), resulting in the maximum recoverability. The incorporation of MMT into 20PEG/PLA composites resulted in an increase in the T_g of the composites, which may have been owing to the chain limitation caused by the MMT particle inclusion. Their shape recovery ratio, on the other hand, is higher than that of 20PEG/PLA film. Because there was no MMT peak (at 6.12°), this showed that the exfoliated MMT might serve as a physical crosslink in PEG/PLA composites, resulting in an increase in the recovery ratio from 93.3 % for 20PEG/PLA to 98 % for 1MMT/20PEG/PLA.

4.2 Effect of PEG content on mechanical and shape memory properties of PLA prepared via melt blending method.

4.2.1 Tensile properties

The stress-strain curves and summary of tensile properties of pure PLA and PLA blended with PEG at various concentrations (5, 10, 15, and 20% wt%) are

shown in Figure 4.4 and Table 4.4. All samples were prepared and formed using melt blending and compression molding, respectively. The stress-strain curve of neat PLA exhibited brittle failure behavior, with a maximum tensile stress of 61.38 MPa at break and a very low elongation at break of 12.64 %. When PEG was added to PLA at a content of up to 10%, the stress-strain curves of PLA blends exhibited a greater degree of plastic deformation than those of pure PLA. Breaking strain increased to a maximum of 480 percent. As expected, the Young's modulus and tensile stress at break of the 10PEG/PLA were reduced to 0.5 GPa and 40 MPa, respectively, when compared to neat PLA. All tensile properties decreased as the PEG content was increased further. This was because at 10% PEG, the plasticizing effect of PEG enabled greater PLA chain mobility, whereas at 15% PEG, the compatibility between PLA and PEG was disrupted. Due to the low degree of compatibility, the tensile properties of the PLA blend have been reduced.

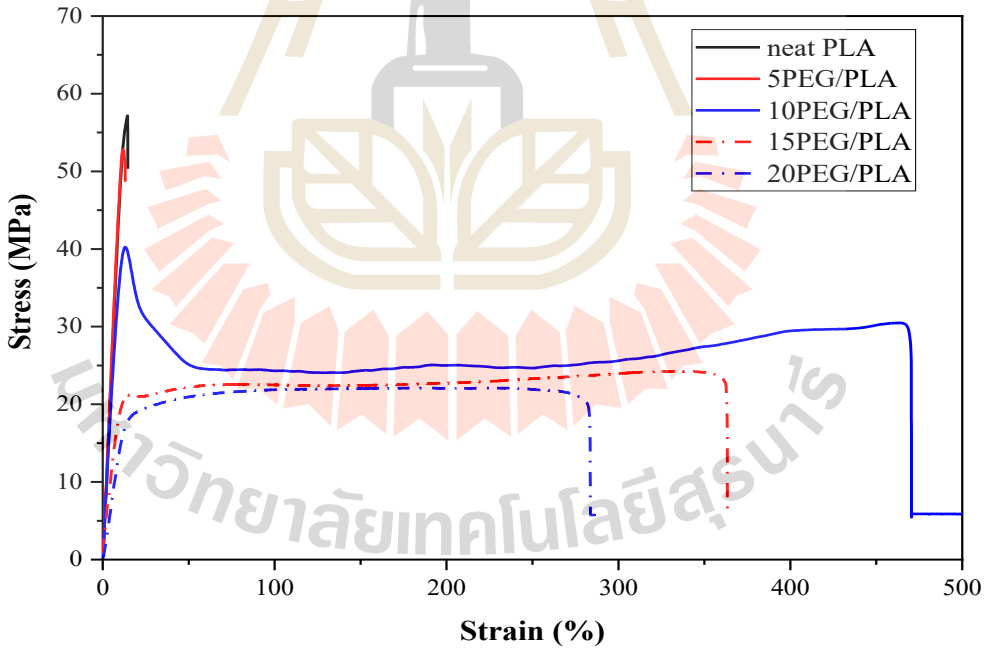

Figure 4.4. Stress-strain curve of PLA and PLA blended with PEG at various contents.

Table 4.4. Mechanical properties of PLA and PEG/PLA blends.

Sample	Tensile strength (MPa)	Young's Modulus (GPa)	Elongation at break (%)
Neat PLA	61.38 ± 1.24	0.70 ± 0.02	12.64 ± 1.19
5PEG/PLA	53.06 ± 1.05	0.50 ± 0.01	13.40 ± 1.59
10PEG/PLA	40.06 ± 1.50	0.50 ± 0.01	480.00 ± 34.59
15PEG/PLA	21.19 ± 0.94	0.24 ± 0.02	358.20 ± 1.41
20PEG/PLA	18.32 ± 1.25	0.13 ± 0.01	282.98 ± 12.73

4.2.2 Shape memory properties by bending test

As detailed in section 3.2.2.4, the specimens' shape memory properties were determined using bending tests. All samples were deformed into a U shape and the recovery ratio was determined at a temperature of 60°C. The shape change of each sample over time is depicted in Figure 4.5 and the recovery ratio of the sample was calculated using equation 3.1 and is stated in Table 4.5. The recovery ratio for PLA and 5PEG/PLA samples was 91 %. When PEG content was increased, the shape recovery ratio decreased. However, as the PEG content increased, the sample recovered more rapidly. This result is consistent with the shape memory testing result of a solution cast film sample. Thus, the same reason was given for why adding PEG to PLA reduces the T_g of PLA, resulting in a lower onset temperature for recovering PLA blends. As a result, the shape-returning properties of PLA blend more quickly than those of neat PLA. In contrast, the recovery ratio is unrelated to the sample's T_g. According to Guo et al. (2018), the addition of PEG, a plastic material, results in irreversible deformation of PLA/PEG blends, resulting in a decrease in R_r.

In solution casting sample, the tensile properties of PLA blend were not drop significantly until the addition of PEG up to 15 wt%. Additionally, adding 20 wt% into PLA, its properties was compromise between tensile properties and shape memory performance. In comparison, the sample with adding 10 wt% prepared by melt blending method had the best improve tensile properties. This result shown the

solution casting method can better mix the PEG and PLA components, thus more PEG content can be homogeneous blended with PLA.

In summary, blending PLA with PEG could improve the tensile properties of PLA and decreased T_g of PLA. Due to lowering T_g led to improve recovery speed of PLA blends. However, shape recovery ratio was destroyed when increasing PEG content.

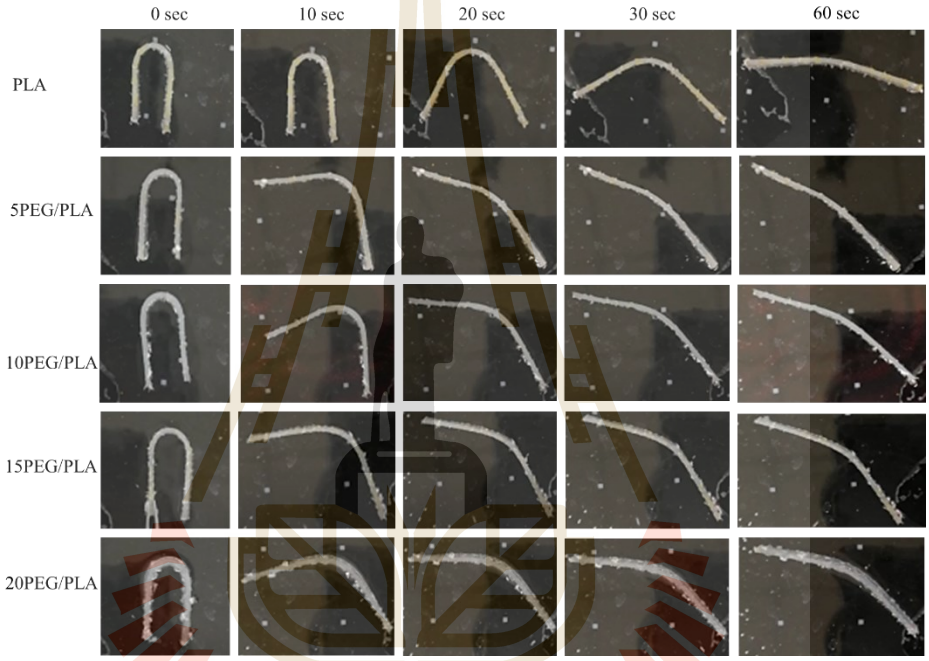

Figure 4.5. Photographs of the shape recovery behaviors of PLA and PEG/PLA blends in a water bath at 60 °C.

Table 4.5. Shape recovery ratio of PLA and PEG/PLA blends

Samples	initial angle (degree)	recovered angle (degree)	Recovery ratio (%)
PLA	180	164.2	91.0
5PEG/PLA	180	164.0	91.0
10PEG/PLA	180	157.0	87.0
15PEG/PLA	180	146.1	81.0
20PEG/PLA	180	149.3	81.0

4.3 Effect of PLA-g-MA content on mechanical, thermal and shape memory properties of PEG/PLA prepared via melt blending method.

4.3.1 Characterizations of PLA-g-MA

PLA-g-MA was prepared by reactive blending to be used as a PLA and PEG compatibilizer. Its grafting MA content was calculated using a titration technique and was 0.45 wt%. Figure 4.6 shows that the PLA-g-MA grafting reaction was also confirmed by FTIR. Figure 4.6(a) shows minimal differences in the FTIR spectra of PLA and PLA-g-MA in the wavenumber range 2000-600 cm^{-1} due to the small amount of MA that has reacted with PLA chains. In Figure 4.6(c), the symmetrical carbonyl (C=O) stretching peak of PLA-g-MA around 1750 cm^{-1} shows a slight shift, peak broadening, and increased intensity as compared to C=O stretching peak of the neat PLA. This was created by the superposition of the MA and PLA C=O peaks. Furthermore, when compared to the neat PLA, the PLA-g-MA spectrum shows additional, broadening absorption bands in the range of 1885-1850 cm^{-1} in Figure 4.6(d). These were consistent with the anhydride group of MA's asymmetric C=O stretching (Hassouna et al., 2011; Hwang et al., 2012). The presence of reactive carbonyl groups of anhydrides in PLA-*g*-MA was observed, which could indicate the presence of a PLA-g-MA grafting reaction.

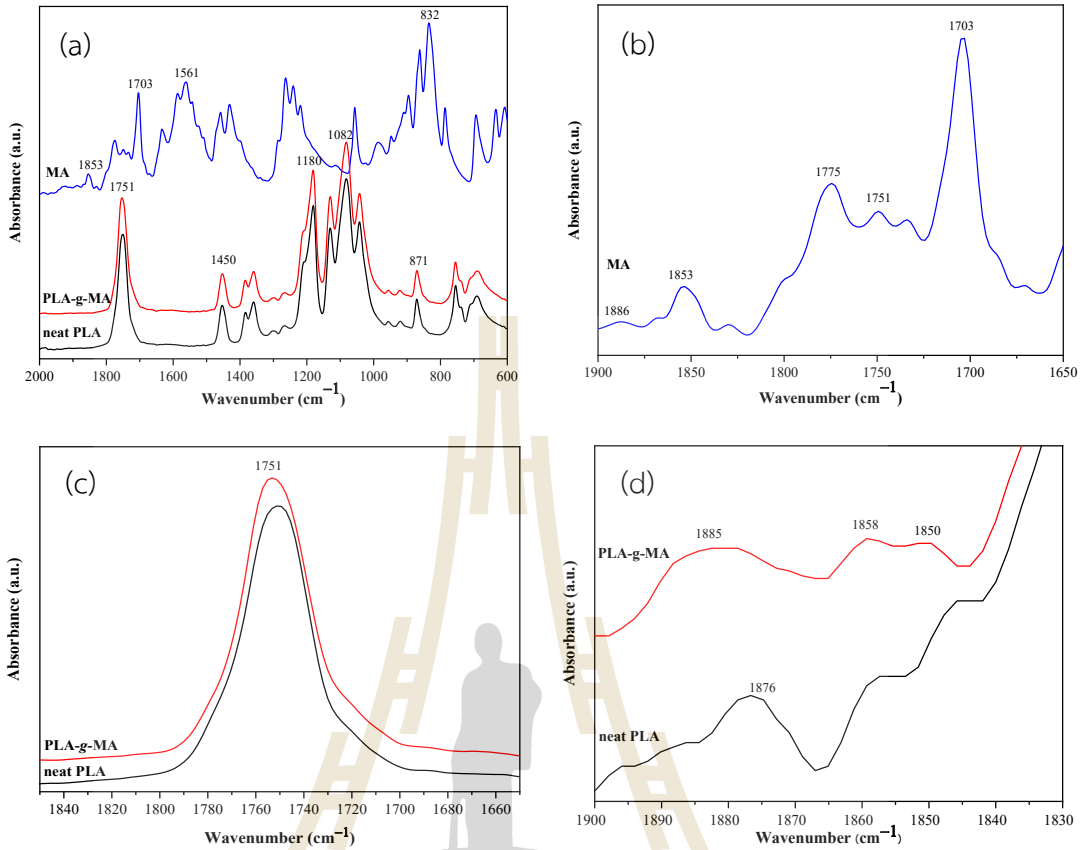

Figure 4.6. FTIR spectra of MA, neat PLA and PLA-*g*-MA.

4.3.2 Tensile properties

The stress-strain curves and summary of tensile properties of 10PEG/PLA blends with and without compatibilizer are shown in the Figure 4.7 and Table 4.6, respectively. As seen in Figure 4.7, neat PLA showed a brittle failure behavior. It possessed the highest Young's modulus of 0.7 GPa and tensile strength of 61.38 MPa, but very low elongation at break of 12.64%. By combining PLA with PEG, the ductility of the PLA was enhanced. The blend's stress-strain curve exhibited a greater degree of plastic deformation than that of PLA. The breaking strain increased to up to 480%. The Young's modulus and yield strength of the 10PEG/PLA expectedly decreased to 0.5 GPa and 40 MPa, respectively. This was the result of the plasticizing effect of PEG that allowed higher PLA chain mobility.(Guo et al., 2018)

The addition of PLA-g-MA to the blends increased Young's modulus and tensile strength, with the values increasing as the PLA-g-MA content increased. The

elongation at break of the blend containing 2 wt% PLA-g-MA was insignificant as compared to that of the uncompatibilized PEG/PLA. This suggested that the existence of 2 wt% PLA-g-MA increased the compatibility of the PLA and PEG phases. The enhanced compatibility steamed from the grafting reaction between the anhydride groups of MA and hydroxyl groups of PLA similar to that reported by Hassouna and coworkers (Hassouna et al., 2011) This interaction increased interfacial adhesion by enhancing stress transfer around the interface, resulting in an increase in tensile strength and retention of elongation at break. However, the addition of PLA-g-MA up to 10 wt% significantly decreased the blend's elongation at break. Other researchers reported similar results. (Kim et al., 2019; H. Liu, Xie, Zhang, Ou, & Yang, 2006) The plausible explanation was that the interface was oversaturated with PLA-g-MA. It is possible for PLA-g-MA coalescence to form, resulting in a decrease in interfacial tension between the polymer components in the blend.

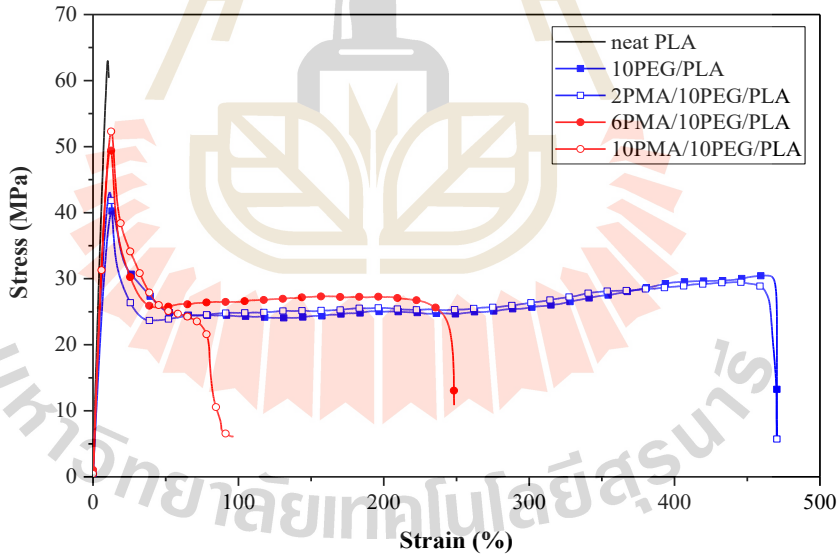

Figure 4.7. Tensile stress-strain curves of neat PLA, 10PEG/PLA blends with/without compatibilizer.

Table 4.6. Summarized tensile properties of PLA and PEG/PLA blends.

Sample	Tensile strength (MPa)	Young's Modulus (GPa)	Elongation at break (%)
Neat PLA	61.38 ± 1.24	0.70 ± 0.02	12.64 ± 1.19
10PEG/PLA	40.06 ± 1.50	0.50 ± 0.01	480.00 ± 34.59
2PMA/10PEG/PLA	44.84 ± 1.41	0.56 ± 0.02	480.75 ± 46.76
6PMA/10PEG/PLA	48.21 ± 0.94	0.56 ± 0.02	246.00 ± 1.41
10PMA/10PEG/PLA	50.32 ± 1.25	0.57 ± 0.01	69.00 ± 12.73

4.3.3 Thermal properties

In this study, DSC technique was used to investigate the changes in thermal properties of the PLA and PEG/PLA blends at different stages of the shape memory test. This included testing the "unstretched sample" from the original shape specimen (L_0) and the "stretched sample" from the temporary shape specimen (L_2). Figure 4.8 depicts DSC thermograms of PLA and PEG/PLA blends in their unstretched and stretched states, and Table 4.7 is a summary of their thermal properties.

DSC thermogram of the neat, unstretched PLA showed T_g and cold crystallization temperature (T_{cc}) at 58.3 °C and 115.5 °C, respectively. The T_g and T_{cc} of the unstretched, uncompatibilized 10PEG/PLA were reduced to 40.3 °C and 87.2 °C, respectively. This result was evidence of the plasticizing effect of PEG, which increased polymer chain mobility and consequently promoted the crystallization of PLA (Guo et al., 2018). The addition of plasticizer also affected the crystal formation as the change of PLA melting peak was observed. The unstretched, uncompatibilized 10PEG/PLA showed a small endothermic peak at a temperature slightly below the main PLA melting peak, which was absent in the unstretched PLA. The small endothermic peak was reported attributed to the be a melting of PLA the α'-crystals, while the main melting peak at 152.2 °C was attributed to the melting of the melting of the PLA α-form crystals (Athanasoulia & Tarantili, 2017). In addition, the 10PEG/PLA crystallinity (X_c) increased to 12.6%, which was significantly greater than the crystallinity (X_c) of the PLA, which was only 2.7%. When PLA-g-MA was added to the blends, the T_g values of

the unstretched, compatibilized blends exhibited a slight upward trend with increasing PLA-g-MA content. At 2 wt% PLA-g-MA loading, the T_{cc} value of the unstretched 2PMA/10PEG/PLA decreased to 84.4 °C (from 87.2 °C of that of the uncompatibilized 10PEG/PLA) with no shift of the main T_m peak (152.4 °C). In addition, the X_c of the unstretched 2PMA/10PEG/PLA was decreased to 8.2 %, as compared to that of the uncompatibilized PEG/PLA (X_c = 12.6%). As the amount of PLA-g-MA was increased above 2 wt%, the T_{cc} and T_m of the compatibilized blends shifted to higher temperatures and the X_c of the 6PMA/10PEG/PLA and 10PMA/10PEG/PLA increased to 14.8% and 12%, respectively. This suggested that the incorporation of PLA-g-MA influenced the lamellar structures of the compatibilized blends (Kim et al., 2019). The addition of 2 wt% PLA-g-MA may improve the interfacial adhesion of the 2PMA/10PEG/PLA, as a result of increased interfacial chain entanglement. This most likely decreased the chain mobility of the PLA, thereby inhibiting crystallization (Tang et al., 2022). Nonetheless, when the PLA-g-MA content exceeded 2 wt%, the X_c of the compatibilized blends increased once more. This is due to the PLA-g-MA coalescence acting as a nucleating agent in the compatibilized blends (H. Liu et al., 2006). Consistent with the tensile properties of the compatibilized blends, the DSC results indicated that the elongation at break of the 6PMA/10PEG/PLA and 10PMA/10PEG/PLA was significantly lower than that of the 2PMA/10PEG/PLA.

In a separate experiment, DSC technique was also used to investigate effect of stretching on thermal properties and crystallinity of neat PLA and 10PEG/PLA blends. During the shape programming procedure, test specimens were stretched to 100% strain at 45 °C and then rapidly cooled using ice packs. In the case of the neat PLA as shown in Figure 4.8, stretching caused an increase in T_g to 62.2 °C and a decrease in T_{cc} to 110.7 °C. Additionally, the shape of the melting peak of the stretched PLA changed, and its T_m decreased to 149.9 °C while its X_c increased by 6.1%. This indicated that rapid PLA recrystallization and crystal disaggregation occurred upon specimen was extended at 45 °C, resulting a higher number of crystals (Wang et al., 2010).

The T_g of all stretched 10PEG/PLA blends, with and without PLA-g-MA, increased marginally. In comparison to their unstretched states, the stretching caused significant decreases in their T_{cc} and cold crystallization enthalpy (ΔH_{cc}), whereas their

crystallinity increased significantly. Moreover, all of the stretched 10PEG/PLA blends exhibited a single endothermic peak, in contrast to the bimodal T_m peaks found in their unstretched states. Crystallization occurred to a greater extent after heating and stretching because the conditions were more favorable for crystal formation. Furthermore, recrystallization completely turned α'-form to α-form crystals after stretching (Athanasoulia & Tarantili, 2017), as evidenced by an increase in the crystallinity and a change in the shape of the melting peaks of the stretched 10PEG/PLA blends.

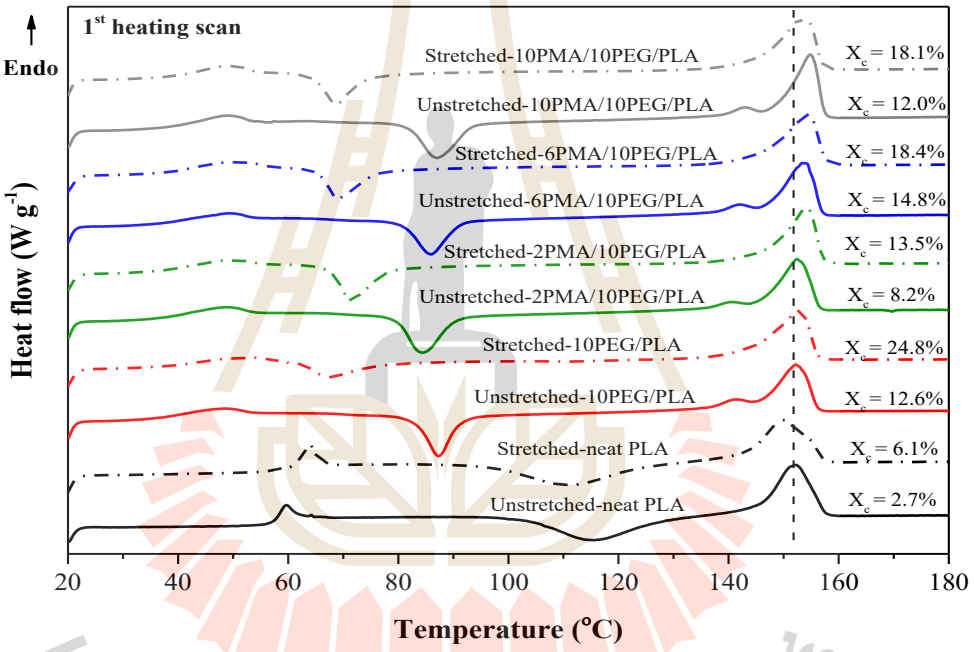

Figure 4.8. DSC thermograms for unstretched and stretched samples of neat PLA, 10PEG/PLA blends with/without compatibilizer.

Table 4.7. Summarized DSC testing results of the samples.

Sample	T_g (°C)	T_{cc} (°C)	$-\Delta H_{cc}$ (J/g)	T_m (°C)	ΔH_m (J/g)	Normalized X_c (%)
Unstretched-PLA	58.3	115.5	24.9	152.3	27.4	2.7
Unstretched-10PEG/PLA	40.3	87.2	15.3	152.2	25.9	12.6
Unstretched-2PMA/10PEG/PLA	41.6	84.4	18.4	152.4	25.2	8.2
Unstretched-6PMA/10PEG/PLA	41.8	85.9	16.3	153.7	28.1	14.8
Unstretched-10PMA/10PEG/PLA	42.3	87.1	18.0	154.9	29.3	12.0
Stretched-PLA	62.2	110.7	21.3	149.9	26.9	6.1
Stretched-10PEG/PLA	43.8	67.5	8.6	152.8	29.5	24.8
Stretched-2PMA/10PEG/PLA	41.8	71.3	16.7	154.1	27.9	13.5
Stretched-6PMA/10PEG/PLA	42.6	69.0	13.0	154.2	27.7	18.4
Stretched-10PMA/10PEG/PLA	42.8	68.8	12.4	153.2	29.4	18.1

4.3.4 Morphology

Morphologies of PLA and 10PEG/PLA blends with various PLA-*g*-MA contents were examined using SEM that are shown in Figure 4.9. The SEM micrograph of the neat PLA in Figure 4.9a shows a smooth cross-sectional area surface, whereas the micrograph of the uncompatibilized 10PEG/PLA in Figure 4.9b reveals a rough surface. This could be a result of PEG droplet dispersion. The addition of 2 wt% PLA-g-MA had no effect on the 2PMA/10PEG/PLA morphology. However, as the compatibilizer content increased up to 6 wt% (Figure 4.9d), the morphology of the 6PMA/10PEG/PLA showed some agglomerations. This could be the coalesces of the excess compatibilizer which resulted in the decrease in an interfacial interaction as mentioned in the tensile result. At 10 wt% PLA-g-MA, as depicted in Figure 4.9e, the surface topography of the 10PMA/10PEG/PLA exhibited a greater degree of agglomeration, with the microvoids being obvious. The compatibility of the 10PEG/PLA blends decreased when the compatibilizer concentration exceeded 2 wt%.

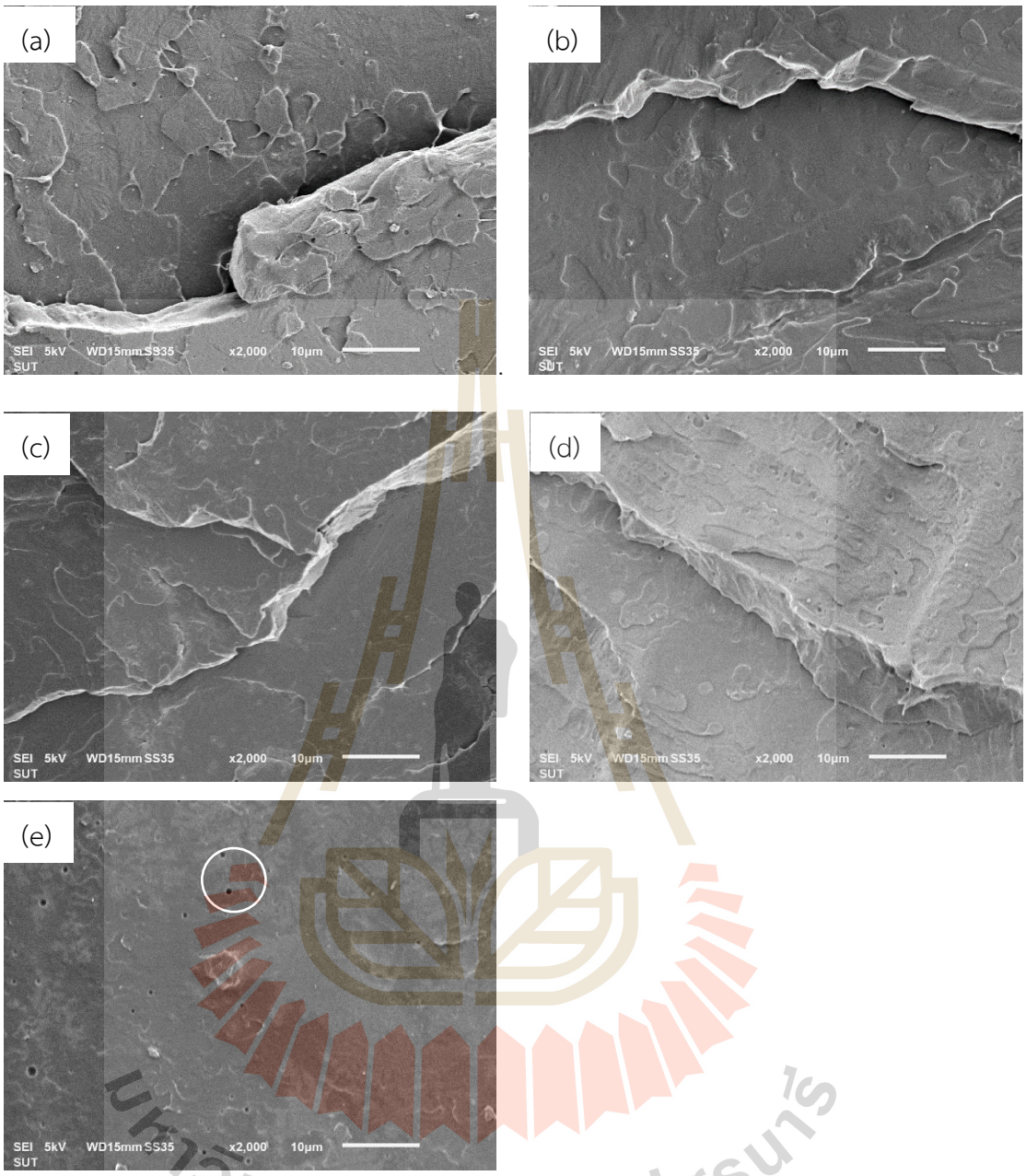

Figure 4.9. SEM micrographs of cryogenically fracture surface specimens of (a) neat PLA, (b) 10PEG/PLA, (c) 2PMA/10PEG/PLA, (d) 6PMA/10PEG/PLA and (e) 10PMA/10PEG/PLA blends.

4.3.5 Shape memory properties by stretching test

4.3.5.1 Shape memory behaviors of the 10PEG/PLA blend at various PLA-g-MA content

Effect of PEG-g-MA content on the shape memory properties of 10PEG/PLA blends are shown in Figure 4.10. As previously stated, the neat PLA exhibited a high recoverability of 98.6%, whereas the R_r of 10PEG/PLA was drastically lowered. Thus, the incorporation of PLA-g-MA into the blend in this work aimed to improve the R_r of the SMP. The compatibilized blend containing 2 wt% PLA-g-MA had the greatest R_r value. Further increased the amount of the compatibilizer to 6 wt% caused a decrease in R_r. This really is the result of the two polymers' interfacial adhesion changing at different amounts of compatibilizer, as discussed previously in the DSC section. With the addition of 2 wt% PLA-g-MA, the blend exhibits increased interaction, resulting in a decrease in crystallinity. In term of fixity ratio, all samples displayed a R_f more than 96%, showing that the presence of PEG and PLA-g-MA had no measurable impact on the R_f value.

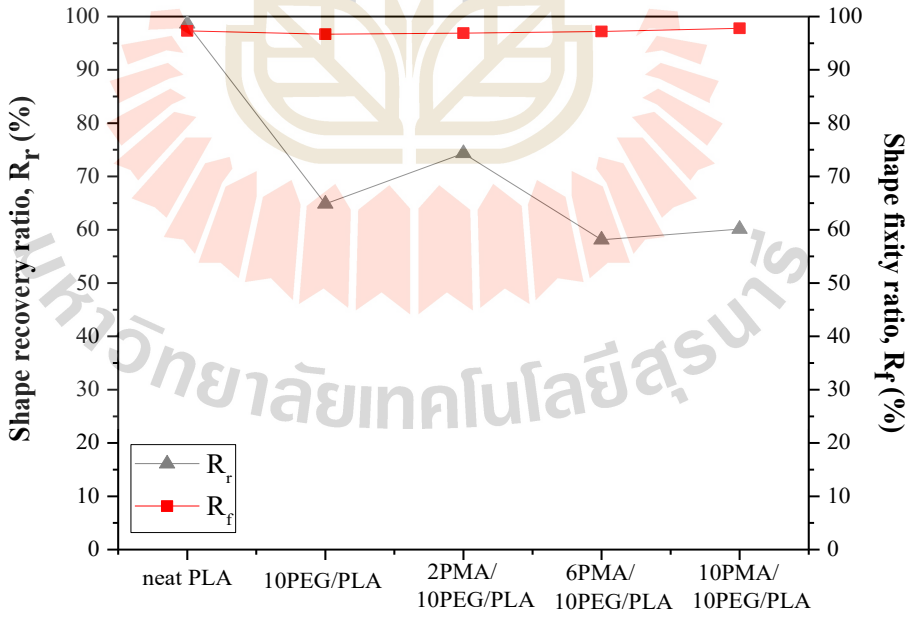

Figure 4.10. Shape recovery and fixity ratios of neat PLA, 10PEG/PLA blends with and without compatibilizer.

4.3.5.2 Shape memory behaviors of the 2PMA/10PEG/PLA blend at various programing temperatures

Moreover, the effect of programming temperature (T_p) on the shape memory behaviors of 2PMA/PEG/PLA blends was investigated. The test specimens were subjected to a 50% strain at programming temperatures in the range of 35 to 50 ℃. They were then restored to their original shape at a temperature of 60 ° C.

Figure 4.11 shows the stress-strain curves of the 2PMA/10PEG/PLA blend at different T_p. At T_p of 35 ℃, the specimen exhibited a noticeable abrupt yielding and a steep initial slope. When the temperature increases to 40 ℃, the stress during stretching of specimen decreased and gradual yielding was observed. However, as T_p increased to 45 and 50 ℃, the mechanical behavior became softer, and no yield point was observed because these T_p were more than the T_g of 2PMA/10PEG/PLA (42 ℃).

In addition, the R_f and R_r values of the 2PMA/10PEG/PLA blend at difference T_p are shown in Figure 4.12. The R_f and R_r values of 2PMA/10PEG/PLA significantly increased when the programming temperature increased from 35 to 45 ℃. When the programming temperature was increased to 50 ℃, the R_f of the 2PMA/10PEG/PLA blend remained stable while its R_r decreased slightly. At T_p < 45 ℃ of the 2PMA/PEG/PLA blend, the polymer chain obtained high stress during the programming process, as indicated by the stress-strain curve, causing the chain structure to become disrupted. In contrast, at T_p of 50 ℃, plastic deformation of the specimen could easily occur due to high chain mobility, causing a drop in the R_r value of the sample.(Koosomsuan et al., 2019) The results revealed that the T_p of 45℃, which was slightly higher than the T_g of the 2PMA/PEG/PLA, was the appropriate programming temperatures for achieving optimal R_r and R_f. Therefore, shape memory properties of PLA and PEG/PLA blends were investigated further in the subsequent experiment at the T_p of 45℃.

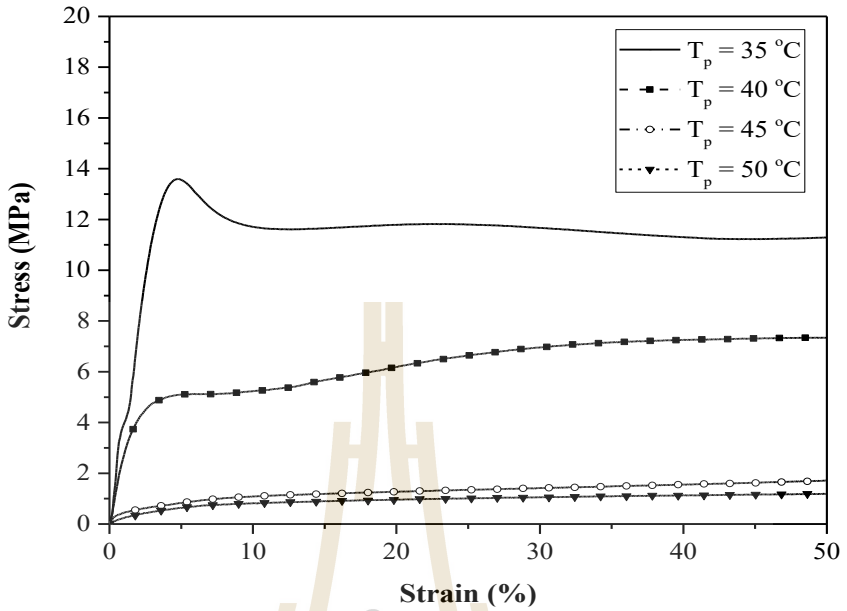

Figure 4.11. Stress-strain curve of 2PMA/10PEG/PLA specimen at various programing temperatures.

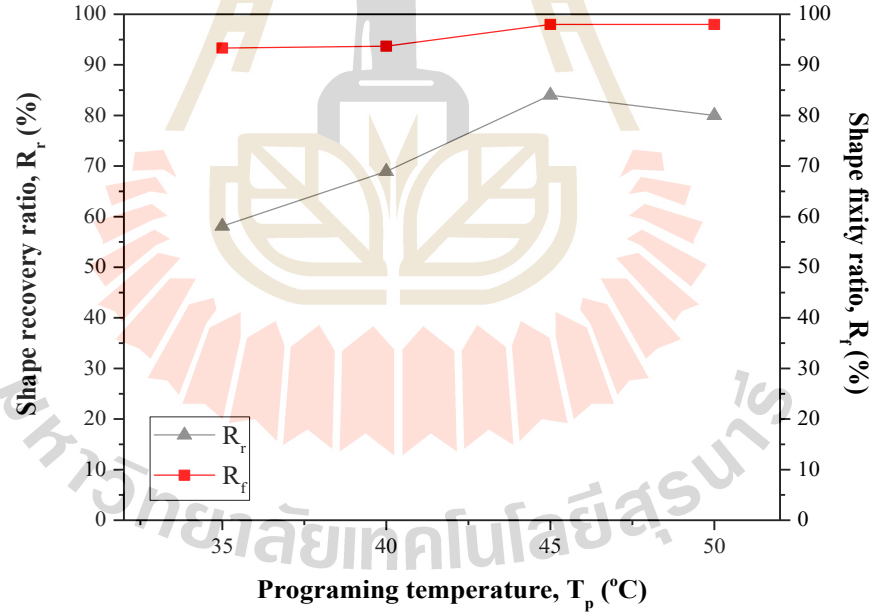

Figure 4.12. Shape recovery and fixity ratios of 2PMA/10PEG/PLA specimen at various programing temperatures.

4.3.5.3 Shape memory behaviors of the 2PMA/10PEG/PLA blend at various recovery temperatures

Additionally, the effect of recovery temperature (T_r) on shape recoverability of PLA and 10PEG/PLA blends was examined. The stretched specimens were subjected to different temperatures of the water bath at 40, 50, and 60 °C to measure the recoverability. Their R_r values are illustrated in Figure 4.13.

For the neat PLA, the specimen could recover with a high R_r value at T_r of 60 °C. However, the neat PLA was difficult to recover at T_r below 60 °C. This was because its T_g was increased to 62 °C during shape programming process. This required more energy or heat to drive the recovery process. The 10PEG/PLA blends had the lower R_r as compared with the neat PLA. Nonetheless, all the 10PEG/PLA blends, with/without compatibilizer, could recover even at temperatures as low as 40 °C. Their R_r increased with the increasing T_r. Among the 10PEG/PLA blends, 2PMA/10PEG/PLA blend had the highest R_r values at all recovery temperatures. It was reported that a lowering of T_g can widen the recovery temperature of a shape memory polymer (Guo et al., 2018). As the T_g of the 10PEG/PLA blends approached 40 °C, their onset recovery temperatures decreased. This could make them more appropriate for the use in biomedical applications.

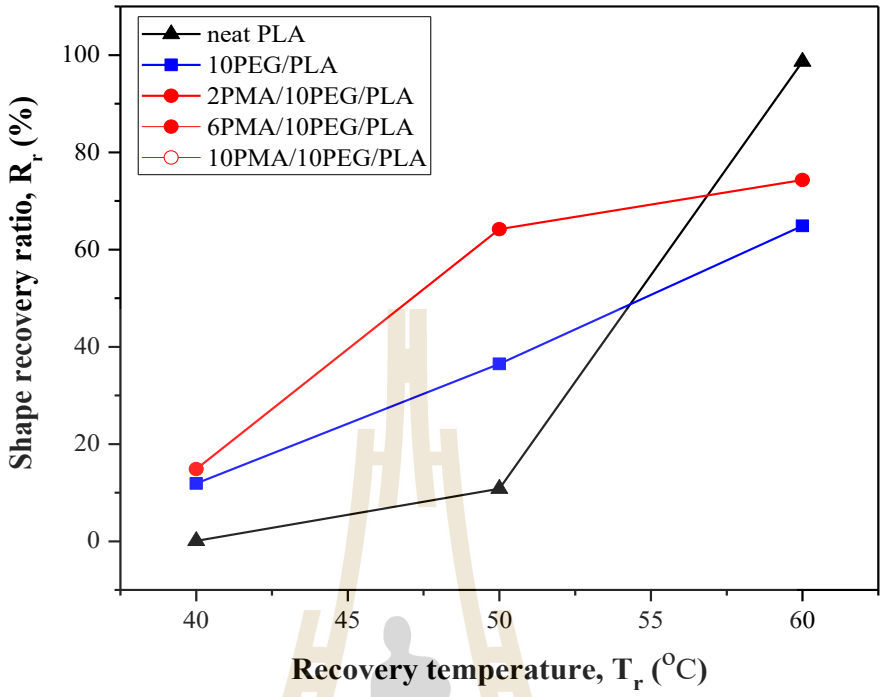

Figure 4.13. Shape recovery ratio of neat PLA and the 10PEG/PLA blends specimens at various recovery temperatures.

4.3.6 Stress relaxation of the 10PEG/PLA blends with various PLA-g-MA contents

According to Tcharkhtchi et al. (Tcharkhtchi et al., 2014), the residual stress could be represented as the driving force behind SMPs regaining their original shape. Shape recovery performance of the 10PEG/PLA blends can be explained by observing their stress relaxation behaviors at the shape programming temperature of 45 °C. The experiment was designed similarly to the shape programming process; the specimen was heated to 45 °C for 5 minutes before being stretched to % strain and the stress reduction was measured for 1 hour. The stress relaxation curves of these specimens are illustrated in Figure 4.14.

As seen from the figure, the residual stress of the 2PMA/10PEG/PLA blend was higher than that of the PEG/PLA blend. However, the residual stress of the compatibilized blends decreased as more PLA-*g*-MA exceeded 2 wt%. This was explained by the effect of the compatibilizer on the crystallinity of the blends. As stated previously, the presence of 2 wt% PLA-g-MA in the blend decreased the X_c

and/or increased the chain entanglement of 2PMA/10PEG/PLA, resulting in a more difficult release of the obtained stress during temporary shape formation and a greater storage of driving stress energy for recovery to its original shape, as compared to those of the 10PEG/PLA blend without PLA-g-MA (Kong & Xiao, 2016). Consequently, when more than 2 wt% PLA-g-MA was added, the X_c increased, which decreased the blends' recoverability. This result was consistent with the results of DSC and shape memory tests.

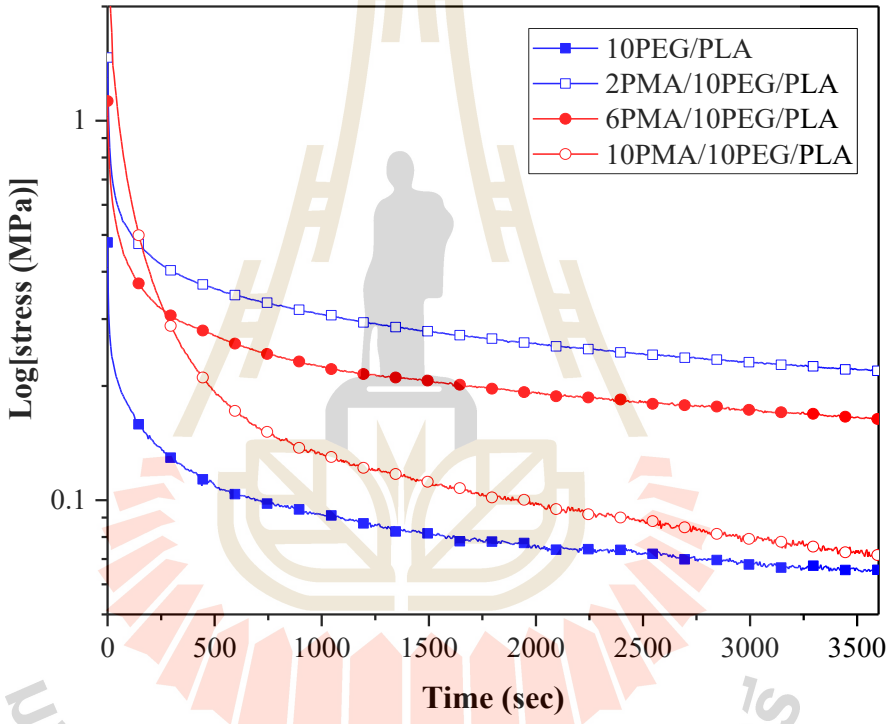

Figure 4.14. Stress versus time during the shape-programming step at T_p of 45 °C for 10PEG/PLA blends with and without a compatibilizer.

4.3.7 Dynamic mechanical properties

The dynamic mechanical properties of 10PEG/PLA blends with/without PLA-g-MA compatibilizer are presented by the storage modulus (E') and $\tan\delta$ from DMA testing, as shown in Figure 4.15. As can be seen in Figure 4.15a, E' of the samples decreased gradually as the temperature increased in the glassy state and abruptly in the rubbery state. The addition of 10 wt% PEG reduced both E' in the glassy state and

the slope of the glass transition. This is because PEG's plasticizing effect can increase the chain mobility of a PLA-based blend. Additionally, as the PLA-g-MA content increased, the glassy modulus increased slightly. It may be understood by the hardening effect of the difference in degree of compatibility between PLA and PEG, as it has been explained by the tensile properties. The E' of the samples significantly decreased at 60°C and 47°C for neat PLA and their blends, respectively. This is consistent with the shape recovability result at various T_r. The result indicated that the percentage of recovery for a blend system was greater than 50% at T_r around 50°C, whereas the onset of T_r for neat PLA began at T_r greater than 60°C.

In Figure 4.15b, for temperatures between 40 and 60°C, the E' curve of 2PMA/10PEG/PLA exhibited the highest modulus when compared to the other blend systems. The high E' value may be due to the sample's great resistance to creep, which results in the storage of more internal energy (Koerner et al., 2013). Consistent with the stress relaxation results at the programming temperature of 45°C, 2PMA/10PEG/PLA had a higher residual stress than the other blend systems, which reflected the additional storage energy necessary to promote the sample's recovery to its original shape.

Indeed, the $\tan\delta$ peak is related to the T_g of materials. In Figure 4.15c, the $\tan\delta$ peak for neat PLA, 10PEG/PLA, 2PMA/10PEG/PLA, 6PMA/10PEG/PLA, and 10PMA/10PEG/PLA were 69.3, 61.6, 60.5, 61.3, and 61.1°C, respectively. These $\tan\delta$ values corresponded to their T_g, which was shown to be more than that of unstretched samples in the DSC data, because the temperature of the low thermal conductivity sample lagged behind the ambient condition in the DMA machine, indicating an insufficient thermal energy (Koerner et al., 2013).

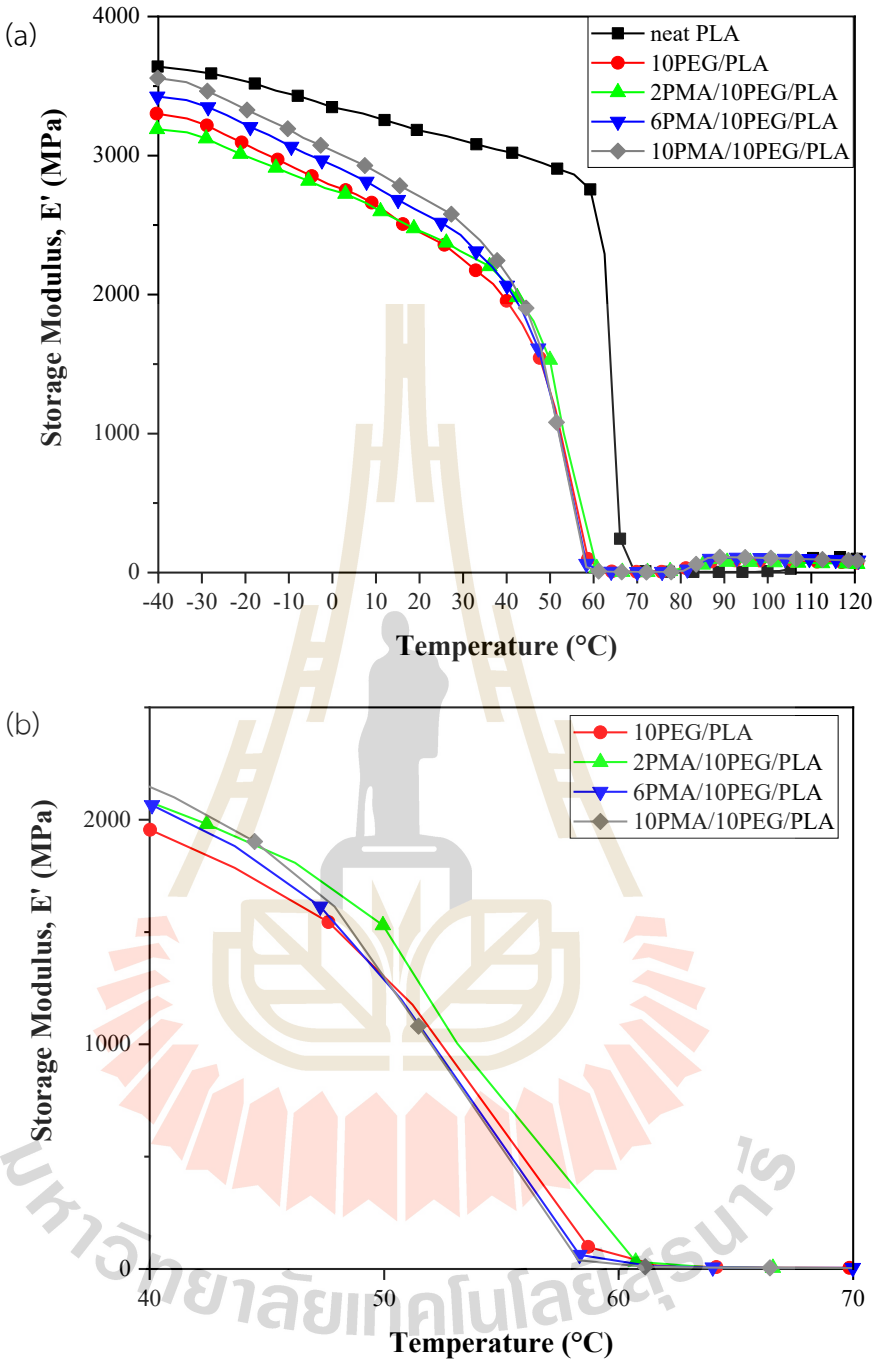

Figure 4.15. Storage Modulus (E') (a), storage modulus at temperatures between 40 and 60 °C (b), and loss factor (tan delta) (c) for neat PLA and 10PEG/PLA blends with and without compatibilizer.

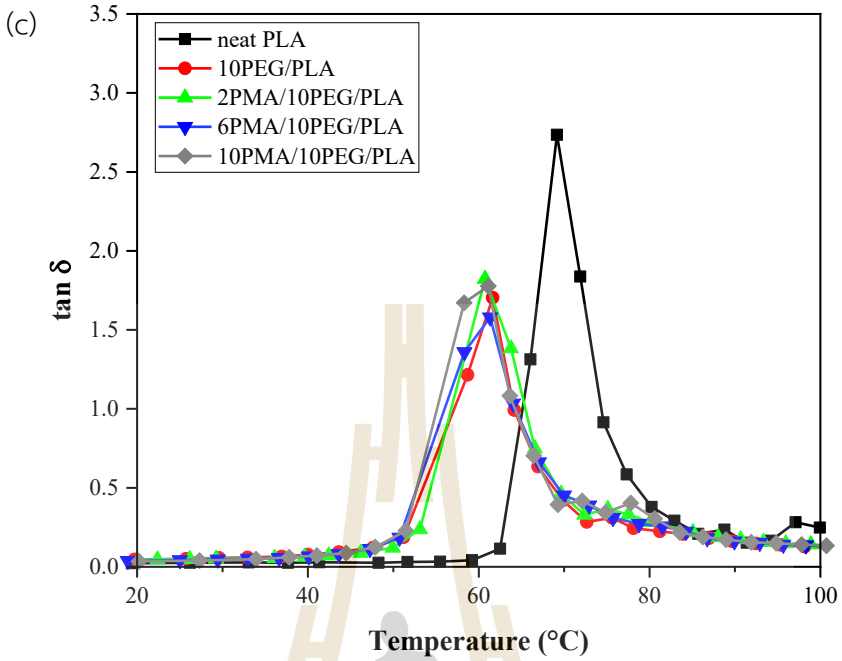

Figure 4.15. Storage Modulus (E') (a), storage modulus at temperatures between 40 and 60 °C (b), and loss factor (tan delta) (c) for neat PLA and 10PEG/PLA blends with and without compatibilizer. (Continued)

4.3.8 Microstructure evolution by SAXS/WAXS techniques

The microstructure evolution of the PEG/PLA and 2PMA/10PEG/PLA blends during the programming and recovery processes were determined by *in situ* SAXS and WAXS measurements. The scattering patterns are shown in Figure 4.16. As labelling in the figure, m and e stand for the meridian and equator directions of scattering profile, respectively. The stretching direction of the specimen was parallel to the meridian axis. The uniform intensity of both amorphous halo (orange colour area) and single ring of crystalline at (200/110) plane around the azimuth angle was observed in the 2D-WAXS pattern of the 10PEG/PLA blend. This suggested that the polymer chains were isotopically oriented in the initial state. The 2D-WAXS of 2PMA/10PEG/PLA blend showed the isotropy of two distinct rings that corresponded to (200/110) and (203) planes of α-form PLA crystallites (Koosomsuan et al., 2019). In the initial state, both specimens exhibited unclear SAXS scattering patterns indicating

the random chain conformation. Nonetheless, their WAXS and SAXS scattering patterns remained unchanged after heating these specimens at 45 °C.

After the programming process, the drawn specimens of the 10PEG/PLA and 2PMA/10PEG/PLA blends showed a higher intensity of the crystallite ring in the equatorial axis in the WAXS pattern and a small equator streak in the SAXS pattern. This suggested that during the shaping process, some amorphous and crystalline regions were weakly anisotropically oriented perpendicular to the stretching direction. Since the specimens were deformed at low strain (100 %strain), it might be insufficient to induce stacking lamellar perpendicular to the stretching direction (Tian et al., 2014). The WAXS and SAXS patterns confirmed the DSC results that the orientation of the drawn specimens promoted an increase in crystallinity.

After recovery at 60 °C, the equator streak in the SAXS pattern of the 10PEG/PLA blend had an asymmetric appearance, which might be due to an unusual recovery direction of the specimens as shown in the image in Figure 4.16. In addition, 1D-SAXS curves in Figure 4.17 show that the intensity of the equator streak of 2PMA/10PEG/PLA blend decreased significantly after recovery, while the intensity of 10PEG/PLA blend did not change. The significant change in the intensity along the equator axis of 2PMA/10PEG/PLA blend may be because this compatibilized blend had less crystallinity or, in other words, the compatibilized blend had relatively more chains in the amorphous region than the uncompatibilized ones. This result might relate to higher residual stress of 2PMA/10PEG/PLA specimen during the shaping step than that of 10PEG/PLA. When the 2PMA/10PEG/PLA specimen was heated to the T_r of 60 °C, the greater number of polymer chains in the amorphous region were returned. As a result, the shape recovery ratio of the 2PMA/10PEG/PLA blend was higher than that of the 10PEG/PLA blend.

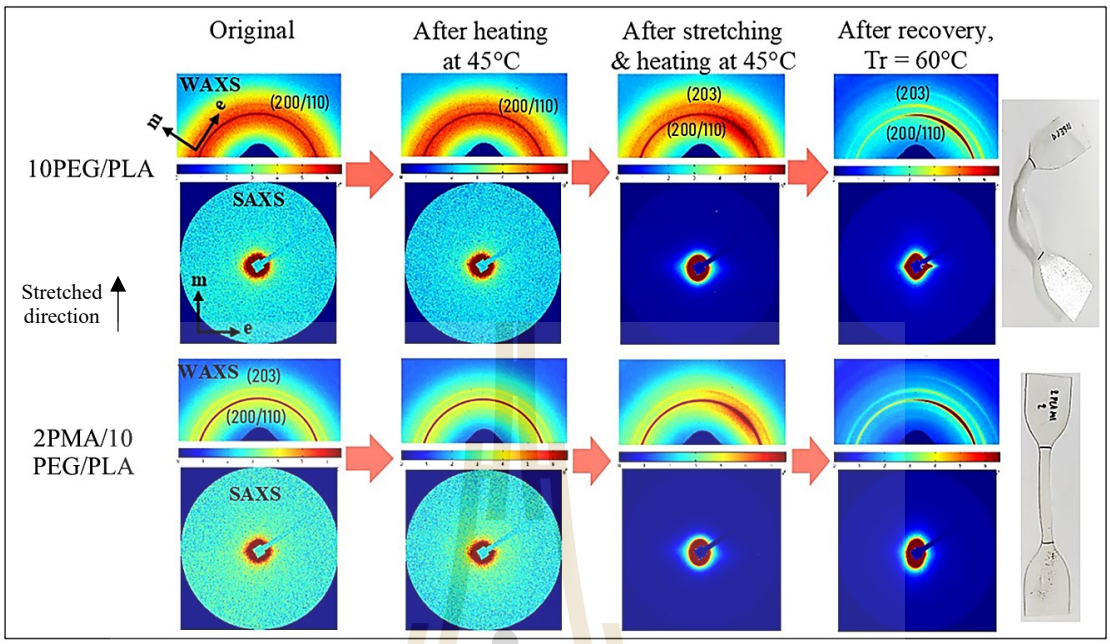

Figure 4.16. 2D-WAXS and SAXS patterns of 10PEG/PLA and 2PMA/10PEG/PLA specimens during shape memory test process.

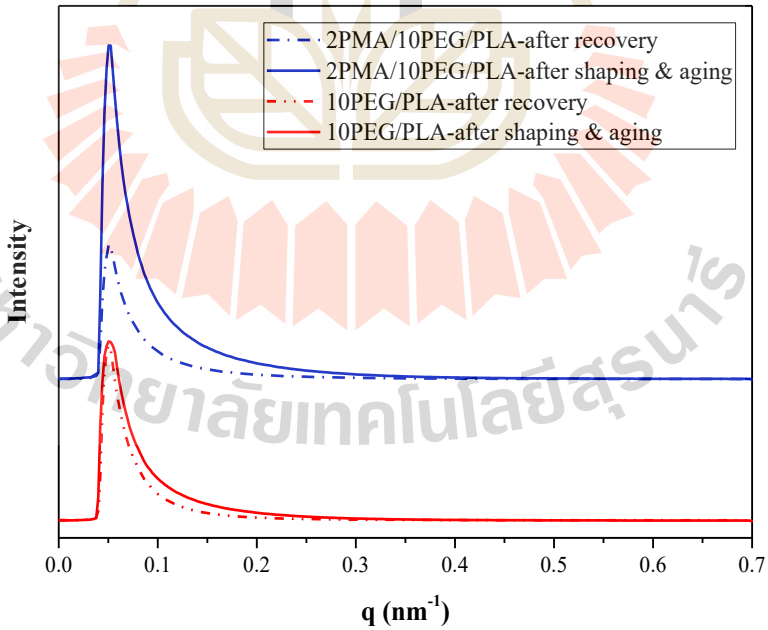

Figure 4.17. 1D-SAXS plots along the equatorial axis of 10PEG/PLA and 2PMA/10PEG/PLA specimens after aging and recovery at 60 °C.

4.4 Effect of organoclay on mechanical, thermal and shape memory properties of PEG/PLA blend prepared via melt blending method

4.4.1 Characterizations of organoclay

4.4.1.1 Structure of MMT and organoclay

The level of exfoliation and intercalation of montmorillonite clay (MMT) with an interlayer space between each triple-sheet layer can be determined by XRD analysis. Figure 4.18 shows X-ray diffraction patterns of MMT (unmodified MMT) and organoclay (OMMT) (modified MMT). According to Bragg's law equation (4.1), the XRD peak of MMT was shifted to lower 2θ, corresponding to an increase in the interlayer space (d value) of OMMT from 1.32 nm to 2.14 nm. This demonstrated OMMT intercalation following surfactant modification with Cetyltrimethylammonium bromide (CTAB).

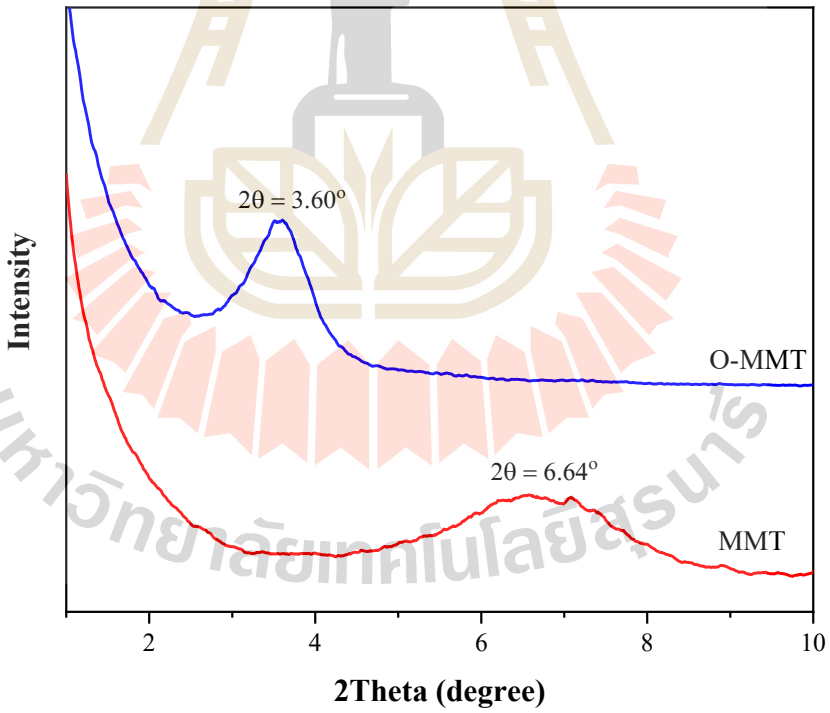

Figure 4.18. XRD patterns of MMT and organoclay.

4.4.1.2 Functional group analysis

The successful modification of MMT with CTAB was confirmed by FTIR as shown in Figure 4.19. The absorption peaks of CTAB, i.e., ammonium moiety band (3435 cm^{-1}), C-H vibration bands of $-CH_2$ (2914-2855 cm^{-1}), stretching vibration band of N^+-CH3 (asymmetric vibration band at 1653 cm^{-1} and symmetric vibration band at 1475 cm^{-1}), $-CH3$ vibration band (915 cm^{-1}), and Br^- band (724 cm^{-1}) were found in OMMT (Yuliana et al., 2020). This indicates that the cationic surfactant is successfully intercalated into the MMT interlayer surface.

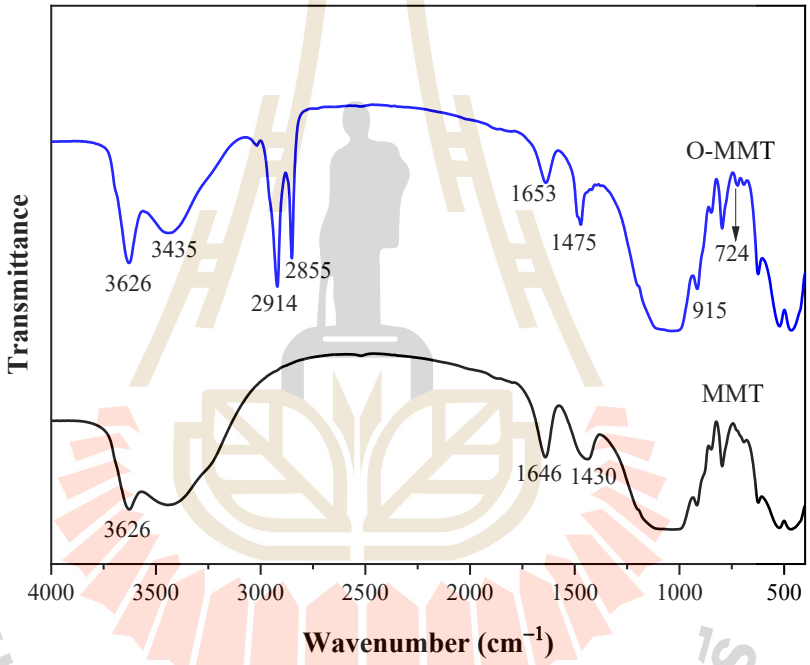

Figure 4.19. FTIR spectra of MMT and organoclay.

4.4.2 Structure of OMMT in the 2PMA/10PEG/PLA composites

Figure 4.20 shows the XRD patterns of OMMT and 2PMA/10PEG/PLA blend and composites that varied OMMT content of 1, 3, 5, and 7 phr. The diffraction peak of pure OMMT clearly can be seen were at 2θ = 3.60° which corresponds to d-spacing 2.14 nm. In the 2PMA/10PEG/PLA composites, two peaks of OMMT were observed at 2θ = 2.55° which corresponds to d-spacing 3.46 nm and at 2θ = 5.22° (1.69 nm). All of the composites had their peaks shifted to lower 2θ, which was caused

by the intercalation of polymer chains in the OMMT interlayer. However, the peak of the composites at 2θ = 5.22° was found to be increased with higher OMMT loading content. This could be because the higher load of OMMT was not spread out well. On the other hand, 5-OMMT/2PMA/10PEG/PLA and 7-OMMT/2PMA/10PEG/PLA show additional peak at 2θ = 16.8°, which correspond to the plane of crystalline PLA (Komal, Lila, & Singh, 2021). The present investigation revealed the sharpness in peak for the composite adding 7 phr OMMT resulted in higher crystallinity of the composites.

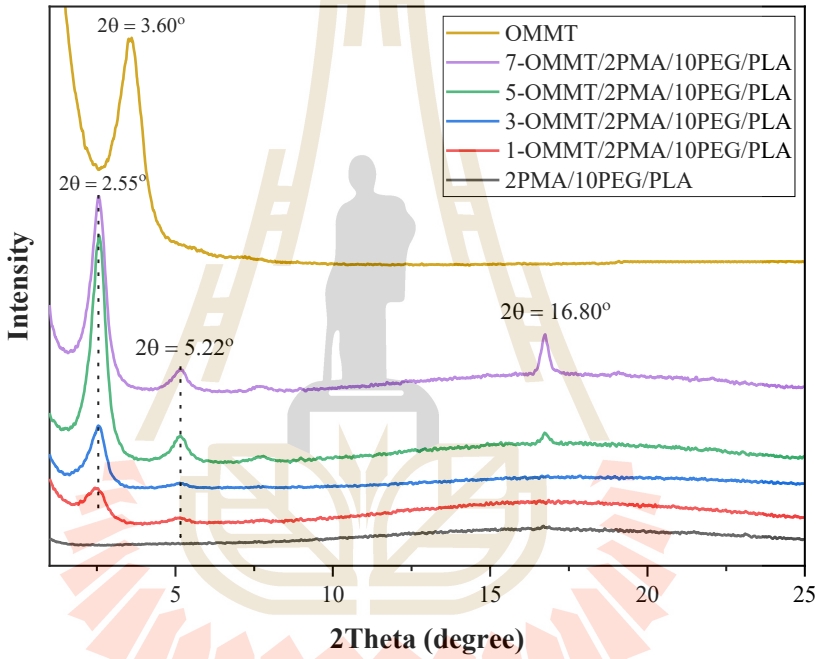

Figure 4.20. XRD patterns of OMMT and 2PMA/10PEG/PLA blend and composites.

4.4.3 Tensile properties

Tensile stress-strain curves and summarized of tensile properties of 2PMA/10PEG/PLA blend and composites with OMMT at various contents are shown in Figure 4.21 and Table 4.8. In Figure 4.21, the composite containing 1 phr OMMT had a higher tensile stress in the plastic deformation zone than the 2PMA/10PEG/PLA blend, whereas the elongation at break was unchanged. This could be due to the intercalation of OMMT interlayer when 1 phr of OMMT was added to the 2PMA/10PEG/PLA blend, which served as physical crosslinking points that also affect the strengthening and toughening (Cui & Du, 2013). However, as the OMMT concentration reached 3 phr, the

yield strength, Young's modulus, and elongation at break of 3-OMMT/2PMA/10PEG/PLA decreased significantly. This is possibly due to a poor dispersion of OMMT's high load, which offered poor adhesion between OMMT and polymer, resulting in a decrease in stress transfer between these phases. Furthermore, when the OMMT concentration reached 7 phr, the Young's modulus of 7-OMMT/2PMA/10PEG/PLA increased and became higher than the 2PMA/10PEG/PLA blend. According to the XRD result of the composites, the addition of 7 phr OMMT appears to increase the crystallinity of the 7-OMMT/2PMA/10PEG/PLA composite, which may result in an increase in its modulus.

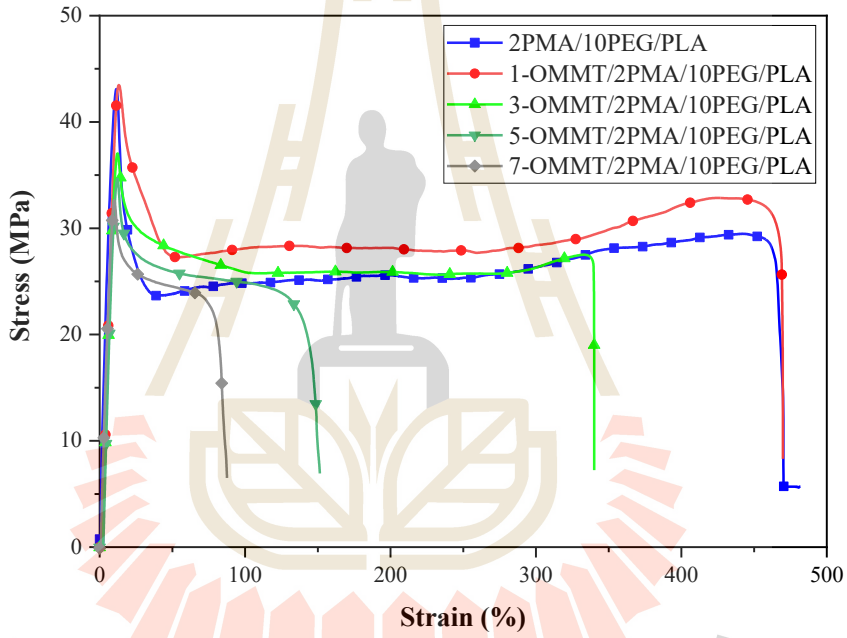

Figure 4.21. Tensile stress-strain curves of 2PMA/10PEG/PLA composite at various OMMT contents.

Table 4.8. Summarized tensile properties of the 2PMA/10PEG/PLA composites.

Sample	Stress at yield (MPa)	Young's Modulus (GPa)	Elongation at break (%)
2PMA/10PEG/PLA	44.84 ± 1.41	0.56 ± 0.02	480.75 ± 46.76
1-OMMT/2PMA/ 10PEG/PLA	43.29 ± 1.37	0.55 ± 0.03	504.00 ± 135.45
3-OMMT/2PMA/ 10PEG/PLA	35.67 ± 2.05	0.49 ± 0.22	305.78 ± 82.68
5-OMMT/2PMA/ 10PEG/PLA	33.75 ± 0.64	0.49 ± 0.03	120.25 ± 20.82
7-OMMT/2PMA/ 10PEG/PLA	31.50 ± 0.87	0.59 ± 0.05	80.80 ± 5.87

4.4.4 Shape memory properties by stretching test

4.4.4.1 Shape memory behaviors of the 2PLA/10PEG/PLA composite at various OMMT contents

The result of shape memory properties of the 2PLA/10PEG/PLA composites are shown in Figure 4.22. To study the effect of strain, the specimen was stretched to 50 and 100% strain during the programming process. At 50% strain, the shape recovery (R_r) and fixity (R_f) ratios are shown in Figure 4.22a. At 50% strain, R_r of 2PMA/10PEG/PLA blend was 84 %. For the composites, the R_r value of 1-OMMT/2PMA/10PEG/PLA did not change, however after increasing OMMT up to 3 phr, the R_r decreased slightly. The R_r decreased significantly as the OMMT load increased to 7 phr, while the OMMT loading had no effect on the R_f value of all specimens. The decrease in R_r with increasing OMMT content due to the decreased adhesion of the composites as mention above.

Figure 4.22b shows the shape recovery behavior of 2PMA/10PEG/PLA and its composites at 100% strain. The R_r of all 100% strain-stretched specimens were less than those of 50% strain-stretched specimens. This was due to

the fact that polymer switching chain was subjected to excessive stress at higher levels of stretching, and that some chains could deform, resulting in a reduced driving force to return to their original shape. However, at 100% strain, the effect of OMMT content on the shape memory capabilities of 2PMA/10PEG/PLA composites was clearly seen that the R_r value of 1-OMMT/2PMA/10PEG/PLA composite increased as compared to non-composite. After OMMT exceeded 3 phr, the R_r value of the composite decreased as OMMT content increased. The increase in R_r of the 1-OMMT/2-PMA/10-PEG/PLA composite may be due to the fact that 1 phr of OMMT was sufficient to boost the system's driving force, as a result of the intercalated OMMT serving as a physical crosslinker as mentioned in the tensile properties result.

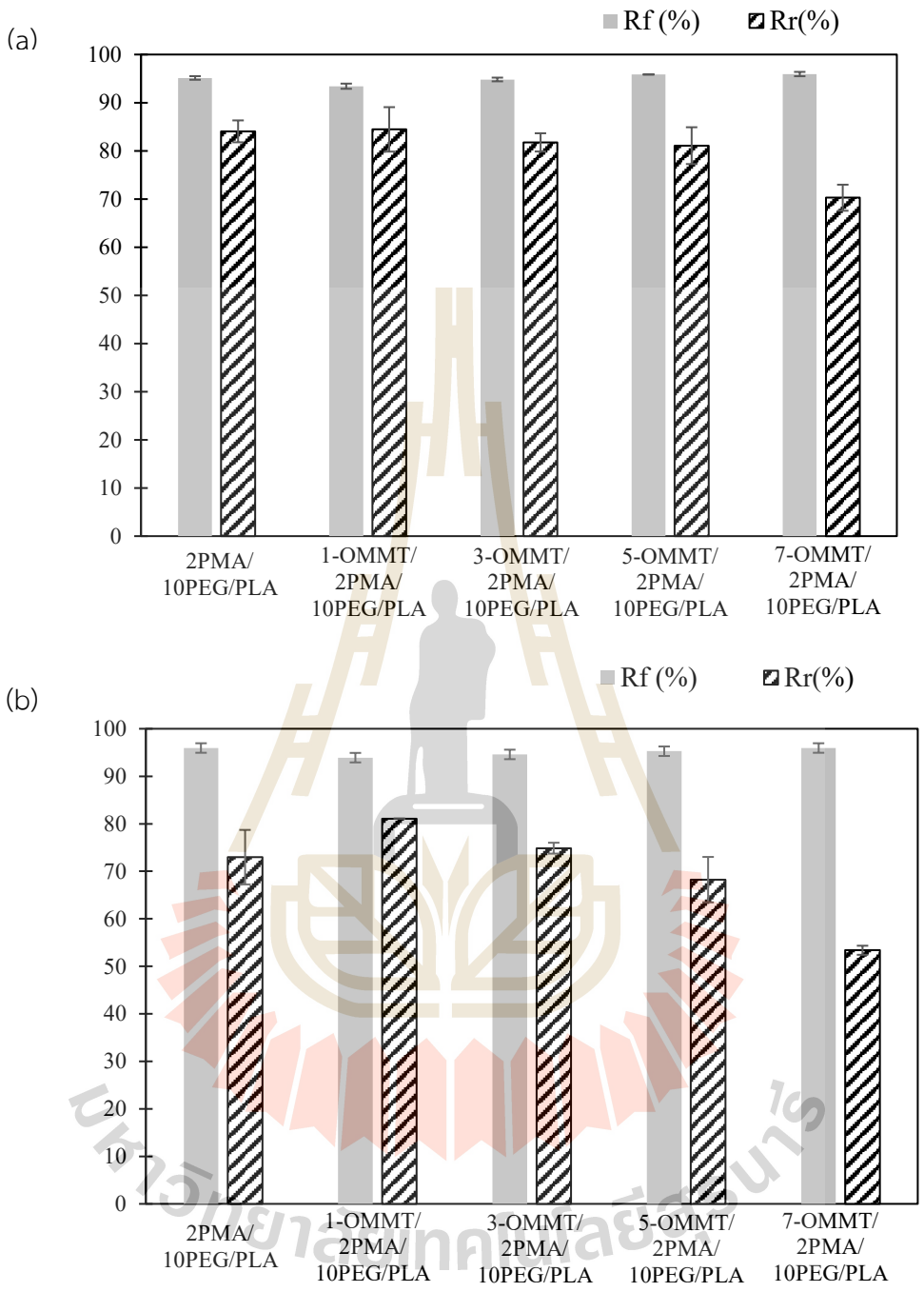

Figure 4.22. Shape recovery (R_r) and shape fixity (R_f) ratios of 2PMA/10PEG/PLA with OMMT at various contents under stretching to (a) 50% strain and (b) 100% strain during the programming process.

4.4.4.2 Shape memory behavior under cyclic stretch and recovery process

To examine the influence of cyclic stretch on the shape recovery performance of the 2PMA/10PEG/PLA blend and its composites, specimens were heated to 45 ℃, stretched to 50 or 100 percent strain, and then allowed to recover at 60 ℃. After then, the initial recovered specimens were stretched and recovered a second and third time. Figure 4.23 depicts the shape recovery ratio (R_r) for each cycle test of 2PMA/10PEG/PLA, 1 -OMMT/2PMA/10PEG/PLA, and 7-OMMT/2PMA/10PEG/PLA.

R_r under cyclic stretched to 50% strain of 2PMA/10PEG/PLA, 1 -OMMT/2PMA/10PEG/PLA, and 7-OMMT/2PMA/10PEG/PLA are shown in Figure 4.23a. The R_r of 2PMA/10PEG/PLA decreased after stretching in third cycle. After the third stretch-recovery cycle, the R_r value of 2PMA/10PEG/PLA decreased from 84% of the first stretch to 75% of the third stretch, whereas the R_r value of 1-OMMT/2PMA10PEG/PLA did not change and remained higher than 80%. However, at high OMMT loading (7 phr), the R_r of 7-OMMT/2PMA/10PEG/PLA decreased proportional to cyclic stretch.

Figure 4.23b shows the R_r result of cyclic stretch and recovery test at 100% strain. After the first cycle, the R_r value of all specimens decreased. This may be due to the fact that the specimen's elongation at higher strain led to chain orientation and crystal structure was easily produced, as described in the following section. As the crystallinity increased after repeated cycle stretch-recovery, the recoverability of the specimen decreased due to the amorphous phase's lower driving force energy as mentioned in the preceding section.

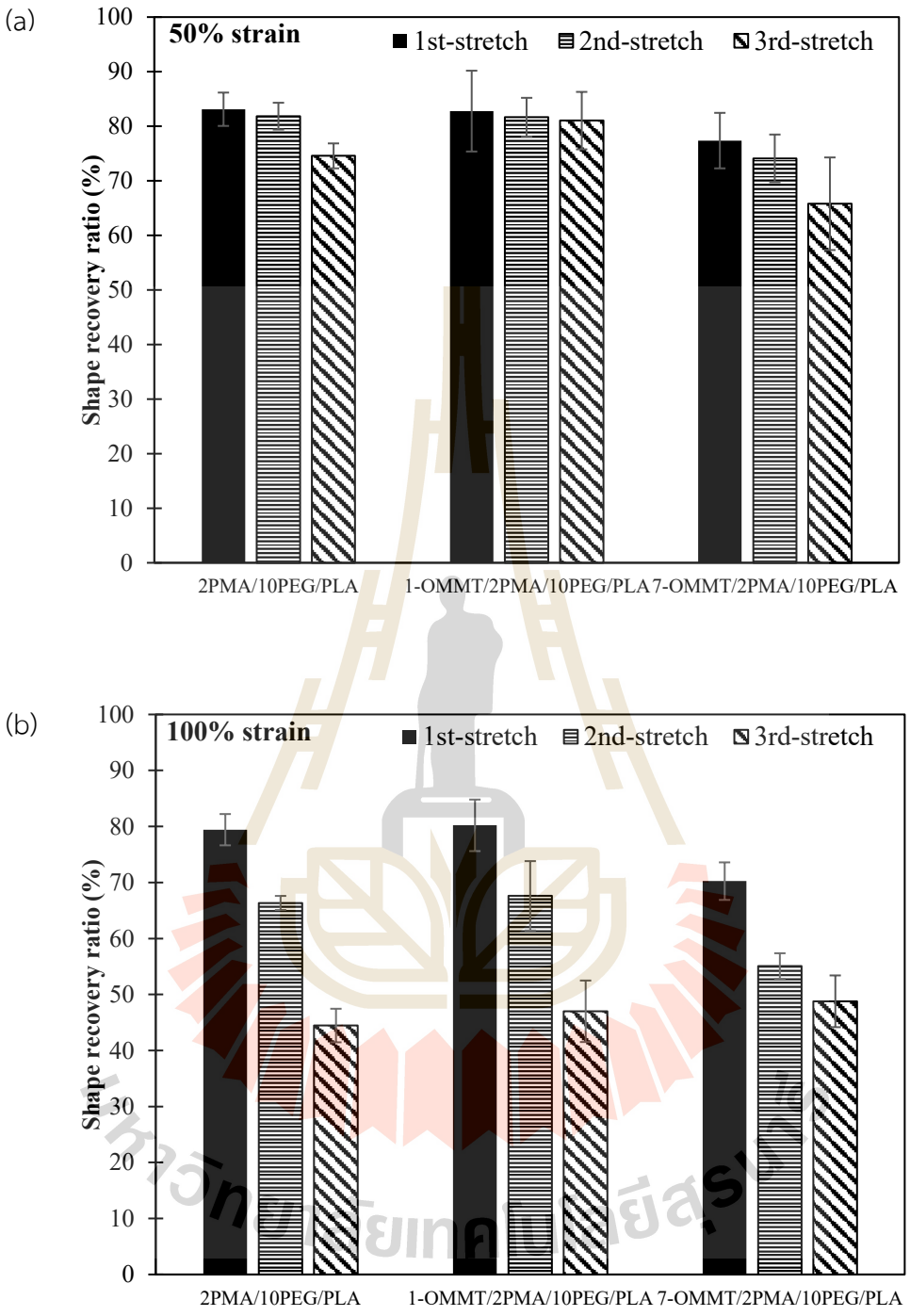

Figure 4.23. Shape recovery ratio (R_r) under cyclic stretched to 50% strain (a) and 100% strain (b) of 2PMA/10PEG/PLA, 1 -OMMT/2PMA/10PEG/PLA, and 7-OMMT/2PMA/10PEG/PLA

According to Kim and coworkers (Kim et al., 2019), the recovery ratio of tensile energy was measured from the tensile energy of the specimen for the second stretch divided by the first stretch of the specimen compare to that of the third stretch divided by the second stretch of the specimen, could be indicative of the shape memory performance of the specimen. Figure 4.24 illustrates an example of stress-strain curve for the 2PMA/10PEG/PLA specimen that was stretched to 50% (in Figure 4.24a) and 100% (in Figure 4.24b) for the third cycle. For the stress-strain curve of the cyclic stretch of 1 -OMMT/2PMA/10PEG/PLA, and 7-OMMT/2PMA/10PEG/PLA, see in Appendix A.

The recovery ratio of tensile energy was measured from the tensile energy of 2PMA/10PEG/PLA, 1-OMMT/2PMA/10PEG/PLA, and 7-OMMT/2PMA/10PEG/PLA elongated to 50% and 100% are shown in Figure 4.25a and Figure 4.25b, respectively. The tensile energy recovery between second stretch/first stretch and third stretch/second stretch of 2PMA/10PEG/PLA, 1-OMMT/2PMA/10PEG/PLA had a small difference as compared to that of 7-OMMT/2PMA/10PEG/PLA, indicating that more stable shape memory behavior was obtained at stretched 50% for 2PMA/10PEG/PLA, 1-OMMT/2PMA/10PEG/PLA but not for 7-OMMT/2PMA/10PEG/PLA. The high difference in the recovery ratio of tensile energy of 7-OMMT/2PMA/10PEG/PLA specimen may be due to the specimen's high degree of crystallinity, which is easily oriented by stress, resulting in its structure requiring more energy to deform following chain alignment in the initial state. This corresponded to the shape recoverability of both 2PMA/10PEG/PLA, 1-OMMT/2PMA/10PEG/PLA which remained unaltered after cyclic stretching to 50% strain, whereas the R_r of 7-OMMT/2PMA/10PEG/PLA deteriorated, as indicated in previous section.

Figure 4.25b, the recovery ratio of tensile energy of the specimen elongated to 100% lower than that of the specimen elongated to 50%. This indicated that the tensile energy for stretching to 100% of each cycle time had changed significantly, which corresponded to a change in the specimen's structure that will be described in the following subsections.

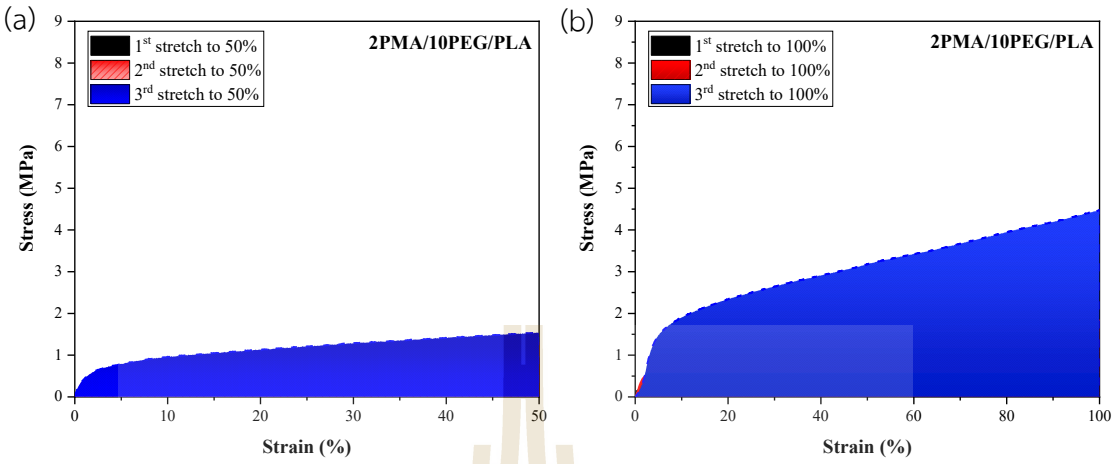

Figure 4.24. Stress-strain curves under cyclic stretched to 50% strain (a) and 100% strain (b) of 2PMA/10PEG/PLA.

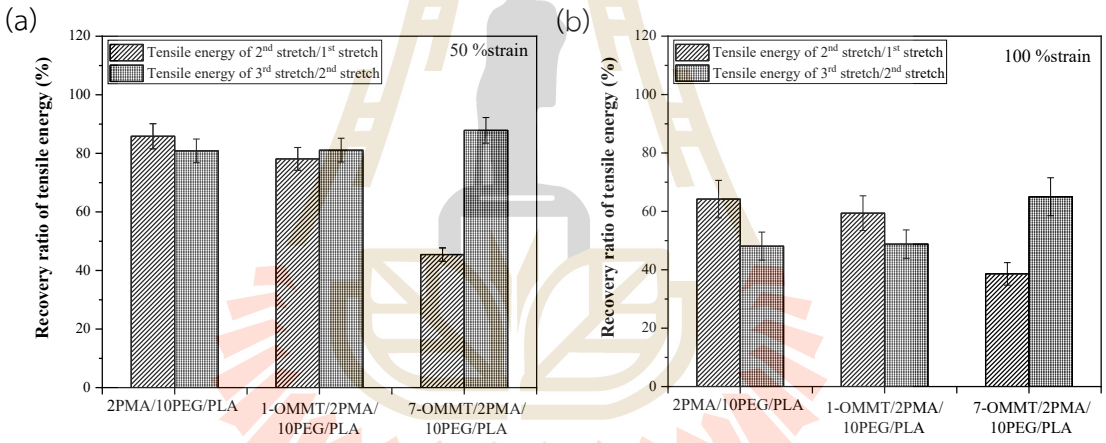

Figure 4.25. Recovery ratio of tensile energy under cyclic stretched to 50% strain (a) and 100% strain (b) of 2PMA/10PEG/PLA, 1 -OMMT/2PMA/10PEG/PLA, and 7-OMMT/2PMA/10PEG/PLA

4.4.5 Microstructure investigated by WAXS

The microstructure and crystallinity of the specimen during cyclic stretch and recovery process were analyzed by synchrotron wide-angle X-ray scattering (WAXS) technique. To evaluate the peak of PLA, the obtained WAXS raw data was analyzed using the SAXSIT4.41 software. As illustrated in Figure 4.26, the WAXS patterns of each specimen can be divided into seven parts: original, first stretching, after first recovery, second stretching, after second recovery, third stretching, and after third

recovery. The specimen was heated during the stretch procedure at 45 °C and recovered at 60 °C.

The X-ray scattering patterns of 2PMA/10PEG/PLA during cyclic stretch-recovery process at 50% strain (Figure 4.26a), contained three amorphous halos at approximately 14.5°, 18.8°, and 31.2°, and a mesomorphous peak at 16.5° that overlayed on the amorphous halo. The mesomorphic form is a well-developed crystalline phase that is an intermediate form of arranging polymer chains between amorphous and crystalline forms (Puchalski, Kwolek, Szparaga, Chrzanowski, & Krucinska, 2017). The crystalline peak did not appear clearly in the original to the second stretch states. The small PLA crystalline peak corresponding to the (110/200) plane of the 2PMA/10PEG/PLA specimen occurred after the second recovery process and increased in intensity after the third stretching and recovery, respectively. This implies that by performing stretch-recovery numerous times, the structure of a 2PMA/10PEG/PLA specimen can change in response to the applied stress and temperature. In Figure 4.26c, the WAXS patterns of 1-OMMT/2PMA/10PEG/PLA were similar in the pattern of 2PMA/10PEG/PLA. This result corroborated the stable structure of both 2PMA/10PEG/PLA and 1-OMMT/2PEG/PLA, resulting in the same recoverability of the specimen after the second cycle shape recovery measurement.

The recorded WAXS peaks of 7-OMMT/2PMA/10PEG/PLA in the original state (Figure 4.26e) showed clear peaks located at 2θ = 18.7°, 22.6°, and 26.2° corresponding to crystal planes at (203), (105), and (216), respectively (Lai, Wu, & Wang, 2016). After first recovery process, the WAXS peaks of 7-OMMT/2PMA/10PEG/PLA had an addition peak at 16.3° corresponds to the (110) and (200) lattice plane of the α and α'crystalline form of PLA, respectively. Furthermore, another minor peak appeared in the WAXS patterns of 7-OMMT/2PMA/10PEG/PLA specimens, which could be the ordered-phase caused by high OMMT loading (7 phr). The change in the crystalline structure of the specimen after the initial cyclic procedure might well have resulted in the unstable tensile energy storage of 7-OMMT/2PMA/10PEG/PLA, resulting in reduced repeatability across the specimen's cyclic operation. This finding supported the shape recovery ratio and tensile energy recovery ratio in the previous section.

Additionally, the crystalline structure of specimens that underwent cyclic stretch-recovery at 100% strain was investigated and shown in Figure 4.26b, d, f. Both 2PMA/10PEG/PLA and 1-OMMT/2PMA/10PEG/PLA showed the identical WAXS patterns at each cyclic stretch-recovery stage; however, the crystalline peak (110/200) was visible after the first recovery state of stretching to 100% and the peak intensity increased over operating more cycles, as the polymer chain became more oriented at 100% strain. This may result in a more significant difference in tensile energy recovery ratio than if the specimen was stretched to 50%, resulting in a decrease in R_r value for the 2PMA/10PEG/PLA and 1-OMMT/2PEG/PLA operating cyclic shape memory test at 100% strain.

The WAXS patterns of 7-OMMT/2PMA/10PEG/PLA that was stretched to 100% in cyclic test exhibited crystalline peaks identical to the specimen that was stretched to 50%; however, the peak intensity at 2θ = 16.3°, which corresponded to (110/200) plane, was higher, showing the crystallinity increased. The crystal structure of the 7-OMMT/2PMA/10PEG/PLA specimen appeared as a result of the specimen's original state, which facilitated the specimen's crystallinity induction at each stretch-recovery cycle. This resulted in the specimen requiring a higher tensile energy to stretch after completing the recovery process of its previous state. This led to a large difference in the recovery ratio of tensile energy, which increased the probability of polymer chain destruction under high stress and lowered the specimen's R_r.

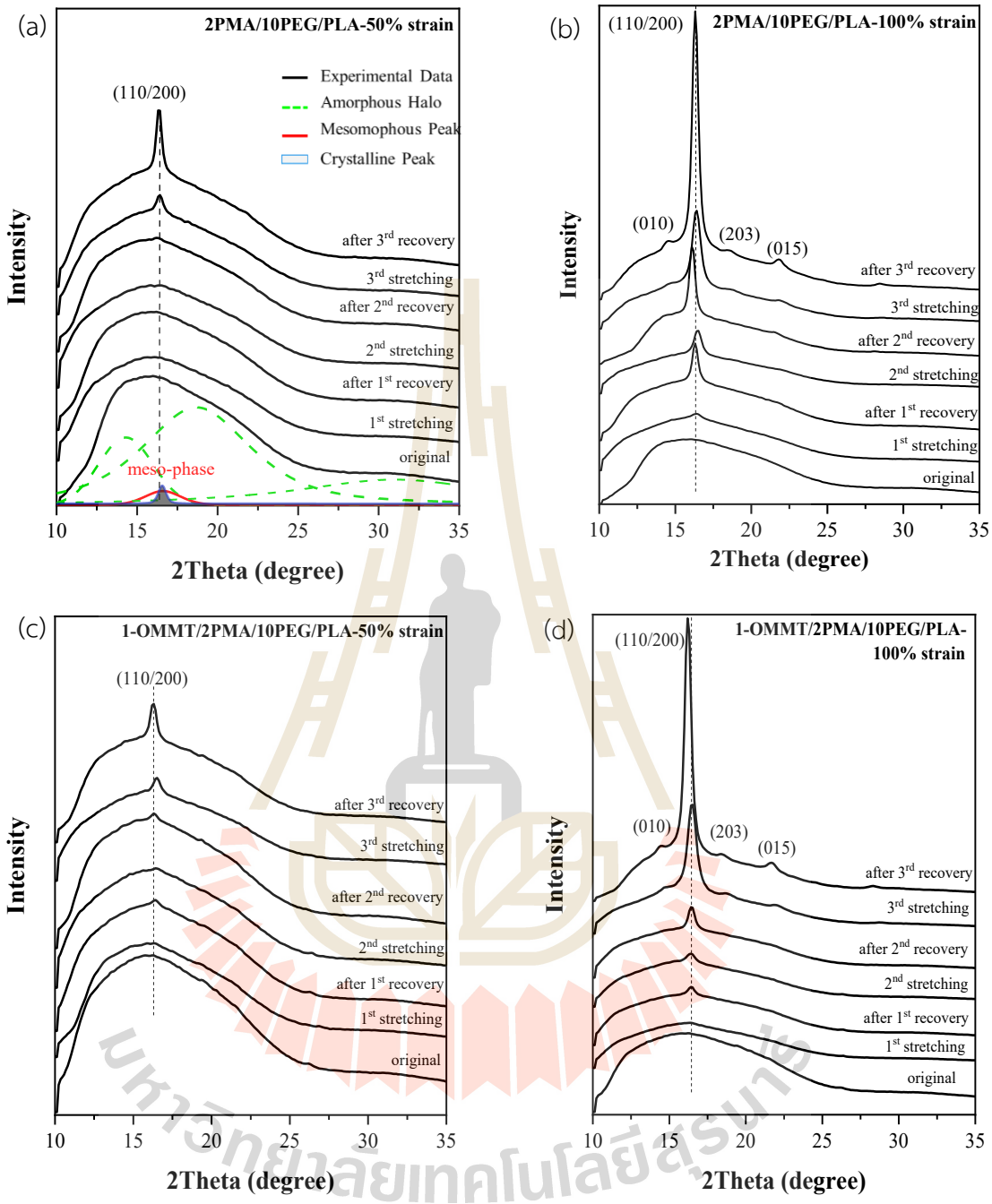

Figure 4.26. WAXS patterns of cyclic stretch and recovery at 50% and 100% strain for 2PMA/10PEG/PLA (a, b), 1 -OMMT/2PMA/10PEG/PLA (c, d), and 7-OMMT/2PMA/10PEG/PLA (e, f)

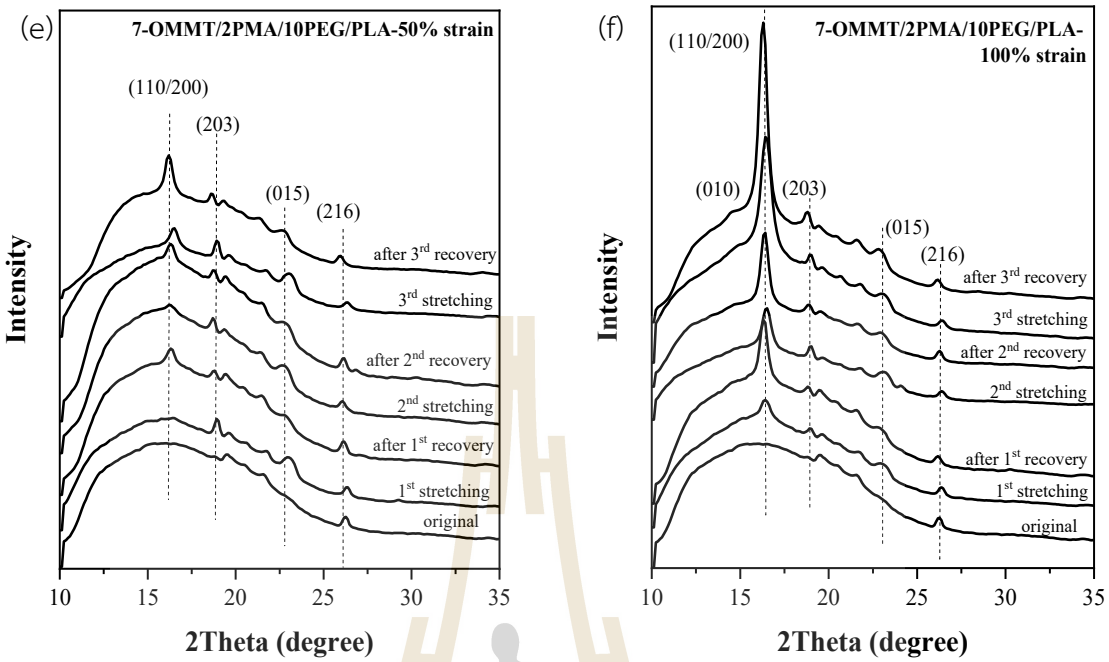

Figure 4.26. WAXS patterns of cyclic stretch and recovery at 50% and 100% strain for 2PMA/10PEG/PLA (a, b), 1 -OMMT/2PMA/10PEG/PLA (c, d), and 7-OMMT/2PMA/10PEG/PLA (e, f) (Continued)

CHAPTER V
CONCLUSION

This work explored the shape memory behavior and mechanical properties of poly (lactic acid) (PLA)-based shape memory polymers (SMPs) and its potential application in intelligent orthopedic splints.

First section was the preliminary investigation of the effect of PEG and unmodified MMT content on the characteristics of PLA blends and composites. The samples were made utilizing the solution casting technique. The addition of PEG to PLA was found to reduce the PLA's brittleness and T_g. When PEG was introduced to PLA blends at concentrations of 10 and 15 wt%, the elongation at break approximately was quadruples. However, the T_g of plasticized PLA with 20% PEG was the lowest (47°C), resulting in the highest recoverability among the blends. MMT was added to 20PEG/PLA, resulting in a higher shape recovery ratio over that of without MMT. The shape recovery ratio increased from 93.3% to 98% of 20PEG/PLA of 20PEG/PLA composite with 1 phr MMT, respectively. This was the result of the exfoliated MMT serving as a physical crosslink between PLA chains.

The preliminary findings suggested that the mechanical and shape memory capabilities of PLA could be improved by blending it with PEG. The effects of PEG content on thermal, mechanical and shape memory properties of PEG/PLA blends were further investigated in the second section. The blends were prepared using the commercial method of melt blending via twin screw extrusion. The tensile characteristics of the blend containing 10 wt% PEG (10PEG/PLA) showed a highest extent of plastic deformation than that of the neat PLA. The result was well agreed with that of prior investigated where the blends were prepared via solution casting. At 10% PEG, the plasticizing effect of PEG allowed for enhanced PLA chain mobility. In addition, the recoverability of 10PEG/PLA was weaker as compared to that of the neat PLA and 5PEG/PLA, and increasing the PEG content diminished the recoverability. This was due to the phase separation of that higher PEG contents in the PEG/PLA blends.

The PLA-g-MA compatibilizer was added to PEG/PLA (10/90) blends to optimize the their mechanical and shape memory properties. The effect of the content of PLA-g-MA on thermal, mechanical, and shape memory properties of 10PEG/PLA blend was examined in the third section. The presence of PLA-g-MA in the 10PEG/PLA blend caused the changes in mechanical and thermal properties, and shape memory behavior. The optimal content of the compatibilizer for 10PEG/PLA blend was found to be at 2 wt% which gave highest tensile properties and lowest T_g and X_c. The 2PMA/10PEG/PLA possessed the maximum shape fixity and recoverability performance among the 10PEG/PLA blends at a programming temperature of 45 °C and a recovery temperature of 60 °C. The shape fixity performance of the compatibilized 10PEG/PLA blends was comparable to that of the neat PLA at the programming temperatures of 45 °C. In situ SAXS and WAXS measurements revealed that higher number of oriented polymer chains in the amorphous region were relaxed in the 2PMA/10PEG/PLA. Consequently, 2PMA/10PEG/PLA possessed a higher shape recovery ratio than that of the uncompatibilized 10PEG/PLA. The finding was well agreed with DSC and stress relaxation results. In conclusion, PLA-g-MA compatibilizer played a complex role in the shape memory behaviors of the PEG/PLA blends. PLA-g-MA provided anchor points for the two polymers in the partially compatible system of 10PEG/PLA blend. With the optimum amount, PLA-g-MA could improve interfacial adhesion between phases, promoted chain entanglement, and accumulated stress during the recovery process.

The final part was to investigate the effect of nanofiller in improving the shape memory properties of the compatibilized blend 2PMA/10PEG/PLA. A modified MMT with CTAB (OMMT) was added into 2PMA/10PEG/PLA to improve mechanical properties and acted as physical crosslinks which were beneficial for shape memory capabilities. The results showed that the composite containing 1 phr OMMT (1-OMMT/2PMA/10PEG/PLA) had a higher tensile stress in the plastic deformation zone than the 2PMA/10PEG/PLA blend, whereas the elongation at break was unchanged. In addition, 1-OMMT/2PMA/10PEG/PLA exhibited a better recovery ratio than the 2PMA/10PEG/PLA blend, as well as superior repeatability of shape recoverability when shape programming at 50% strain. The cyclic shape memory test was also performed at 100% strain and the results were significantly different that when programed at 50%

strain. With 100% strain shape programing, the shape recovery ratio of all specimens changed since the first cycle. From the results of tensile energy of the specimen preformed the cyclic stretch-recovery test, the specimen that stretched to 100% had more change in the structure than that of the specimen that stretched to 50%. This could be due to the difference in crystallinity or degree of damages inside the samples, which affected in the shape memory behavior.

This thesis demonstrated the feasibility of optimizing the properties of shape-memory PLA to meet the requirements of applications involving smart orthopedic splints. The PLA based SMPs including PEG/PLA blends and composites overcame the limitations of the neat PLA for the use in the medical industry. The decrease in T_g of the SMP to close to the required temperature for the use with the human body and the improvement in ductility were critically important achievement from this work. The optimized blend of 2PMA/10PEG/PLA was capable of regaining their original shape at a lower temperature than that of neat PLA. In addition, the study discovered that the 1-OMMT/2PMA/10PEG/PLA composite was superior to the 10PEG/PLA blends for functions requiring good shape memory recoverability under high strain (100% strain) and outstanding repeatability at low strain (50% strain).

REFERENCES

Athanasoulia, I.-G., & Tarantili, P. A. (2017). Preparation and characterization of polyethylene glycol/poly(L-lactic acid) blends. *Pure and Applied Chemistry, 89*(1), 141-152. doi:10.1515/pac-2016-0919

Chow, W. S., Tham, W. L., & Seow, P. C. (2012). Effects of maleated-PLA compatibilizer on the properties of poly(lactic acid)/halloysite clay composites. *Journal of Thermoplastic Composite Materials, 26*(10), 1349-1363. doi:10.1177/0892705712439569

Cui, H.-W., & Du, G.-B. (2013). Influence of Synthesis Processes on the Properties of PVAc-MMT-STAB Exfoliated Nanocomposites. *Polymer-Plastics Technology and Engineering, 52*(6), 571-580. doi:10.1080/03602559.2012.762522

Fu, L., Wu, F., Xu, C., Cao, T., Wang, R., & Guo, S. (2018). Anisotropic Shape Memory Behaviors of Polylactic Acid/Citric Acid–Bentonite Composite with a Gradient Filler Concentration in Thickness Direction. *Industrial & Engineering Chemistry Research, 57*(18), 6265-6274. doi:10.1021/acs.iecr.8b00602

Green, R. L., NJ). (1984). United States Patent No.

Guo, Y., Ma, J., Lv, Z., Zhao, N., Wang, L., & Li, Q. (2018). The effect of plasticizer on the shape memory properties of poly(lactide acid)/poly(ethylene glycol) blends. *Journal of Materials Research, 33*(23), 4101-4112. doi:10.1557/jmr.2018.359

Hassouna, F., Raquez, J.-M., Addiego, F., Dubois, P., Toniazzo, V., & Ruch, D. (2011). New approach on the development of plasticized polylactide (PLA): Grafting of poly(ethylene glycol) (PEG) via reactive extrusion. *European Polymer Journal, 47*(11), 2134-2144. doi:10.1016/j.eurpolymj.2011.08.001

Hwang, S. W., Lee, S. B., Lee, C. K., Lee, J. Y., Shim, J. K., Selke, S. E. M., . . . Auras, R. (2012). Grafting of maleic anhydride on poly(L-lactic acid). Effects on physical and mechanical properties. *Polymer Testing, 31*(2), 333-344. doi:10.1016/j.polymertesting.2011.12.005

Jinsong, L., Lan, X., Liu, Y., & Du, S. (2011). Shape-memory polymers and their composites: Stimulus methods and applications. *Progress in Materials Science, 56*, 1077–1135. doi:10.1016/j.pmatsci.2011.03.001

Joseph, M. A., CO, US). (2015). United States Patent No.

Kim, S. K., Jang, R., & Kim, W. N. (2019). Effects of compatibilizer on the mechanical, rheological, and shape memory behaviors of poly(lactic acid) and poly(MnBM) blends. *Journal of Applied Polymer Science, 137*(16). doi:10.1002/app.48591

Koerner, H., Strong, R. J., Smith, M. L., Wang, D. H., Tan, L.-S., Lee, K. M., . . . Vaia, R. A. (2013). Polymer design for high temperature shape memory: Low crosslink density polyimides. *Polymer, 54*(1), 391-402. doi:10.1016/j.polymer.2012.11.007

Komal, U., Lila, M., & Singh, I. (2021). Processing of PLA/pineapple fiber based next generation composites. *Materials and Manufacturing Processes, 36*. doi:10.1080/10426914.2021.1942904

Kong, D., & Xiao, X. (2016). High Cycle-life Shape Memory Polymer at High Temperature. *Sci Rep, 6*, 33610. doi:10.1038/srep33610

Koosomsuan, W., Yamaguchi, M., Phinyocheep, P., & Sirisinha, K. (2019). High-Strain Shape Memory Behavior of PLA-PEG Multiblock Copolymers and Its Microstructural Origin. *Journal of Polymer Science Part B: Polymer Physics, 57*(5), 241-256. doi:10.1002/polb.24775

Lai, S.-M., Li, C.-H., Kao, H.-C., & Liu, L.-C. (2019). Shape Memory Properties of Melt-Blended Olefin Block Copolymer (OBC)/Ethylene-Vinyl Acetate Blends. *Journal of Macromolecular Science, Part B, 58*(1), 174-191. doi:10.1080/00222348.2018.1558593

Lai, S.-M., Wu, W.-L., & Wang, Y.-J. (2016). Annealing effect on the shape memory properties of polylactic acid (PLA)/thermoplastic polyurethane (TPU) bio-based blends. *Journal of Polymer Research, 23*(5). doi:10.1007/s10965-016-0993-6

Li, S.-C., & Tao, L. (2010). Melt Rheological and Thermoresponsive Shape Memory Properties of HDPE/PA6/POE-g-MAH Blends. *Polymer-Plastics Technology and Engineering, 49*(2), 218-222. doi:10.1080/03602550903147320

Liu, H., Xie, T., Zhang, Y., Ou, Y., & Yang, G. (2006). Crystallization Behaviors of Polypropylene/Polyamide-6 Blends Modified by a Maleated Thermoplastic Elastomer. *Polymer Journal, 38*(1), 21-30. doi:10.1295/polymj.38.21

Liu, J., Zhou, K., Wen, P., Wang, B., Hu, Y., & Gui, Z. (2015). The influence of multiple modified MMT on the thermal and fire behavior of poly (lactic acid) nanocomposites. *Polymers for Advanced Technologies, 26*(6), 626-634. doi: https://doi.org/10.1002/pat.3497

Liu, Y., Li, Y., Yang, G., Zheng, X., & Zhou, S. (2015). Multi-stimulus-responsive shape-memory polymer nanocomposite network cross-linked by cellulose nanocrystals. *ACS Appl Mater Interfaces, 7*(7), 4118-4126. doi:10.1021/am 5081056

Navarro-Baena, I., Sessini, V., Dominici, F., Torre, L., Kenny, J. M., & Peponi, L. (2016). Design of biodegradable blends based on PLA and PCL: From morphological, thermal and mechanical studies to shape memory behavior. *Polymer Degradation and Stability, 132*, 97-108. doi:https://doi.org/10.1016/j.polym degradstab.2016.03.037

Oliver, K., Seddon, A., & Trask, R. S. (2016). Morphing in nature and beyond: a review of natural and synthetic shape-changing materials and mechanisms. *Journal of Materials Science, 51*(24), 10663-10689. doi:10.1007/s10853-016-0295-8

Peponi, L., Navarro-Baena, I., & Kenny, J. M. (2014). Shape memory polymers: properties, synthesis and applications. In *Smart Polymers and their Applications* (pp. 204-236).

Phanthong, P., Reubroycharoen, P., Hao, X., Xu, G., Abudula, A., & Guan, G. (2018). Nanocellulose: Extraction and application. *Carbon Resources Conversion, 1*(1), 32-43. doi:10.1016/j.crcon.2018.05.004

Puchalski, M., Kwolek, S., Szparaga, G., Chrzanowski, M., & Krucinska, I. (2017). Investigation of the Influence of PLA Molecular Structure on the Crystalline Forms (alpha' and alpha) and Mechanical Properties of Wet Spinning Fibres. *Polymers (Basel), 9*(1). doi:10.3390/polym9010018

Qi, X., Dong, P., Liu, Z., Liu, T., & Fu, Q. (2016). Selective localization of multi-walled carbon nanotubes in bi-component biodegradable polyester blend for rapid

electroactive shape memory performance. *Composites Science and Technology, 125*, 38-46. doi:10.1016/j.compscitech.2016.01.023

Qi, X., Jing, M., Liu, Z., Dong, P., Liu, T., & Fu, Q. (2016). Microfibrillated cellulose reinforced bio-based poly(propylene carbonate) with dual-responsive shape memory properties. *RSC Advances, 6*(9), 7560-7567. doi:10.1039/c5ra22215j

Qin, S.-X., Yu, C.-X., Chen, X.-Y., Zhou, H.-P., & Zhao, L.-F. (2018). Fully Biodegradable Poly(lactic acid)/Poly(propylene carbonate) Shape Memory Materials with Low Recovery Temperature Based on in situ Compatibilization by Dicumyl Peroxide. *Chinese Journal of Polymer Science, 36*(6), 783-790. doi:10.1007/s10118-018-2065-3

Raghunath, S., Kumar, S., Samal, S. K., Mohanty, S., & Nayak, S. K. (2018). PLA/ESO/MWCNT nanocomposite: a study on mechanical, thermal and electroactive shape memory properties. *Journal of Polymer Research, 25*(5). doi:10.1007/s10965-018-1523-5

Sessini, V., Navarro-Baena, I., Arrieta, M. P., Dominici, F., López, D., Torre, L., . . . Peponi, L. (2018). Effect of the addition of polyester-grafted-cellulose nanocrystals on the shape memory properties of biodegradable PLA/PCL nanocomposites. *Polymer Degradation and Stability, 152*, 126-138. doi:10.1016/j.polymdegradstab.2018.04.012

Shen, T., Lu, M., Zhou, D., & Liang, L. (2012). Influence of blocked polyisocyanate on thermomechanical, shape memory and biodegradable properties of poly(lactic acid)/poly(ethylene glycol) blends. *Iranian Polymer Journal, 21*(5), 317-323. doi:10.1007/s13726-012-0031-4

Tang, X., Liu, C., Keum, J., Chen, J., Dial, B. E., Wang, Y., . . . Chen, X. C. (2022). Upcycling of semicrystalline polymers by compatibilization: mechanism and location of compatibilizers. *RSC Advances, 12*(18), 10886-10894. doi:10.1039/D1RA09452A

Tanoue, S., Hasook, A., Iemoto, Y., & Unryu, T. (2006). Preparation of poly(lactic acid)/poly(ethylene glycol)/organoclay nanocomposites by melt compounding. *Polymer Composites, 27*(3), 256-263. doi:10.1002/pc.20174

Tcharkhtchi, A., Abdallah-Elhirtsi, S., Ebrahimi, K., Fitoussi, J., Shirinbayan, M., & Farzaneh, S. (2014). Some New Concepts of Shape Memory Effect of Polymers. *Polymers, 6*(4), 1144-1163. doi:10.3390/polym6041144

Tian, Y., Zhu, C., Gong, J., Yang, S., Ma, J., & Xu, J. (2014). Lamellae break induced formation of shish-kebab during hot stretching of ultra-high molecular weight polyethylene precursor fibers investigated by in situ small angle X-ray scattering. *Polymer, 55*(16), 4299-4306. doi:https://doi.org/10.1016/j.polymer.2014.06.056

Wang, W., Jin, Y., Ping, P., Chen, X., Jing, X., & Su, Z. (2010). Structure Evolution in Segmented Poly(ester urethane) in Shape-Memory Process. *Macromolecules, 43*(6), 2942-2947. doi:10.1021/ma902781e

Xu, J., & Song, J. (2011). Thermal Responsive Shape Memory Polymers for Biomedical Applications. *Orthopedics and Physical Rehabilitation Publications and Presentations.*

Xu, J., & Song, J. (2015). Polylactic acid (PLA)-based shape-memory materials for biomedical applications. In *Shape Memory Polymers for Biomedical Applications* (pp. 197-217).

Yuliana, M., Sutrisno, R. J., Hermanto, S., Ismadji, S., Wijaya, C. J., Santoso, S. P., . . . Ju, Y. H. (2020). Hydrophobic Cetyltrimethylammonium Bromide-Pillared Bentonite as an Effective Palm Oil Bleaching Agent. *ACS Omega, 5*(44), 28844-28855. doi:10.1021/acsomega.0c04238

Zhu, Y., Radlauer, M. R., Schneiderman, D. K., Shaffer, M. S. P., Hillmyer, M. A., & Williams, C. K. (2018). Multiblock Polyesters Demonstrating High Elasticity and Shape Memory Effects. *Macromolecules, 51*(7), 2466-2475. doi:10.1021/acs.macromol.7b02690

APPENDIX A

Stress-strain curves under cyclic stretched to 50% strain and 100% strain of the specimen

APPENDIX A

Stress-strain curves under cyclic stretched to 50% strain and 100% strain of the specimen

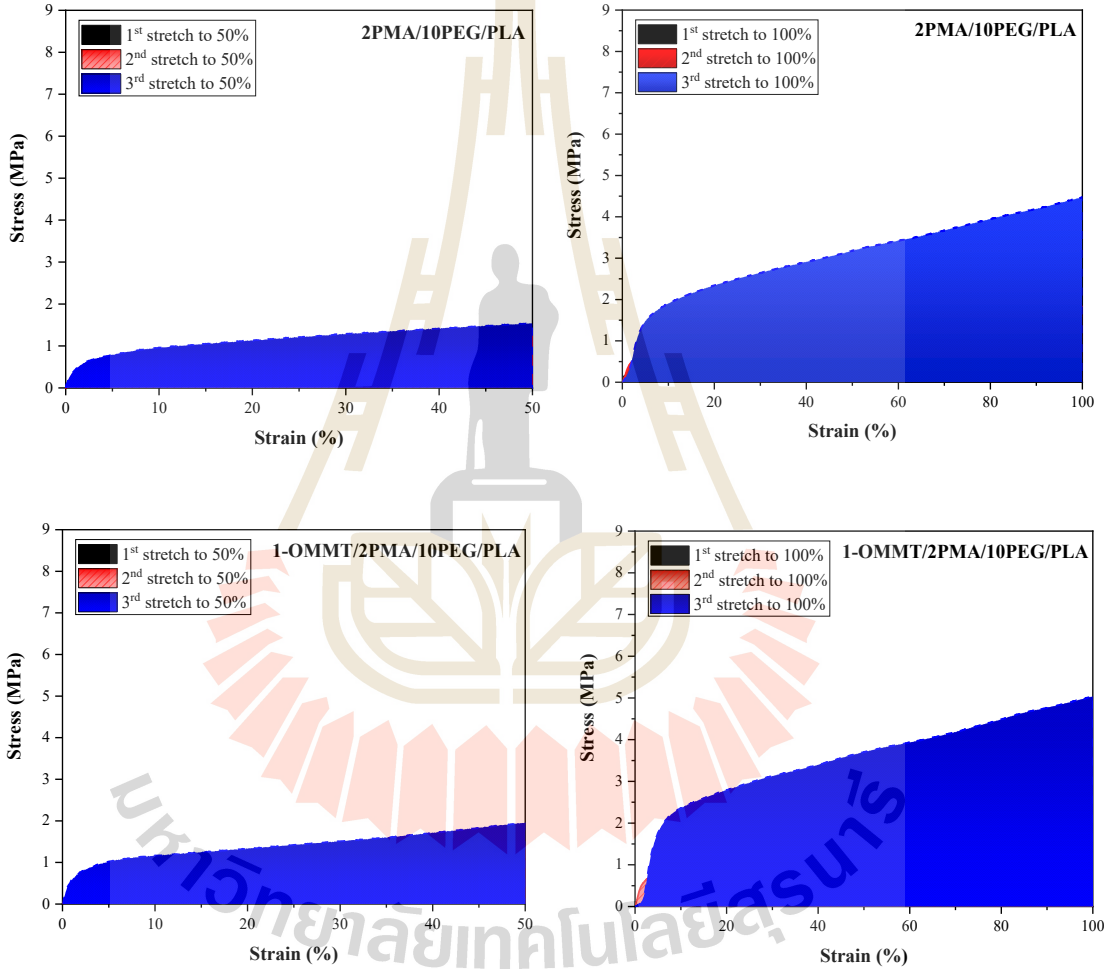

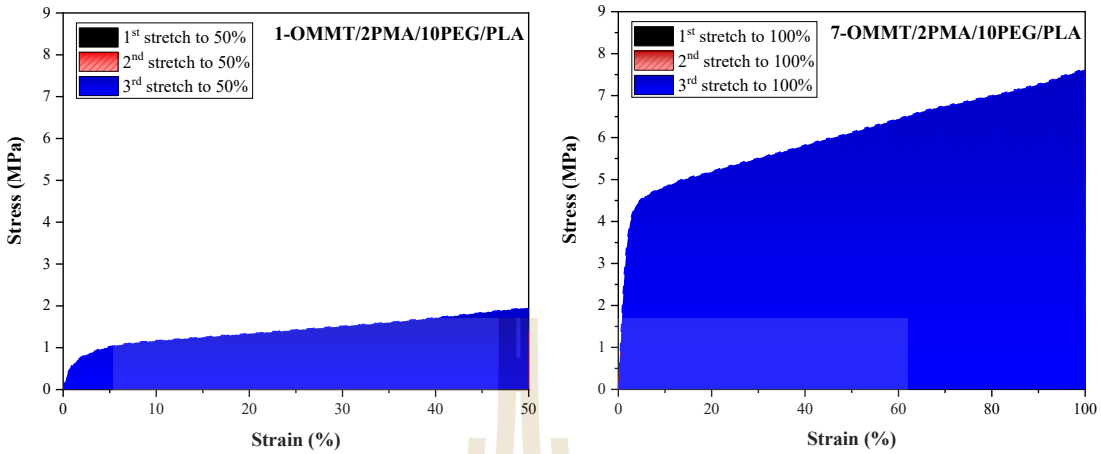

APPENDIX B

List of Publication

List of Publications

1. Wasana Nonkrathok, Nitinat Suppakarn, Tatiya Trongsatitkul, Effects of PEG and MMT Contents on Mechanical, Thermal, and Shape Memory Properties of MMT/PEG/PLA Nanocomposites, The 2nd Materials Research Society of Thailand International Conference (MRS-Thailand 2019), July 10 - 12, 2019, The Zign Hotel, Pattaya,Thailand.
2. Wasana Nonkrathok, Nitinat Suppakarn, Tatiya Trongsatitkul, Role of PLA-g-MA in Improving Shape Memory Properties of Thermally-responsive PEG/PLA Blends, The 4th International Conference on Materials Engineering and Nanotechnology (ICMEN 2021), April 3rd - 4th, 2021, Kuala Lumpur, Malaysia.
3. Wasana Nonkrathok, Nitinat Suppakarn, Tatiya Trongsatitkul, Role of Maleic Anhydride-Grafted Poly(lactic acid) in Improving Shape Memory Properties of Thermoresponsive Poly(ethylene glycol) and Poly(lactic acid) Blends. *Polymers* **2022**, *14*, 3923. https://doi.org/10.3390/polym14183923

AIP Conference Proceedings

Effects of PEG and MMT contents on mechanical, thermal, and shape memory properties of MMT/PEG/PLA nanocomposites

Cite as: AIP Conference Proceedings **2279**, 070006 (2020); https://doi.org/10.1063/5.0023117
Published Online: 26 October 2020

W. Nonkrathok, N. Suppakarn and T. Trongsatitkul

AIP Publishing

Effects of PEG and MMT Contents on Mechanical, Thermal, and Shape Memory Properties of MMT/PEG/PLA Nanocomposites

W. Nonkrathok[1], N. Suppakarn[1, 2], and T. Trongsatitkul[1, 3, a)]

[1]School of Polymer Engineering, Suranaree University of Technology, Nakhon Ratchasima 30000, Thailand
[2]Center of Excellence in Microbial Technology for Agricultural Industry, Suranaree University of Technology, Nakhon Ratchasima 30000, Thailand
[3]Center of Excellence in Biomechanics Medicine, Suranaree University of Technology, Nakhon Ratchasima 30000, Thailand

[a)]Corresponding author: tatiya@sut.ac.th

Abstract. Shape memory polymer of poly (lactic acid) (PLA) has attracted a significant attention, especially in the field of biomedical application. This is mainly because of its biocompatibility rendering it safe to use in human body. The glass transition temperature (T_g) of PLA is used as a mechanism to activate the shape memory effect. Nonetheless, utilization of PLA in medical application is limited due to its brittleness and relatively high T_g (about 60°C). In this work, poly (ethylene glycol) (PEG) with molecular weight of 4,000 g/mol was used as a plasticizer for PLA. Effect of PEG contents (10, 15, 20, 30, and 40 wt%) on thermal and mechanical properties were investigated by differential scanning calorimetry (DSC) and tensile test, respectively. Furthermore, influence of PEG on shape recovery ratio was investigated at a constant temperature of 65°C. It was found that tensile strength, tensile modulus, and T_g values of the plasticized PLA decreased, while elongation at break increased with the increasing PEG content. The shape recovery of plasticized PLA was slightly decreased as PEG content increased. In order to enhance the shape memory performance of PLA blends, montmorillonite (MMT) nanoparticles were added into the plasticized PLA. Nanocomposites of plasticized PLA with 20 wt% PEG (20PEG/PLA) were prepared with the filler loadings of 1 and 3 phr. The exfoliation of MMT in polymer matrix was confirmed with the observation of a peak position angle of MMT via X-ray diffraction (XRD). The presence of MMT in 20PEG/PLA was found to increase the tensile modulus and shape recovery ratio over those of 20PEG/PLA. In this work, we have illustrated that shape memory performance of PLA can be enhanced by the incorporations of PEG and MMT.

INTRODUCTION

Shape memory polymers (SMPs) have received an increasing attention. This is not only because they can offer shape memory properties, but they are also light in weight, easy to fabricate, and some are biocompatible. SMPs can be processed into temporary shapes, then rapidly restored to their original shapes under external stimuli such as heat, electromagnetism, solvent, light, and so on. Thermally induced SMPs are the most extensively explored. A temporary shape of this SMP can be obtained by heating the polymer at temperature above their transition temperature (T_{trans}). Force is applied to the polymer to form a desired shape before cooling down to below the T_{trans} to fix the temporary form. When they are reheated to the T_{trans}, the elastic force, stored in the reversible phase, turns them back to the initial shape. Using of thermally induced SMPs in the field of biomedical is rather challenging. This is due to the narrow working window of temperature (37-45°C). SMPs are required to possess T_{trans} slightly above human body temperature to ensure stable shape fixing in a minimally invasive configuration during surgical delivery. The examples of materials that possess such transition temperatures include poly (lactic acid) (PLA), poly (ε-caprolactone) (PCL), Thermoplastic polyurethane (TPU), etc.

The Second Materials Research Society of Thailand International Conference
AIP Conf. Proc. 2279, 070006-1–070006-6; https://doi.org/10.1063/5.0023117
Published by AIP Publishing. 978-0-7354-4009-8/$30.00

Nowadays, biodegradable polymer, poly (lactic acid) (PLA) is of great interests in biomedical applications such as tissue engineering, drug delivery systems, resorbable sutures, and implant materials. This is because of its biocompatibility, nontoxicity, and biodegradability. Moreover, many researches have reported the excellent shape memory properties of PLA. J. Xu and J. Song (2015) reported that the crystalline phase in PLA acted as the shape-fixing parts that maintained dimensional stability during deformation and recovery while the amorphous phase acted as the shape-switching parts, which could be triggered above glass transition temperature (T_g). However, high T_g (about 60°C) and brittleness can be harmful to human tissue [1].

The approaches to improve the performance of PLA based SMPs include, copolymerization and blending. The blending method is more practical and economical strategy to modify the polymer properties than copolymerization. The second polymer to be incorporated into PLA should function as a plasticizer to improve ductility and processability of the brittle polymer. The most common plasticizer used for PLA is Poly (ethylene glycol) (PEG), which is biodegradable, non-volatile, and non-toxic. Numerous researchers have reported the plasticizing effect of PEG in PLA. PEG with different molecular weights (M_w of 400, 600, and 2,000 g/mol) have been investigated in order to understand the role of PEG in the improvements of the mechanical and thermal properties of PLA blends. Yijun Guo and Jing Ma (2018) studied effect of PEG on shape memory and physical properties of PLA/PEG blends. They found that an increase of a PEG content significantly increased the elongation at break and decreased T_g of the PLA/PEG blends. Nonetheless, the shape memory performance and tensile modulus of PLA/PEG blends were decreased with the increased PEG content [2].

To improve the mechanical and shape memory properties of PLA/PEG blends, an incorporation of inorganic nano-additive is one of the most effective ways to improve the material's performance [3]. The nano-additive is believed to restrict chain movements of PLA, which improves PLA's ability to response to temperature change, thus better shape recovery, and increases the modulus of the material [4].

The aims of this paper were to investigate shape memory properties of PLA and PEG blends. PEG with molecular weight of 4,000 g/mol were used at 10, 15, 20, 30, and 40 wt%. The contents of plasticizer and MMT nanofiller were varied (1 phr and 3 phr). Results and discussion on the mechanical, thermal, and shape memory properties of the PLA blends and plasticized PLA nanocomposites are reported.

MATERIALS AND METHODS

Poly (lactic acid) (PLA, 4043D, pellet) was purchased from Nature Works Co. (Minnetonka, Minnesota, USA) with a melting temperature (T_m) of 150°C and the glass transition temperature (T_g) of 55°C. Poly (ethylene glycol) (PEG) with a molecular weight of 4,000 g/mol was kindly donated by Innovation Group (Thailand) Ltd,. The commercial montmorillonite (MMT) was supplied by Thai Nippon Chemical Industry Co. Ltd., Thailand. Dichloromethane (DCM) was purchased from P. WAI CO., Ltd. PLA, PEG and MMT were dried under vacuum at 50°C for 24 h prior to use.

PLA base SMPs films were prepared via solvent casting method. To prepare PLA shape memory film, PLA 8 g was added in to 100 ml of DCM in an enclosed bottle. The mixture was stirred using magnetic at a constant speed of 350 rpm at room temperature for at least 4 h until clear and homogeneous solution was obtained. The solution was then carefully poured into a Petri dish glass and let dry at room temperature for 24 h, followed by second drying step in an oven at 60°C for 4 h to ensure a complete removal of DCM. The PEG/PLA blends and PEG/PLA nanocomposites were prepared the same method as described above. Solutions of PLA or PEG/PLA blends were prepared at a constant solids content of 8 w/v %. The PLA based blend films were prepared with various PEG contents i.e. 10, 15, 20, 30, and 40 wt%. The plasticized PLA nanocomposites with different MMT contents of 1 and 3 phr were also prepared using the same method described above. Prior to mixing MMT with PEG/PLA blend solution, MMT was dispersed in DCM and sonicated for 30 min to ensure its uniform dispersion. The obtained film samples possess thicknesses around 0.20 ± 0.01 mm. The samples were named according to the weight percentage of PEG in the PEG/PLA blends and MMT content. For example, a PLA blend containing PEG of 20 wt% was named 20PEG/PLA. The 20PEG/PLA blend containing MMT of 1 phr was named 1MMT/20PEG/PLA. Non-plasticized PLA containing MMT of 3 phr was named 3MMT/PLA.

CHARACTERIZATION

Thermal characteristics of PLA and plasticized-PLA films were determined using differential scanning calorimeter (DSC) (TGA/DSC 1 Instruments SDT 2960, USA). The tests were performed using a temperature range from 35 to 200°C at a heating rate of 10°C/min under a nitrogen atmosphere.

Tensile test was performed at room temperature using Universal Testing Machine (UTM) (5565 Model, Instron, UK) according to ASTM D882 with a load cell of 1 kN and a cross head speed of 50 mm/min. The rectangular specimens with the length of 100 mm and the width of 10 mm were prepared.

The interlayer spacing and peak position angle of MMT were determined by X-ray diffraction (XRD) performed on D8-Advance Bruker, model AXS with CuKα radiation having a $\lambda = 1.542 \times 10^{-10}$ (1.542 Å). The MMT, PLA, 3MMT/PLA, 20PEG/PLA, and 3MMT/20PEG/PLA were characterized using a scanning range of $2\theta = 3 - 25°$, with a constant scanning speed 0.2°/min.

Shape memory performance of samples were evaluated by shape recovery test. The size of sample was 60 mm x 5 mm x 0.20 mm. To test shape recovery, the samples were formed into spiral shape at 65°C followed by rapid cooling in cold water (10°C) to obtain a temporary shape as seen in Fig. 1 To observe shape recovery performance, the sample was reheated by immerse in a water bath at 65°C. At this temperature the polymer was relaxed the residual stress was relieved which allowed the recovery of the sample to take place. The samples were found to be able to return to their initial shapes within 2 min. The values of shape recovery ratio (R_r) were calculated using the following equation, [5]

$$R_r = \frac{\theta_r}{180} \times 100\%$$

where R_r: is shape recovery in percent and θ_r: is recovered angle

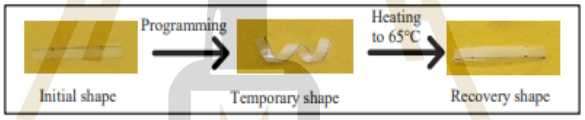

FIGURE 1. Pictures showing the shape memory process.

RESULTS AND DISCUSSION

The thermally induced shape recovery of PLA usually takes place around its T_g (55°C). The presences of plasticizer PEG and nanofiller MMT are known to affect polymer chain mobility, hence T_g. Therefore, investigating the T_g value influenced by PEG content and incorporation of MMT are necessary for exploring the shape memory properties of PLA blends and PLA nanocomposites, respectively. DSC thermograms of PLA, PEG/PLA blends, and MMT/PEG/PLA nanocomposite are illustrated in Fig. 2. From the DSC curve of PLA, the T_g was found to be equal to 55°C. The presence of PEG of 15 and 20 wt% in PLA resulted in the decrease of T_g of PLA to 50°C and 47°C, respectively. These indicate that the polymer chains can easily slip pass each other due to plasticizing effect of PEG, which, as a consequence, the system requires less energy for phase transition process. However, the blend with PEG content of 30 wt% possesses T_g of 52°C close to that of PLA. This could be the result of PEG and PLA phase separation [2]. The cold crystallization temperature (T_c) of PLA also changed from about 135°C to 98°C as PEG content increased. This might be due to plasticizing effect of PEG that helps increase polymer chain mobility which facilitates crystallization of PLA. The melting temperature (T_m) of PLA decreased as a result of the addition of plasticizer [6]. However, as PEG content in the blend increased up to 40 wt%, the T_g of PLA could not be found. This was because the melting peak of PEG at 52°C overshadowed the T_g of PLA.

From this result, the 20PEG/PLA blend showed the lowest T_g of 47°C, which should be beneficial for medical application, therefore was chosen to be further investigated. Nanocomposites of PLA and 20PEG/PLA were prepared with MMT content of 1 and 3 phr. From Fig. 2, it was found that the presence of 3 wt% MMT in PLA showed little to no effect on the T_g of PLA but its T_m. The melting peak of PLA shifted to higher temperature which might be because the MMT acts as a nucleating agent. This results in more nuclei with smaller crystal of PLA [7], which, as a consequence, required higher energy to destroy the crystalline structure. This was well agreed with XRD

result of 3MMT/PLA which present an intensity of the PLA crystalline peak was increased as compared to those of PLA.

The DSC curve in Fig. 2 of the plasticized nanocomposite of 3MMT/20PEG/PLA shows the effect of the presence of PEG together with MMT. It was found that the T_g and T_m of PLA were 53°C and 150°C respectively. Its DSC curve seems to be similar to that of PLA. This revealed that the effect of PEG on the lubricated PLA chain might be obliterated by chain restriction of MMT may cause as the T_g and T_m of PLA were unaffected after combining of PEG and MMT.

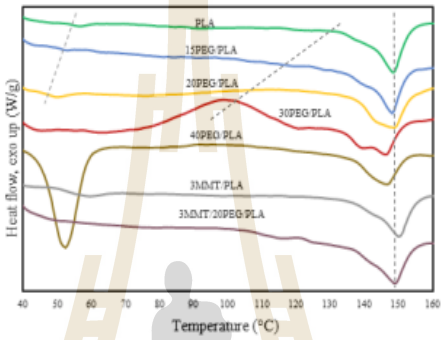

FIGURE 2. DSC thermograms of PLA, PEG/PLA blends and MMT/PEG/PLA nanocomposites.

The tensile properties including tensile strength at yield, tensile stress at break, tensile modulus, and elongation at break of PLA, PEG/PLA blends and MMT/PEG/PLA nanocomposites are summarized in Table 1. PLA exhibited the highest modulus of around 1.67 GPa and lowest elongation at break of 4.65%. When introduced 3 phr of MMT into PLA, the tensile properties of 3MMT/PLA nanocomposite declined as compared with those of the neat PLA. This could be due to the unexfoliated MMT in PLA, which was well agreed with the XRD result discussed in later section of this report. With the addition of PEG into PLA matrix, the ductility of plasticized PLA significantly was improved, as can be seen by an increase of the elongation at break up to 20 folds over that of PLA. The tensile strength at yield, tensile stress at break, and tensile modulus were, as expected, significantly decreased with the increasing PEG content. This was because the presence of PEG in PLA matrix resulted in an increase in PLA's chain mobility, which was also well agreed with the DSC result in which the decrease of T_g in plasticized PLA was observed. The addition of 1 and 3 phr of MMT into plasticized 20PEG/PLA resulted in increases of the tensile moduli to 1.19 and 1.49 GPa for 1MMT/20PEG/PLA and 3MMT/20PEG/PLA nanocomposites, respectively. Nonetheless, their elongation at break decreased as compared with those of 20PEG/PLA blend. These can be because the incorporation of MMT particles reduced the chain mobility of PLA.

TABLE 1. Tensile properties of PLA, PEG/PLA blends, and MMT/PEG/PLA nanocomposite films

Sample	Strength at yield (MPa)	Stress at break (MPa)	Modulus (GPa)	Elongation at break (%)
PLA	-	43.76 ± 1.36	1.67 ± 0.26	4.65 ± 0.30
10PEG/PLA	21.64 ± 1.02	16.87 ± 0.91	1.03 ± 0.09	86.56 ± 4.03
15PEG/PLA	24.83 ± 1.47	18.70 ± 0.76	1.12 ± 0.16	86.71 ± 6.08
20PEG/PLA	24.43 ± 1.34	15.72 ± 0.98	1.10 ± 0.11	51.78 ± 5.02
30PEG/PLA	16.01 ± 1.13	11.09 ± 1.07	0.72 ± 0.11	47.74 ± 4.43
40PEG/PLA	12.89 ± 0.44	10.77 ± 1.36	0.24 ± 0.17	56.24 ± 10.23
1MMT/20PEG/PLA	16.41 ± 1.58	13.04 ± 1.79	1.19 ± 0.12	14.07 ± 5.48
3MMT/20PEG/PLA	19.15 ± 1.87	15.61 ± 1.85	1.49 ± 0.22	23.01 ± 7.08
3MMT/PLA	-	37.78 ± 1.48	1.16 ± 0.57	3.13 ± 1.27

XRD was performed to confirm if nanocomposites with fully exfoliated nanofiller were obtained. The XRD patterns of MMT, PLA, 3MMT/PLA, 20PEG/PLA, and 3MMT/20PEG/PLA are shown in Fig. 3. Characteristic

peak of MMT was observed at 2θ equal to 6.12° which corresponded to a basal spacing of 1.44 nm, according to Bragg's law ($n\lambda = 2d \sin\theta$). For semi-crystalline polymer PLA characteristic peaks of crystalline phase appear at 2θ equal to 16.5° and 19° along with the nearby broaden peak of amorphous phase [8]. With the addition of MMT into PLA matrix, XRD pattern of 3MMT/PLA nanocomposite showed additional peaks at 2θ equal to 6.12°,16.5°, and 19° while XRD peak of MMT (2θ equal to 6.12°) was not shifted. Note that, a peak intensity of PLA crystalline phase appears at 2θ equal to 16.5° of 3MMT/PLA significantly increased as compared to those of PLA. These indicated that MMT formed unexfoliated agglomerates and polymer chains could not penetrated between MMT layers [9]. Moreover, the MMT layers may be increased the nucleation density of the PLA led to its crystalline phase was increased as reported previously for DSC part. Blending PLA with 20 wt% PEG, intensity of PLA crystalline phase seemed slightly decreased as compared to those of PLA. These could plausibly be due to plasticizing effect of PEG which caused molecular structure of PLA to align perpendicular to helical chain direction, led to the reduction of the crystallinity of PLA [10]. For the 3MMT/20PEG/PLA, the XRD peak of MMT was not clearly observed. This may be because the small segmental mobility of PEG assisted the MMT particles in more dispersed into PLA.

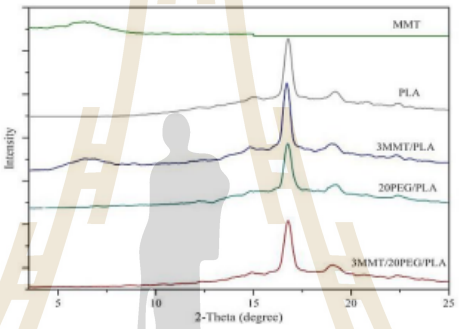

FIGURE 3. XRD patterns of MMT, PLA, 3MMT/PLA, 20PEG/PLA, and 3MMT/20PEG/PLA.

From the DSC results, the T_g of all samples can be observed in range of 47 to 55°C. Therefore, the thermal recovery test was performed by selected T_{trans} of 65°C on the PLA, PEG/PLA, and MMT/20PEG/PLA films, which result in Table 2 and the photographs of the shape recovery behaviors are shown in Fig. 4. PLA film possessed the highest shape recovery ratio of 98.2 %. With the addition PEG, the shape recovery ratio of plasticized PLA films significantly decreased as compared with that of PLA. The results might be reasoned that the presence of PEG decreased the tensile modulus of plasticized PLA. The modulus is known to be associated to shape fixity phase of SMPs. Thus, the shape memory performance can be suffered if the modulus decreases. However, the shape recovery ratio of 20PEG/PLA showed the highest value of PEG/PLA blends. This suggested that the lowest T_g of 20PEG/PLA facilitated the polymer chains in amorphous phases of PLA to be oriented easily, which consequently offered the strong driving force for recovered to its initial shape. With the addition of MMT into plasticized PLA, the shape recovery ratio of MMT/20PEG/PLA films were greater than 20PEG/PLA film. This is because the restriction effect of MMT resulted in higher orientation of PLA chains, leading to the increment of shape recovery ratio from 93.3% of 20PEG/PLA to 98% of 1MMT/20PEG/PLA films [4].

TABLE 2. Shape recovery tests of PLA, PEG/PLA blends and MMT/PEG/PLA nanocompositesfinal key points to consider

Sample	Recovery ratio (%)
PLA	98.2
10PEG/PLA	56.1
15PEG/PLA	81.7
20PEG/PLA	93.3
30PEG/PLA	88.9
40PEG/PLA	87.2
1MMT/20PEG/PLA	98.0
3MMT/20PEG/PLA	97.2

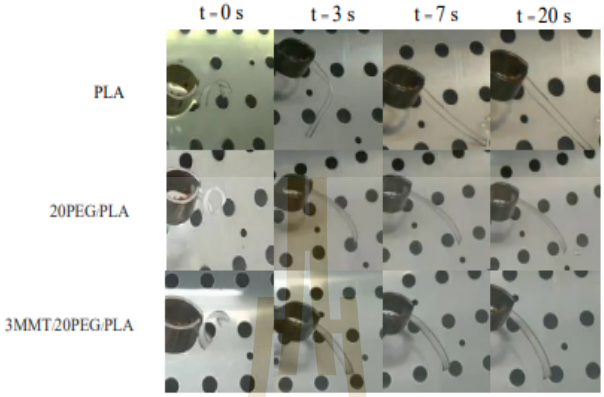

FIGURE 4. Photographs of the shape recovery behaviors of PLA, 20PEG/PLA, and 3MMT/20PEG/PLA films in a water bath at 65 °C.

CONCLUSIONS

Shape memory films of PLA, its blends, and its nanocomposites have been investigated. PEG was incorporate into PLA to moderate the brittleness and high T_g of PLA. The contents of PEG were varied from 10 to 40 wt%. Ductility of PLA film was significantly improved with increasing the percentage of PEG. The elongation at break of PLA blends increase about 20 times after adding PEG of 10 and 15 wt%. The T_g of plasticized PLA with 20wt% PEG possessed the lowest T_g of 47°C. While an incorporation of MMT into 20PEG/PLA was founded to increase the T_g of 3MMT/20PEG/PLA because MMT particles may cause chain restriction. In shape memory test result, most of samples obtained high recovery ratio reflected the excellent ability to recover from the temporary shape to the permanent shape. Moreover, the introduction of MMT can increase the shape recovery ratio from 93.3% of 20PEG/PLA to 98% of 1MMT/20PEG/PLA.

REFERENCES

1. J. Xu, J. Song, in Shape Memory Polymers for Biomedical Applications. 197-217 (2015).
2. Y. Guo, J. Ma, Z. Lv, N. Zhao, L. Wang, Q. Li, J. Mat. Re. **33**, 23, 4101-4112 (2018).
3. J. Liu, K. Zhou, P. Wen, B. Wang, Y. Hu, Z. Gui, Polym. Adv. Tech. **26**, 6, 626-634 (2015).
4. L. Fu, F. Wu, C. Xu, T. Cao, R. Wang, S. Guo, Indus. & Eng. Chem. Re. **57**, 18, 6265-6274 (2018).
5. S. Lashgari, M. Karrabi, I. Ghasemi, H. Azizi, M. Messori, K. Paderni, Express Polym. Lett. **10**, 4, 349-359 (2016).
6. S. Raghunath, S. Kumar, S. K. Samal, S. Mohanty, S. K. Nayak, J. Polym Re. **25**, 5 (2018).
7. Y.-F. Huang, P.-C. Wang, J.-H. Lee, J.-Y. Lee, H.-J. Liu, Polym.-Plas. Tech. Eng. **54**, 4, 433-439 (2015).
8. S. Dadashi, S.-M. Mousavi, Z.-E. Djomeh, A. Oromiehie, Int. J. Nanosci. Nanotechnol. **10**, 4 (2014).
9. E. Picard, E. Espuche, R. Fulchiron, Appl. Clay Sci. **53**, 1, 58-65 (2011).
10. K.-M. Choi, S.-W. Lim, M.-C. Choi, D.-H. Han, C.-S. Ha, Macro. Re. **22**, 12, 1312-1319 (2014).

polymers

MDPI

Article

Role of Maleic Anhydride-Grafted Poly(lactic acid) in Improving Shape Memory Properties of Thermoresponsive Poly(ethylene glycol) and Poly(lactic acid) Blends

Wasana Nonkrathok [1], Tatiya Trongsatitkul [1,2,3,*] and Nitinat Suppakarn [1,2,4,*]

[1] School of Polymer Engineering, Institute of Engineering, Suranaree University of Technology, Nakhon Ratchasima 30000, Thailand
[2] Research Center for Biocomposite Materials for Medical Industry and Agricultural and Food Industry, Suranaree University of Technology, Nakhon Ratchasima 30000, Thailand
[3] Center of Excellence in Biomechanics Medicine, Suranaree University of Technology, Nakhon Ratchasima 30000, Thailand
[4] Center of Excellence in Microbial Technology for Agricultural Industry, Suranaree University of Technology, Nakhon Ratchasima 30000, Thailand
* Correspondence: tatiya@sut.ac.th (T.T.); nitinat@sut.ac.th (N.S.)

Abstract: Generally, poly(ethylene glycol) (PEG) is added to poly(lactic acid) (PLA) to reduce brittleness and improve mechanical properties. However, shape memory properties of PEG/PLA blends suffered due to the blend's incompatibility. To enhance shape memory abilities of the blends, 0.45% maleic anhydride-grafted poly(lactic acid) (PLA-*g*-MA) was used as a compatibilizer. Thermal and mechanical properties, morphologies, microstructures, and shape memory properties of the blends containing different PLA-*g*-MA contents were investigated. The compatibilized blend with 2 wt% PLA-*g*-MA exhibited enhanced tensile modulus, strength, and elongation at break, as well as a lower glass transition temperature and degree of crystallinity than the uncompatibilized blend. Results revealed that PLA-*g*-MA improved interfacial adhesion between phases and promoted chain entanglement. Shape fixity performance of the compatibilized blends were comparable to that of neat PLA. The compatibilized blend containing 2 wt% PLA-*g*-MA possessed the best shape fixity and recovery performance. Although a high recovery temperature was expected to enhance the recovery of the PEG/PLA blends, the compatibilized blends can be recovered to their original shape at a lower temperature than the PLA. This study illustrated the possibility of optimizing PLA properties to meet requirements necessary for biomedical applications.

Keywords: poly(lactic acid); poly(ethylene glycol); shape memory polymer; compatibilizer

Citation: Nonkrathok, W.; Trongsatitkul, T.; Suppakarn, N. Role of Maleic Anhydride-Grafted Poly(lactic acid) in Improving Shape Memory Properties of Thermoresponsive Poly(ethylene glycol) and Poly(lactic acid) Blends. *Polymers* **2022**, *14*, 3923. https://doi.org/10.3390/polym14183923

Academic Editors: Rui A. S. Moreira and Mónica Oliveira

Received: 3 August 2022
Accepted: 10 September 2022
Published: 19 September 2022

1. Introduction

Shape memory polymers (SMPs) have attracted considerable attention over the last decades due to their light weight, ease of fabrication, and ability to retain their initial shape in the presence of a stimulus. They can be formed into the temporary shape and then restored to their permanent shape in response to an external stimulus [1–4], such as heat [5,6], light [7], electrical field [8], magnetic field [9], pH [10], solvent [11], etc. Polymeric materials, in general, undergo a noticeable change in physiochemical properties as a function of temperature. As a result, thermally induced SMPs are the most common and extensively studied [5,6]. These SMPs can be triggered directly by heat, such as hot gas or warm water.

SMPs are typically comprised of two components: a hard segment and a soft segment. The hard segment acts as netpoints that memorize the permanent shape via physical or chemical cross-linking. The soft segment, also known as the reversible phase, acts as a switch, allowing the molecular chains to temporarily deform and is responsible for the shape recovery process [12]. A temporary shape of SMPs is achieved through applying mechanical force,

while heating above its transition temperature (T_{trans}), i.e., glass transition (T_g) or melting temperature (T_m) of the reversible part, which is referred to as programming temperature (T_p). The deformed shape is maintained upon cooling down. The restoration of the permanent shape can be achieved by reheating above T_{trans} (called recovery temperature (T_r)) [13–16].

Poly(lactic acid) (PLA) is a well-known biodegradable polyester with a wide range of applications, particularly in medical fields, due to its good mechanical strength, high biocompatibility, and nontoxicity [17,18]. Furthermore, several studies have revealed the use of PLA as a shape memory material with triggering temperatures close to its T_g of about 60 °C. At temperatures below its T_g, PLA can be programmed into a temporary shape, and it returns almost entirely to its original shape at temperatures above its T_g [19–21]. However, PLA still has some drawbacks such as brittleness, and high T_g, which may cause tissue damage in humans when used in some medical applications [22,23].

The addition of plasticizers is an interesting approach for tuning T_g and reducing the brittleness of PLA [24]. Poly(ethylene glycol) (PEG) is considered as an effective plasticizer for PLA due to its miscibility, biodegradability, and nontoxicity. Many research groups investigated the properties of PLA blended with PEG of molecular weights ranging from 1000 to 20,000 g/mol [25–31]. In general, the addition of PEG to PLA decreases T_g and increases elongation at break. Nonetheless, low molecular weight PEG has a tendency to migrate from the PLA matrix or evaporate during the process, and a PLA-PEG phase separation occurs when the PEG content exceeds a certain threshold. In addition, Guo et al. [28] reported that shape memory properties of PEG/PLA blends were marginally reduced when the PEG content was increased to 15 wt%, but significantly reduced when the PEG content was increased to 20 wt%. This was due to phase separation, which occurred in particular at a PEG content of 20 wt%.

Compatibility between two polymer components has a significant impact on the properties of a polymer blend and can be enhanced by introducing block or grafted copolymers with segments capable of physical or chemical interacting with the blend components [32,33]. Several studies have reported the use of maleic anhydride-grafted on polymer matrix as a compatibilizer to improve the compatibility of polymer blends [34–37]. Hwang et al. [35] studied effect of the maleic anhydride and DCP concentrations on the grafting and the properties of PLA. They found that T_g and percent crystallinity of the PLA decreased, but its mechanical properties remained unchanged. Hassouna et al. [36] investigated effect of low molecular PEG (MW = 400 g/mol) and maleic anhydride-grafted PLA (PLA-*g*-MA) copolymer on the ductility of PLA blends. Their findings revealed that the T_g of the PLA blend containing 20 wt% PEG decreased to 23 °C when compared to the T_g of the neat PLA at 60 °C. They also found that adding 10 wt% PLA-*g*-MA reduced the T_g of the PEG/PLA blend to 14 °C. In addition, Kim et al. [37] found that increasing the compatibility between two polymer phases enhanced the mechanical properties of the system as well as its shape memory behaviors. In their research, styrene–acrylonitrile-maleic anhydride (SAN-MAH) copolymer was used as a compatibilizer for poly(lactic acid) (PLA) and poly(methyl methacrylate-block-n-butyl acrylate-block-methyl methacrylate) (80/20) (PLA/Poly(MnBM)) blend. The shape recovery ratios for the PLA/Poly(MnBM) blends with and without the addition of 1 wt% SAN-MAH were 83 and 56%, respectively. Although the maleic anhydride-graft-poly(lactic acid) (PLA-*g*-MA) has been studied for its effect as a compatibilizer on the physical properties of PEG/PLA blends, the shape memory performance of the compatibilized materials has not yet been investigated.

In this study, we investigated the effect of the PLA-*g*-MA, used as a compatibilizer on shape memory abilities of PEG/PLA (10/90) blends. Our hypothesis was that by increasing the compatibility of PEG and PLA matrix, shape memory properties of the PEG/PLA blends such as shape recovery ratio (R_r), shape fixity ratio (R_f), and recovery rate would be improved. Additionally, thermal and mechanical properties, morphologies, and microstructures of the PEG/PLA blends containing different PLA-*g*-MA contents were respectively studied by differential scanning calorimetry (DSC), tensile test, scanning electron microscopy (SEM), and in situ synchrotron small-angle X-ray scattering and wide-angle X-ray scattering (SAXS and WAXS) microscopies.

2. Experimental

2.1. Materials

A semi-crystalline poly(lactic acid) (PLA) with a 4% D-isomer content, under the trade name Ingeo™ biopolymer PLA, was purchased from Nature Works LLC (Minnetonka, MN, USA). Poly(ethylene glycol) (PEG) with a molecular weight of 4000 g/mol was supplied by Dow Chemical Company (Midland, MI, USA). Maleic anhydride (MA) was purchased from Loba Chemie Pvt. Ltd. (Mumbai, Maharashtra, India). Dicumyl peroxide (DCP) was purchased from Sigma-Aldrich Co., LLC (Burlington, MA, USA). Maleic anhydride-grafted poly(lactic acid) (PLA-*g*-MA) was prepared in house using PLA, MA and DCP.

2.2. Preparation of PLA-g-MA and PEG/PLA Blends

To prepare PLA-*g*-MA and PEG/PLA blends, a twin-screw extruder (Charoen Tut Model CTE-D16L32, Samutprakarn, Thailand) (L/D = 32) with a die diameter of 3 mm was used. The extruder temperature profile, from the feed throat to the die, was 50/160/180/180/180/180/175 °C. The screw speed used was 80 rpm (r/min). Rod extrudates were cooled by air and cut into small pellets using a pelletizer.

The PLA-*g*-MA compatibilizer was synthesized by grafting of poly(lactic acid) with maleic anhydride via reactive extrusion using the twin-screw extruder. PLA, DCP (1 phr), and MA (5 phr) were pre-mixed before being fed into the extruder. The obtained PLA-*g*-MA pellets were dried at 100 °C under a vacuum for 4 h to remove any unreacted MA.

To investigate influence of the compatibilizer on properties of the PEG/PLA blends, PLA and 10 wt% PEG, designated as PEG/PLA, were mixed with various PLA-*g*-MA contents, i.e., 2, 6 and 10 wt%. The samples were named according to the weight percentages of PLA-*g*-MA in the blends. For example, the PEG/PLA blend containing PLA-*g*-MA of 2 wt% was named 2PMA/PEG/PLA.

All test specimens were compressed molded at 175 °C for 10 min under a pressure of 100 MPa in a compression molding machine (LabTech Model LP20-B, Samutprakarn, Thailand) being allowed to cool at room temperature.

2.3. Characterizations of PLA-g-MA

The proportion of maleic anhydride grafted to PLA was determined using the titration technique. The dried PLA-*g*-MA sample was purified prior to use. At room temperature, the sample was dissolved in chloroform (RCI Labscan, Bangkok, Thailand) and magnetically stirred at 350 rpm to obtain a homogeneous solution. Methanol (RCI Labscan, Bangkok, Thailand) was then gradually added to the solution to re-precipitate it. Purified PLA-*g*-MA was filtered and dried in a vacuum at 80 °C for 4 h. To determine the amount of maleic anhydride grafted to PLA, the purified PLA-*g*-MA was dissolved in chloroform and titrated with methanolic potassium hydroxide (QREC, Chon Buri, Thailand) solution (KOH). The percentage of grafted maleic anhydride was calculated using Equation (1).

$$\%\text{MA}\ (\%) = \frac{(N_{KOH} \times V_{KOH} \times 98.06)}{2W_{sample}} \times 100 \quad (1)$$

where N_{KOH} is the normality of KOH (mol/L); V_{KOH}, the volume of KOH (mL); W_{sample}, the weight of sample (g); and the molecular weight of maleic anhydride is 98.06 g/mol.

Fourier transform infrared (FT-IR) (Bruker Tensor 27, Billerica, MA, USA) spectrometer with an attenuated total reflection (ATR) accessory was used to identify functional groups of PLA and PLA-*g*-MA. Spectrum of a sample was recorded in a wavenumber range of 4000 to 400 cm^{-1} with a resolution of 2 cm^{-1} and a number of scans of 64.

2.4. Characterizations of PEG/PLA Blends

2.4.1. Tensile Testing

Tensile testing was carried out on a universal testing machine (UTM) (Instron 5565 Model, Norwood, MA, USA) with a load cell of 5 kN and a cross head speed of 10 mm/min. The

test specimens were prepared in accordance with the ASTM D 638 standard (Type V). At least five specimens were tested, and the average value was reported.

The data from of the tensile test were statistically analyzed using IBM SPSS Statistic, version 24.0. (Armonk, NY, USA). The data was evaluated using one-way ANOVA and Turkey's post hoc comparison test on three replication values ($n = 3$) from five examined specimens. To identify statistical differences between the comparison groups, the level of statistical significance was set at $p < 0.5$.

2.4.2. Thermal Characteristics

Thermal characteristics i.e., glass transition temperature (T_g), crystallization temperature (T_c), cold crystallization temperature (T_{cc}), melting temperature (T_m), and crystallinity (X_c) of specimens, before and after stretching, were determined using a differential scanning calorimeter (DSC) (Perkin Elmer, Waltham, MA , USA). To compare their actual thermal properties, unstretched and stretched samples were subjected to a single heating step between 25 and 200 °C at a rate of 10 °C/min under a nitrogen atmosphere. The crystallinity (X_c) of each sample was estimated using the following Equation (2):

$$X_c(\%) = \left(\frac{\Delta H_m - \Delta H_{cc}}{\omega \Delta H_m^o}\right) \times 100 \quad (2)$$

where ΔH_m and ΔH_{cc} are the enthalpies of melting and cold crystallization, respectively. ω is the weight fraction of PLA and ΔH_m^o is melting enthalpy of 100% crystalline PLA (93.7 J/g) [38].

2.4.3. Morphology

Morphologies of the PEG/PLA blends were analyzed by using a scanning electron microscope (SEM) (JEOL JSM-6010LV, Peabody, MA, USA) at a voltage of 5 kV. Samples were cryo-fractured in liquid nitrogen and coated with gold for 3 min to ensure suitable electrical conductivity.

2.4.4. Shape Memory Behaviors

Shape memory behaviors of the PEG/PLA blends were quantified using two parameters, R_f and R_r. The shape fixity ratio (R_f) quantifies the ability of a specimen to fix temporary deformations that occur during the programming process. The shape recovery ratio (R_r) measures how well a specimen can return to its original shape.

Shape memory tests were performed using a universal testing machine (UTM) (Instron 5569 Model, Norwood, MA, USA) equipped with a heating chamber. The following steps were performed: (1) The specimen with an initial length of L_0 was heated to a constant programming temperature (T_p) and maintained at that temperature for 5 min. It was then stretched to a specified% strain at a constant strain rate of 10 mm/min. (L_1). This constraint was maintained while the specimen was quenched with an ice pack. (3) After removing the specimen from the test equipment, it was kept at room temperature for 24 h (L_2). (4) The stretched specimens were immersed in a water bath at a specific recovery temperature (T_r) to observe the recoverability of the specimen (L_3). The test specimen collected at each stage of the shape memory test is illustrated in Figure 1. Tests were done on at least five specimens from each experimental condition. Shape recovery ratio (R_r) and shape fixity ratio (R_f) values of the specimens were determined as follows [39]:

$$R_r(\%) = \left(\frac{L_2 - L_3}{L_2 - L_0}\right) \times 100 \quad (3)$$

$$R_f(\%) = \left(\frac{L_2}{L_1}\right) \times 100 \quad (4)$$

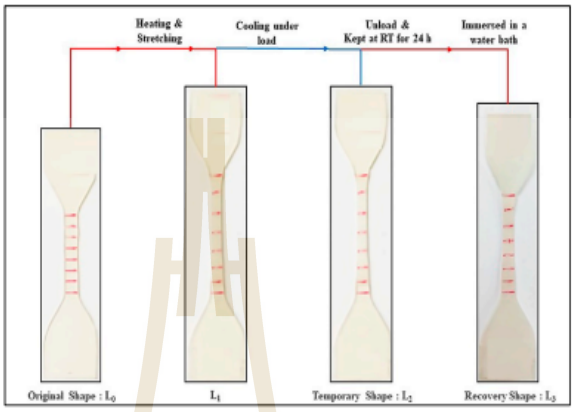

Figure 1. Diagram of a test specimen at different stages of the shape memory test.

The effects of compatibilizer concentration, and recovery temperature (T_r) on the shape memory properties of PEG/PLA blends were investigated. To determine the effect of compatibilizer concentration, the specimens were stored at T_p of 45 °C and recovered at T_r 60 °C. To examine the effect of recovery temperature, specimens were kept at T_p of 45 °C before being immersed in a water bath at 40, 50 and 60 °C to observe their recoverability.

2.4.5. Stress Relaxation Test

Stress relaxation test was conducted with the assistance of a Dynamic mechanical analyzer (DMA) (NETZSCH GABO EPLEXOR® Serie ultra-high, Ahlden, Germany). The dimensions of a test specimen were 10 mm × 4 mm × 1.0 mm. Each specimen was kept at 45 °C for 5 min. It was then stretched to 100% strain at a rate of 10 mm/min. The tension was maintained throughout the experiment, and the stress reduction was plotted against time.

2.4.6. Microstructure Evaluation

In situ Small-angle X-ray scattering and wide-angle X-ray scattering (SAXS/WAXS) measurements using BL1.3W beamline of Synchrotron Light, was applied to study microstructure evolution of specimens during shape memory test including the initial state, after heating, after stretching, and after recovery. X-ray energy of 9 keV (λ = 1.38 Å) was applied with the exposure duration of 60 s. q-range for SAXS measurement was 0.04–0.7 nm^{-1}. The specimen-to-detector distances for WAXS and SAXS measurements were 0.24 and 5.18 m, respectively. WAXS and SAXS scattering data were processed by using the SAXSIT4.41 software (Synchrotron Light Research Institute, Nakhon Ratchasima, Thailand).

3. Results and Discussion

3.1. Characterizations of PLA-g-MA

PLA-*g*-MA was synthesized through reactive blending to be utilized as a compatibilizer for PLA and PEG. Its grafting MA content was determined using titration technique, and the value was 0.45 wt%. The PLA-*g*-MA grafting reaction was also confirmed by FTIR, as shown in Figure 2. Due to the small amount of MA that has reacted with PLA chains, Figure 2a reveals minimal differences between the FTIR spectra of PLA and PLA-*g*-MA in the wavenumber range 2000–600 cm^{-1}. The symmetrical carbonyl (C=O) stretching peak of PLA-*g*-MA around 1750 cm^{-1}, in Figure 2b, shows a slight shift, peak broadening, and enhanced intensity in comparison to the C=O stretching peak of the neat PLA. This was due to the superposition of the C=O peaks of MA and PLA. Additionally, in Figure 2c, PLA-*g*-MA spectrum exhibits additional, broadening absorption bands in the

range of 1885–1850 cm^{-1} as compared with those of the neat PLA. These corresponded to the asymmetric C=O stretching of the anhydride group of MA [35,36]. The results revealed the presence of reactive carbonyl groups of anhydrides in PLA-*g*-MA, which could indicate the occurrence of a PLA-*g*-MA grafting reaction.

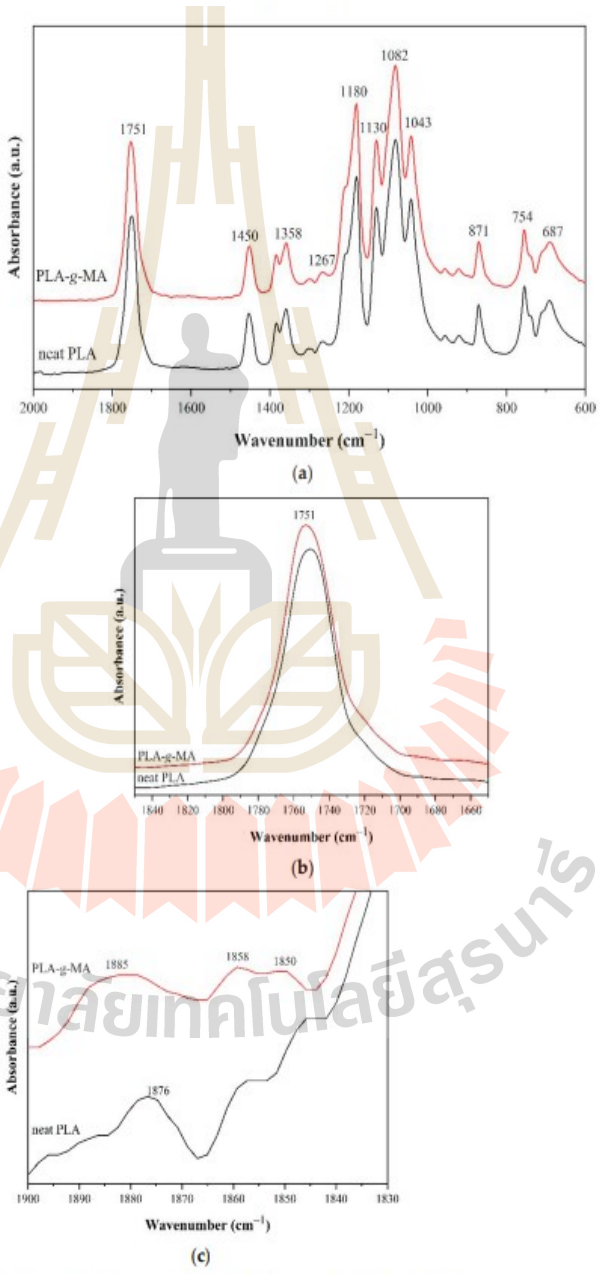

Figure 2. FTIR spectra of neat PLA and PLA-*g*-MA. (**a**) wavenumber range 2000–600 cm^{-1} (**b**) wavenumber range 1840–1660 cm^{-1} (**c**) wavenumber range 1900–1830 cm^{-1}.

3.2. *Tensile Properties of PLA and PEG/PLA Blends with Various PLA-g-MA Contents*

The stress-strain curves and summary of tensile properties of neat PLA and PEG/PLA blends with/without compatibilizer are shown in the Figure 3 and Table 1, respectively. As seen in Figure 3, neat PLA showed a brittle failure behavior. It possessed the highest Young's modulus of 0.7 GPa and yield strength of 61.38 MPa, but very low elongation at break of 12.97%. The brittleness of PLA makes it unsuitable to be used for any shape memory application. By combining PLA with PEG, the ductility of the PLA was strengthened. The stress-strain curves of the uncompatibilized PEG/PLA blend exhibited a greater degree of plastic deformation than that of neat PLA. The breaking strain increased to up to 477%. Its Young's modulus and yield strength expectedly decreased to 0.49 GPa and 40.22 MPa, respectively. This was the result of the plasticizing effect of PEG that allowed higher PLA chain mobility [28].

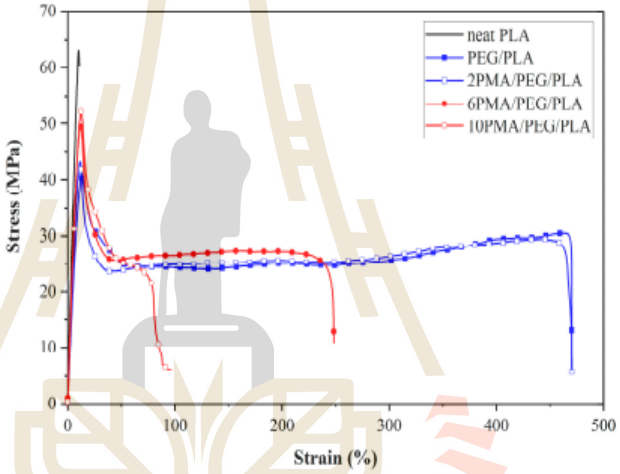

Figure 3. Stress-strain curves of PLA and PEG/PLA blends with various PLA-*g*-MA contents.

Table 1. Summarized tensile properties of PLA and PEG/PLA blends.

Sample	Tensile Strength [MPa]	Young's Modulus [GPa]	Elongation at Break [%]
neat PLA	61.38 ± 1.24 #	0.70 ± 0.02 #	12.97 ± 0.92 #
PEG/PLA	40.22 ± 0.60 *	0.49 ± 0.01 *	477.01 ± 62.03 *
2PMA/PEG/PLA	45.04 ± 1.32 *,#	0.53 ± 0.01 *,#	475.51 ± 88.87 *
6PMA/PEG/PLA	48.07 ± 0.90 *,#	0.55 ± 0.01 *,#	205.23 ± 73.74 *,#
10PMA/PEG/PLA	50.15 ± 1.53 *,#	0.56 ± 0.01 *,#	74.74 ± 11.78 #

* $p < 0.05$, compared with the neat PLA. # $p < 0.05$, compared with the PEG/PLA.

The addition of PLA-*g*-MA increased Young's modulus and tensile strength of the compatibilized PEG/PLA blends, and the values increased with increasing PLA-*g*-MA content. The change in elongation at break of the 2PMA/PEG/PLA was statistically insignificant as compared to that of the uncompatibilized PEG/PLA. The results suggested that the existence of 2 wt% PLA-*g*-MA increased the compatibility of the PLA and PEG phases. The enhanced compatibility steamed from the grafting reaction between the anhydride groups of MA and hydroxyl groups of PLA similar to that reported by Hassouna et al. [36]. This interaction enhanced the interfacial adhesion by improving stress transfer around the interface, resulting in an increase in tensile strength while elongation at break remain unchanged. As PLA-*g*-MA concentrations increased up to 10 wt%, the elongation at break of the 6PMA/PEG/PLA and 10PMA/PEG/PLA significantly dropped. The plausible

explanation was that an excess of PLA-*g*-MA was oversaturated at the interface. PLA-*g*-MA coalescence may form, consequently causing the decline of interfacial tension between the polymer components in the blend [40,41]. Similar findings were reported by Tang et al. [40] in the system of ethylene terpolymer as a compatibilizer of poly(ethylene terephthalate) (PET) and high-density polyethylene (HDPE) blends, and Liu et al. [41] in the system of maleated thermoplastic elastomer as a compatibilizer of polypropylene (PP)/polyamide-6 (PA6) blends.

3.3. Thermal Behaviors of PLA and PEG/PLA Blends with Various PLA-g-MA Contents

In this study, DSC technique was used to investigate the changes in thermal properties of the PLA and PEG/PLA blends at different stages of the shape memory test. This included testing the "unstretched sample" from the original shape specimen (L_0) and the "stretched sample" from the temporary shape specimen (L_2). Figure 4 depicts DSC thermograms of PLA and PEG/PLA blends in their unstretched and stretched states, and Table 2 is a summary of their thermal properties.

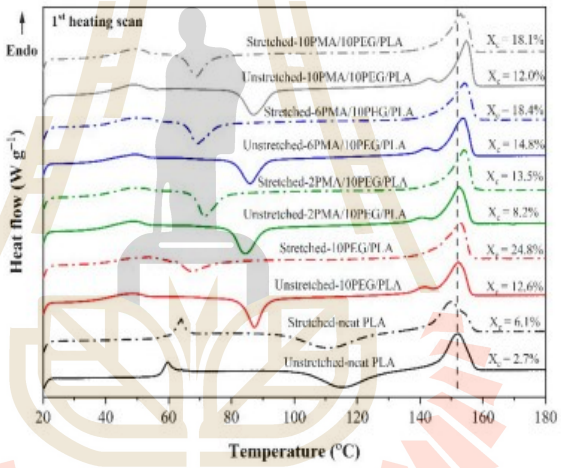

Figure 4. DSC thermograms of PLA and PEG/PLA blends in their unstretched and stretched states. Vertical line is used as a visual guideline for the shift of melting peak of the samples.

Table 2. Summarized DSC results of PLA and PEG/PLA blends in their unstretched and stretched states.

Sample	T_g [°C]	T_{cc} [°C]	$-\Delta H_{cc}$ [J/g]	T_m [°C]	ΔH_m [J/g]	Normalized X_c [%]
Unstretched-PLA	58.3	115.5	24.9	152.3	27.4	2.7
Unstretched-PEG/PLA	40.3	87.2	15.3	152.2	25.9	12.6
Unstretched-2PMA/PEG/PLA	41.6	84.4	18.4	152.4	25.2	8.2
Unstretched-6PMA/PEG/PLA	41.8	85.9	16.3	153.7	28.1	14.8
Unstretched-10PMA/PEG/PLA	42.3	87.1	18.0	154.9	29.3	12.0
Stretched-PLA	62.2	110.7	21.3	149.9	26.9	6.1
Stretched-PEG/PLA	43.8	67.5	8.6	152.8	29.5	24.8
Stretched-2PMA/PEG/PLA	41.8	71.3	16.7	154.1	27.9	13.5
Stretched-6PMA/PEG/PLA	42.6	69.0	13.0	154.2	27.7	18.4
Stretched-10PMA/PEG/PLA	42.8	68.8	12.4	153.2	29.4	18.1

DSC thermogram of the neat, unstretched PLA showed T_g and cold crystallization temperature (T_{cc}) at 58.3 °C and 115.5 °C, respectively. Because of the presence of 10 wt% PEG, the T_g and T_{cc} of the unstretched, uncompatibilized PEG/PLA were reduced to

40.3 °C, and 87.2 °C, respectively. This finding was the evidence of the plasticizing effect of PEG which enhanced polymer chain mobility and thus promoted PLA crystallization [28]. The addition of plasticizer also affected the crystal formation as the change of PLA melting peak was observed. The unstretched, uncompatibilized PEG/PLA exhibited a small endothermic peak at a temperature slightly below the main PLA melting peak, which was not present in the unstretched PLA. The small endothermic peak was attributed to the melting of PLA α′-crystals, while the main melting peak at 152.2 °C was attributed to the melting of PLA α-form crystals [42]. Moreover, the crystallinity (X_c) of the PEG/PLA increased to 12.6% which was significantly higher than that of the PLA, which was just 2.7%.

When PLA-*g*-MA was added to the blends, the T_g values of the unstretched, compatibilized blends showed a slight upward trend as PLA-*g*-MA content increased. At 2 wt% PLA-*g*-MA loading, the T_{cc} value of the unstretched 2PMA/PEG/PLA decreased to 84.4 °C (from 87.2 °C of that of the uncompatibilized PEG/PLA) with no shift of the main T_m peak (152.4 °C). In addition, the X_c of the unstretched 2PMA/PEG/PLA was decreased to 8.2%, as compared to that of the uncompatibilized PEG/PLA (X_c = 12.6%). As the amount of PLA-*g*-MA was increased above 2 wt%, the T_{cc} and T_m of the compatibilized blends shifted to higher temperatures and the X_c of the 6PMA/PEG/PLA and 10PMA/PEG/PLA increased to 14.8% and 12%, respectively. This indicated that the addition of PLA-*g*-MA affected the lamellar structures of the compatibilized blends [37]. The addition of 2 wt% PLA-*g*-MA may improve the interfacial adhesion of the 2PMA/PEG/PLA, as a result of increased interfacial chain entanglement. This probably reduced the chain mobility of the PLA hence restricting crystallization [40]. However, as the PLA-*g*-MA content exceeded 2 wt%, the X_c of the compatibilized blends rose once again. This could be attributed to the PLA-*g*-MA coalescence serving as a nucleating agent in the compatibilized blends [41]. The DSC results were consistent with the tensile properties of the compatibilized blends that the elongation at break of the 6PMA/PEG/PLA and 10PMA/PEG/PLA significantly dropped as compared to that of the 2PMA/PEG/PLA.

In a separate experiment, DSC technique was also used to study effect of stretching on thermal properties and crystallinity of neat PLA and PEG/PLA blends. The test specimens were extended to 100% strain at 45 °C during the shape programming process then rapidly cooled down using ice packs. In the case of the neat PLA as shown in Figure 4, stretching caused an increase in T_g to 62.2 °C and a decrease in T_{cc} to 110.7 °C. In addition, the shape of the melting peak of the stretched PLA altered, and its T_m decreased to 149.9 °C while its X_c increased to 6.1%. This indicated that rapid PLA recrystallization and crystal disaggregation occurred when the specimen was extended at 45 °C, resulting a higher number of crystals [43].

The T_g of all stretched PEG/PLA blends, with and without PLA-*g*-MA, increased marginally. In comparison to their unstretched states, the stretching caused significant decreases in their T_{cc} and cold crystallization enthalpy (ΔH_{cc}), whereas their crystallinity increased significantly. Moreover, all the stretched PEG/PLA blends showed a single endothermic peak, as opposed to the bimodal T_m peaks found in their unstretched states. Upon heating and stretching, crystallization occurred at a greater degree as the condition was more favorable for crystal formation. Furthermore, the recrystallization fully turned α′-form to α-form crystals after stretching [42], as evidently shown by an increase in the crystallinity and the altered shape of the melting peaks of the stretched PEG/PLA blends.

3.4. Morphologies of PLA and PEG/PLA Blends with Various PLA-g-MA Contents

Morphologies of PLA and PEG/PLA blends with various PLA-*g*-MA contents were examined using SEM. The results are shown in Figure 5. The SEM micrograph of the neat PLA in Figure 5a reveals a smooth surface of the cross-sectional area, whereas the micrograph of the uncompatibilized PEG/PLA in Figure 5b reveals a rough surface. The PEG minor phase dispersed in the continuous matrix of PLA in a non-spherical form without distinctive boundary or voids. This indicated the partial miscibility of the two polymers in the system. Several studies have found that PLA blended with PEG with a molecular

weight of 1000–10,000 g/mol was found to be partially miscible at the critical PEG content of 10 wt% and became immiscible at the PEG content above 10 wt% [28,30,31]. The addition of 2 wt% PLA-*g*-MA caused no effect on the morphology of the 2PMA/PEG/PLA. However, as the compatibilizer content increased up to 6 wt% (Figure 5d), some agglomerations were observed in the morphology of the 6PMA/PEG/PLA. This could be the coalesces of the excess compatibilizer that led to the diminish in an interfacial interaction as mentioned in the tensile result. At the 10 wt% PLA-*g*-MA, in Figure 5e, the surface topography of the 10PMA/PEG/PLA showed a higher degree of agglomeration, with the microvoids easily visible. It can be inferred that when the compatibilizer content exceeded 2 wt%, there was a decline in the compatibility of the PEG/PLA blends. The schematic diagram of PEG/PLA blends with various PLA-*g*-MA contents is shown in Figure 6.

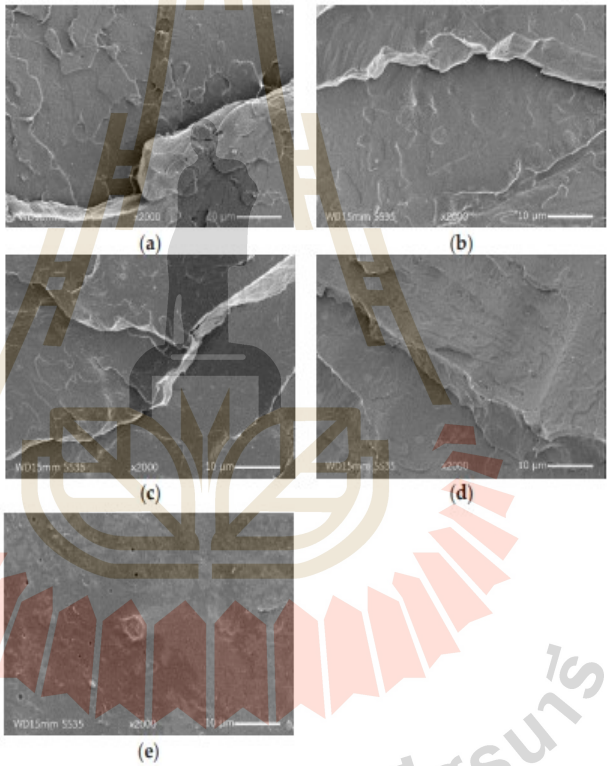

Figure 5. SEM micrographs of cryogenically fracture surfaces of (**a**) neat PLA, (**b**) PEG/PLA, (**c**) 2PMA/PEG/PLA, (**d**) 6PMA/PEG/PLA and (**e**) 10PMA/PEG/PLA.

3.5. Shape Memory Behaviors of PLA and PEG/PLA Blends

The shape memory mechanism of the PEG/PLA blends can be explained by the work of the two major components in the system: i.e., switching phase or soft segment and fixing phase or hard segment. PEG and PLA chains in an amorphous region act as a switching phase. Physical chain entanglement and crystal of the blend act as netpoints or a fixity phase. In order to obtain highest shape fixity and shape recovery, the polymer chains in the amorphous phase must store the applied energy during the temporary shaping as much as possible. This could be possible if higher number of netpoints in the amorphous phase were available.

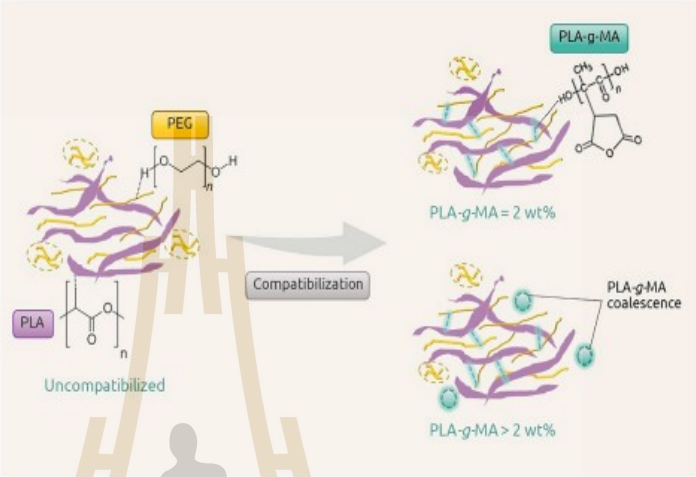

Figure 6. Schematic diagram for interaction between PLA, PEG, and PLA-*g*-MA.

3.5.1. Shape Memory Behaviors of the PLA and PEG/PLA Blends with Various PLA-*g*-MA Contents

Shape recovery (R_r) and fixity (R_f) ratios of neat PLA and PEG/PLA blends with various PLA-*g*-MA contents are shown in Figure 7. In this experiment, the programming and recovery temperatures were 45 and 60 °C, respectively, since these temperatures were slightly higher than T_g of the PEG/PLA blends.

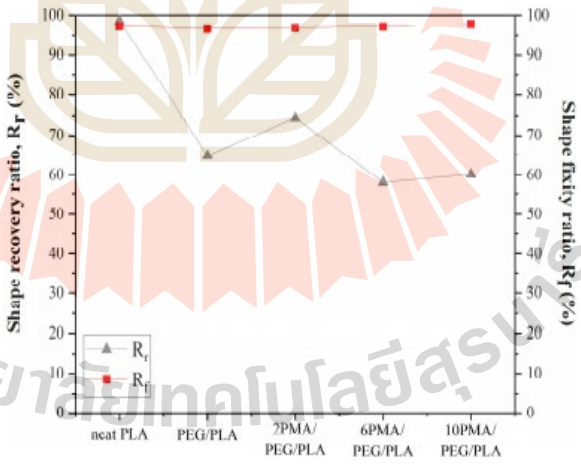

Figure 7. Shape recovery and fixity ratios of PLA and PEG/PLA blends.

R_r and R_f of the neat PLA were nearly perfect, exceeding 98%. All PEG/PLA blends with and without the PLA-*g*-MA compatibilizer demonstrated R_f values greater than 96%, indicating that the presence of PEG and PLA-*g*-MA had no obvious influence on the shape fixity ratio. When R_r was considered, the compatibilized PEG/PLA blend containing 2 wt% PLA-*g*-MA, 2PMA/PEG/PLA, had the highest R_r value among all the PEG/PLA blends. Further increased the amount of the compatibilizer to 6 wt% and 10 wt% caused the decreases in R_r values of the 6PMA/PEG/PLA and 10PMA/PEG/PLA. According to the DSC results of the PEG/PLA blends at various stages of the shape

memory test, the stretching of the PEG/PLA blends resulted in a considerable increase in the crystallinity of the blends as compared to their corresponding unstretched states. This may account for the high R_f values seen in all PEG/PLA blends. Nonetheless, the stretched 2PMA/PEG/PLA had the lowest T_g and degree of crystallinity among the compatibilized PEG/PLA blends. This could be due to the enhanced interfacial adhesion in the 2PMA/PEG/PLA, which constrained the PLA crystallization process. Consequently, the PLA chains in 2PMA/PEG/PLA may have the highest tendency to return to their initial state at the recovery temperatures of 60 °C among the PEG/PLA blends. This gave 2PMA/PEG/PLA the highest R_r value. Guo et al. [28] also found that adding excess PEG to uncompatibilized PEG/PLA blends may cause irreversible deformation of the blends resulting in a reduction in R_r.

3.5.2. Shape Memory Behaviors of the PLA and PEG/PLA Blends at Various Recovery Temperatures

Additionally, the effect of recovery temperature (T_r) on shape recoverability of PLA and PEG/PLA blends was examined. The stretched specimens were subjected to different temperatures of the water bath at 40, 50, and 60 °C to measure the recoverability. Their R_r values are illustrated in Figure 8.

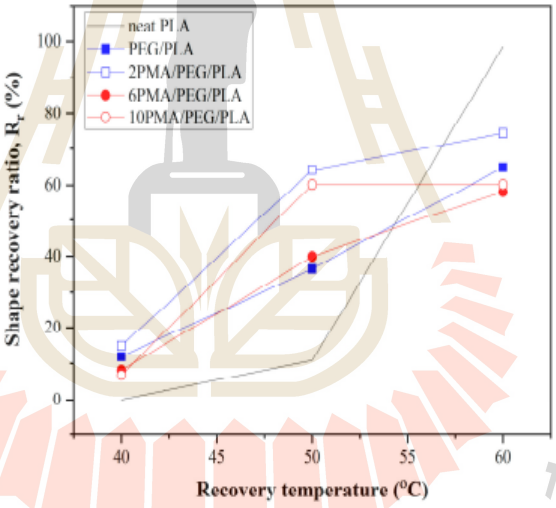

Figure 8. Shape recovery ratios of PLA and PEG/PLA blends at various recovery temperatures.

For the neat PLA, the specimen could recover with a high R_r value at T_r of 60 °C. However, the neat PLA was difficult to recover at T_r below 60 °C. This was because its T_g was increased to 62 °C during shape programming process. This required more energy or heat to drive the recovery process. The PEG/PLA blends had the lower R_r as compared with the neat PLA. Nonetheless, all the PEG/PLA blends, with/without compatibilizer, could recover even at temperatures as low as 40 °C. Their R_r increased with the increasing T_r. Among the PEG/PLA blends, 2PMA/PEG/PLA blend had the highest R_r values at all recovery temperatures. It was reported that a lowering of T_g can widen the recovery temperature of a shape memory polymer [28]. As the T_g of the PEG/PLA blends approached 40 °C, their onset recovery temperatures decreased. This could make them more appropriate for the use in biomedical applications.

3.6. Stress Relaxation of the PEG/PLA Blends with Various PLA-g-MA Contents

According to Tcharkhtchi et al. [44], the residual stress can be considered as the driving force for a SMP to regain its original shape. Shape recovery performance of the PEG/PLA blends can be explained by observing their stress relaxation behaviors at the shape programming temperature of 45 °C. The experiment was designed in a manner similar to the shape programming procedure; the specimen was first heated to 45 °C for 5 min before being stretched to 100% strain and monitored the stress reduction for 1 h. The stress relaxation curves of these specimens are illustrated in Figure 9.

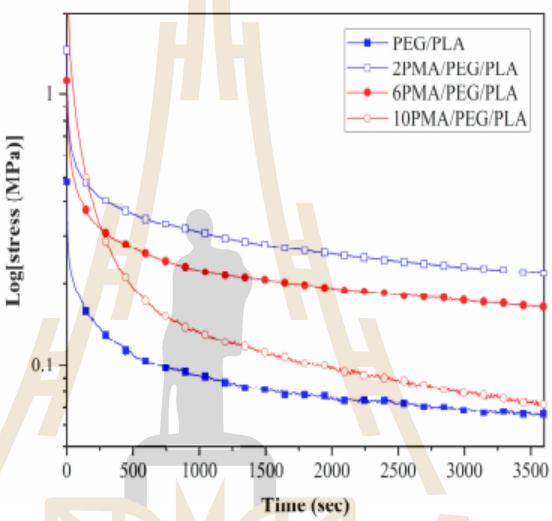

Figure 9. Stress relaxation of PLA and PEG/PLA blends at the shape programming temperature of 45 °C.

As seen from the figure, 2PMA/PEG/PLA had the highest residual stress among the PEG/PLA blends. This could give the highest R_f value of the 2PMA/PEG/PLA. The residual stress of the compatibilized blends decreased as the added PLA-*g*-MA content exceeded 2 wt%. This was explained by the compatibilizer's role in affecting the crystallinity of the blends. As previously stated, the presence of 2 wt% PLA-*g*-MA in the blend reduced the X_c and increased the chain entanglement of 2PMA/PEG/PLA as compared to that of the uncompatibilized PEG/PLA. Consequently, the 2PMA/PEG/PLA had a more difficult time releasing stress accumulated during temporary shape formation and a greater capacity to store driving stress energy for recovery to its original shape than the uncompatibilized PEG [45,46]. The addition of PLA-*g*-MA in excess of 2 wt% increased the X_c, which lowered the recoverability of the blends. This result was consistent with DSC and shape memory test results.

3.7. Microstructures of PEG/PLA and 2PMA/PEG/PLA Blends during Shape Memory Test

In order to gain a better understanding of the function of PLA-*g*-MA in the PEG/PLA blends, in situ SAXS and WAXS measurements were used to determine the microstructure evolution of the uncompatibilized PEG/PLA and 2PMA/PEG/PLA during the programming and recovery processes. Scattering patterns of the blends are shown in Figure 10. As labeled in the figure, m and e represent the meridian and equator directions of the scattering profile, respectively. The stretching direction of the specimen was parallel to the meridian axis.

In the initial state, both uncompatibilized PEG/PLA and 2PMA/PEG/PLA exhibited unclear SAXS scattering patterns, indicating the random conformation of the poly-

mer chains. The 2D-WAXS pattern of the uncompatibilized PEG/PLA demonstrated the uniform intensity of both the amorphous halo (orange color area) and the single ring of crystalline at (200/110) plane around the azimuth angle. The 2D-WAXS pattern of 2PMA/PEG/PLA demonstrated the isotropy of two distinct rings corresponding to (200/110) and (203) planes of α-form PLA crystallites [27]. These suggested that the polymer chains were isotopically oriented in the initial state. In addition, their WAXS and SAXS scattering patterns remained unchanged after heating these specimens at 45 °C.

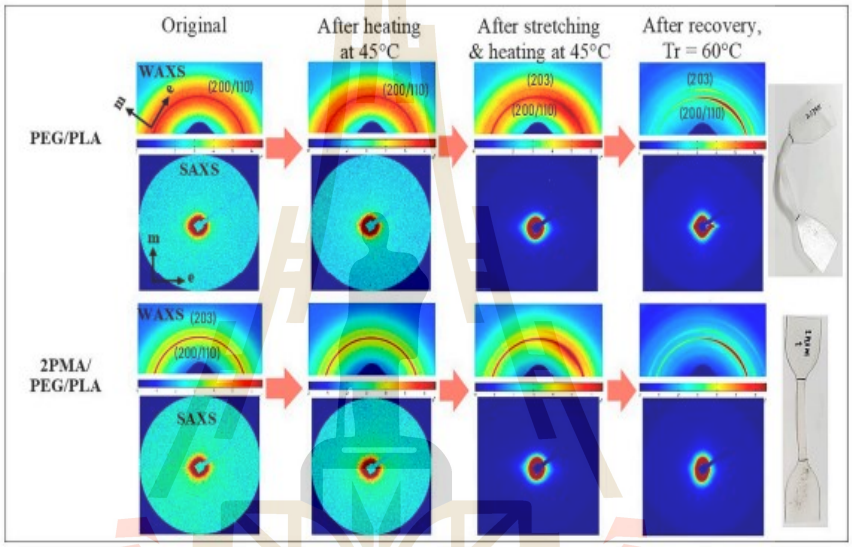

Figure 10. 2D-WAXS and SAXS patterns of PEG/PLA and 2PMA/PEG/PLA specimens during shape memory test process.

After the shape programming process, the WAXS patterns of the stretched PEG/PLA and 2PMA/PEG/PLA specimens revealed a greater intensity of the crystallite ring along the equatorial axis, while their SAXS patterns revealed a small equator streak. These results suggested that polymer chains in both amorphous and crystalline regions were weakly anisotopically oriented perpendicular to the stretching direction during the shaping process. Since the specimens were deformed at low strain (100% strain), it might be insufficient to induce stacking lamellar perpendicular to the stretching direction [47]. The WAXS and SAXS patterns confirmed the DSC results that the polymer chains were oriented along the stretching direction, thereby increasing the crystallinity of the specimens.

After shape recovery at 60 °C, the equator streak in the SAXS pattern of the PEG/PLA had an asymmetrical appearance, which could be attributed to an unusual specimen recovery direction. In addition, the 1D-SAXS curves in Figure 11 demonstrate that the intensity of the equator streak in the 2PMA/PEG/PLA decreased significantly after recovery, while it remained unchanged in the PEG/PLA. The significant change in the intensity along the equator axis of the 2PMA/PEG/PLA may occur because this compatibilized specimen had less crystallinity or, in other words, the compatibilized blend contain relatively more polymer chains in the amorphous region than the uncompatibilized ones. This result explained why 2PMA/PEG/PLA exhibited greater residual stress than the PEG/PLA. When the 2PMA/PEG/PLA specimen was heated to 60 °C, the polymer chains in the amorphous region relaxed, hence restoring the chain to its original state. Consequently, the shape recovery ratio of the 2PMA/PEG/PLA was higher than that of the uncompatibilized PEG/PLA blend.

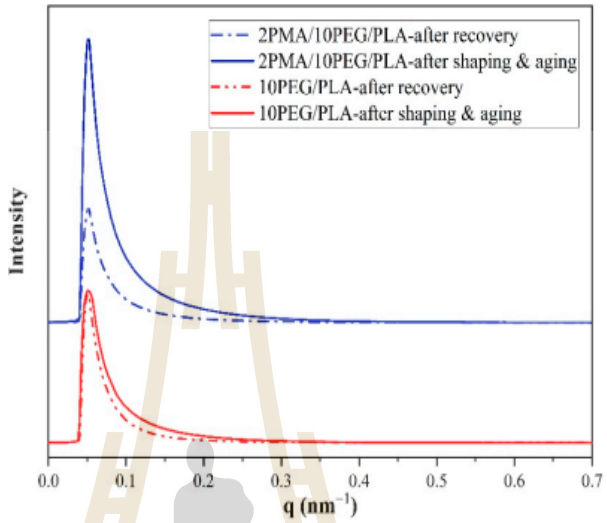

Figure 11. 1D-SAXS plots along the equatorial axis of PEG/PLA and 2PMA/PEG/PLA specimens after aging and recovery at 60 °C.

4. Conclusions

In this work, we investigated the role of PLA-*g*-MA in the PEG/PLA (10/90) blends in improving shape memory properties. The PEG (4000 g/mol) was added to PLA to reduce brittleness and lower recovery temperature to be in a useful range, close to physiological temperature. However, shape fixity and recovery ratio of the PEG/PLA blend were diminished. Poor compatibility was found to cause the decreases of the shape memory properties. The use of the PLA-*g*-MA as a compatibilizer in PEG/PLA was chosen to be a remedy for the issue. The presence of PLA-*g*-MA in the PEG/PLA blend caused the changes in mechanical and thermal properties, and shape memory behavior. The optimal content of the compatibilizer for PEG/PLA blend was found to be at 2 wt% which gave the highest tensile properties and lowest T_g and X_c. The 2PMA/PEG/PLA possessed the maximum shape fixity and recoverability performance among the PEG/PLA blends at a programming temperature of 45 °C and a recovery temperature of 60 °C. The shape fixity performance of the compatibilized PEG/PLA blends was comparable to that of the neat PLA at the programming temperature of 45 °C. Although, a higher T_r was found to be beneficial for increasing recovery of the PEG/PLA blends, the compatibilized PEG/PLA blends can be recovered to their original shape at the temperature lower than the neat PLA. In situ SAXS and WAXS measurements revealed that higher number of oriented polymer chains in the amorphous region were relaxed in the 2PMA/PEG/PLA. Consequently, 2PMA/PEG/PLA possessed a higher shape recovery ratio than that of the uncompatibilized PEG/PLA. The finding was well agreed with DSC and stress relaxation results. In conclusion, PLA-*g*-MA as a compatibilizer plays a complex role in the shape memory behaviors of the PEG/PLA blends. PLA-*g*-MA provide anchor points for the two polymers in the partially compatible system of PEG/PLA blend. As optimum amount, PLA-*g*-MA could improve interfacial adhesion between phases, promote chain entanglement, and accumulate stress during the recovery process. Systematic studies are required in order to fully understand and utilize the polymer for its best performance.

Author Contributions: Conceptualization, T.T. and N.S.; methodology, W.N., T.T. and N.S.; validation, W.N., T.T. and N.S.; formal analysis, W.N., T.T. and N.S.; investigation, W.N., T.T. and N.S.; resources, T.T. and N.S.; data curation, W.N.; writing—original draft preparation, W.N.; writing—review and editing, T.T. and N.S.; supervision, T.T. and N.S.; project administration, T.T. and N.S.; funding acquisition, T.T. and N.S. All authors have read and agreed to the published version of the manuscript.

Funding: This research was funded by Suranaree University of Technology and Thailand Science Research and Innovation (TSRI) and National Science, Research, and Innovation Fund (NSRF) NRIIS number 42853.

Institutional Review Board Statement: Not applicable.

Informed Consent Statement: Not applicable.

Data Availability Statement: The data used to support the findings of this study are available from the corresponding author upon request.

Acknowledgments: The authors would also like to thank Chemical Innovation Co., Ltd. in Bangkok, Thailand, for facilitating the DMA measurement, and the Synchrotron Light Research Institute in Nakhon Ratchasima, Thailand, for supporting the SAXS and WAXS experiments at beamline BL1.3W. Additionally, the first author wishes to express her gratitude to Kitibandit Scholar from Suranaree University of Technology for providing scholarship support.

Conflicts of Interest: The authors declare no conflict of interest.

References

1. Wang, K.; Jia, Y.-G.; Zhao, C.; Zhu, X.X. Multiple and two-way reversible shape memory polymers: Design strategies and applications. *Prog. Mater. Sci.* **2019**, *105*, 100572. [CrossRef]
2. Hager, M.D.; Bode, S.; Weber, C.; Schubert, U.S. Shape memory polymers: Past, present and future developments. *Prog. Mater. Sci.* **2015**, *49–50*, 3–33. [CrossRef]
3. Lendlein, A.; Gould, O.E.C. Reprogrammable recovery and actuation behaviour of shape-memory polymers. *Nat. Rev. Mater.* **2019**, *4*, 116–133. [CrossRef]
4. Yang, J.-M.; Panda, P.K.; Jie, C.J.; Dash, P.; Chang, Y.-H. Poly(vinyl alcohol)/chitosan/sodium alginate composite blended membrane: Preparation, characterization, and water-induced shape memory phenomenon. *Polym. Eng. Sci.* **2022**, *62*, 1526–1537. [CrossRef]
5. Chatterjee, T.; Dey, P.; Nando, G.B.; Naskar, K. Thermo-responsive shape memory polymer blends based on alpha olefin and ethylene propylene diene rubber. *Polymer* **2015**, *78*, 180–192. [CrossRef]
6. Tonndorf, R.; Aibibu, D.; Cherif, C. Thermoresponsive Shape Memory Fibers for Compression Garments. *Polymers* **2020**, *12*, 2989. [CrossRef] [PubMed]
7. Herath, M.; Epaarachchi, J.; Islam, M.; Fang, L.; Leng, J. Light activated shape memory polymers and composites: A review. *Eur. Polym. J.* **2020**, *136*, 109912. [CrossRef]
8. Yao, J.; Liu, X.; Sun, H.; Liu, S.; Jiang, Y.; Yu, B.; Ning, N.; Tian, M.; Zhang, L. Thermoplastic Polyurethane Dielectric Elastomers with High Actuated Strain and Good Mechanical Strength by Introducing Ester Group Grafted Polymethylvinylsiloxane. *Ind. Eng. Chem. Res.* **2021**, *60*, 4883–4891. [CrossRef]
9. Ze, Q.; Kuang, X.; Wu, S.; Wong, J.; Montgomery, S.M.; Zhang, R.; Kovitz, J.M.; Yang, F.; Qi, H.J.; Zhao, R. Magnetic Shape Memory Polymers with Integrated Multifunctional Shape Manipulation. *Adv. Mater.* **2020**, *32*, 1906657. [CrossRef]
10. He, H.; Shi, X.; Chen, W.; Chen, R.; Zhao, C.; Wang, S. Temperature/pH Smart Nanofibers with Excellent Biocompatibility and Their Dual Interactions Stimulus-Responsive Mechanism. *J. Agric. Food Chem.* **2020**, *68*, 7425–7433. [CrossRef]
11. Guo, Y.; Lv, Z.; Huo, Y.; Sun, L.; Chen, S.; Liu, Z.; He, C.; Bi, X.; Fan, X.; You, Z. A biodegradable functional water-responsive shape memory polymer for biomedical applications. *J. Mater. Chem. B* **2019**, *7*, 123–132. [CrossRef] [PubMed]
12. Cai, S.; Sun, Y.C.; Ren, J.; Naguib, H.E. Toward the low actuation temperature of flexible shape memory polymer composites with room temperature deformability via induced plasticizing effect. *J. Mater. Chem. B* **2017**, *5*, 8845–8853. [CrossRef] [PubMed]
13. Zhuo, J.; Wu, B.; Zhang, J.; Peng, Y.; Lu, H.; Le, X.; Wei, S.; Chen, T. Supramolecular Assembly of Shape Memory and Actuating Hydrogels for Programmable Shape Transformation. *ACS Appl. Mater. Interfaces* **2022**, *14*, 3551–3558. [CrossRef] [PubMed]
14. Panda, P.K.; Dash, P.; Biswal, A.K.; Chang, Y.-H.; Misra, P.K.; Yang, J.-M. Synthesis and Characterization of Modified Poly(vinyl alcohol) Membrane and Study of Its Enhanced Water-Induced Shape-Memory Behavior. *J. Polym. Environ.* **2022**, *30*, 3409–3419. [CrossRef]
15. Wang, X.; Yang, X.; Xu, C.; Lin, B.; Fu, L. Enhanced, hydrophobic, initial-shape programmable shape-memory composites with a bio-based nano-framework via gradient metal-ligand cross-linking. *Compos. Sci. Technol.* **2022**, *220*, 109255. [CrossRef]
16. Wu, M.; Yang, L.; Shen, Q.; Zheng, Z.; Xu, C. Endeavour to balance mechanical properties and self-healing of nature rubber by increasing covalent crosslinks via a controlled vulcanization. *Eur. Polym. J.* **2021**, *161*, 110823. [CrossRef]

17. Xu, J.; Song, J. Polylactic acid (PLA)-based shape-memory materials for biomedical applications. In *Shape Memory Polymers for Biomedical Applications*; Yahia, L., Ed.; Elsevier: Amsterdam, The Netherlands, 2015; pp. 197–217.
18. Li, G.; Zhao, M.; Xu, F.; Yang, B.; Li, X.; Meng, X.; Teng, L.; Sun, F.; Li, Y. Synthesis and Biological Application of Polylactic Acid. *Molecules* **2020**, *25*, 5023. [CrossRef]
19. Kumar Panda, P.; Jebastine, J.; Ramarao, M.; Fairooz, S.; Reddy, C.K.; Nasif, O.; Alfarraj, S.; Manikandan, V.; Jenish, I.; Ganeshan, P. Exploration on Mechanical Behaviours of Hyacinth Fibre Particles Reinforced Polymer Matrix-Based Hybrid Composites for Electronic Applications. *Adv. Mater. Sci. Eng.* **2021**, *2021*, 4933450. [CrossRef]
20. Mehrpouya, M.; Vahabi, H.; Janbaz, S.; Darafsheh, A.; Mazur, T.R.; Ramakrishna, S. 4D printing of shape memory polylactic acid (PLA). *Polymer* **2021**, *230*, 124080. [CrossRef]
21. Barletta, M.; Gisario, A.; Mehrpouya, M. 4D printing of shape memory polylactic acid (PLA) components: Investigating the role of the operational parameters in fused deposition modelling (FDM). *J. Manuf. Process.* **2021**, *61*, 473–480. [CrossRef]
22. Navarro-Baena, I.; Sessini, V.; Dominici, F.; Torre, L.; Kenny, J.M.; Peponi, L. Design of biodegradable blends based on PLA and PCL: From morphological, thermal and mechanical studies to shape memory behavior. *Polym. Degrad. Stab.* **2016**, *132*, 97–108. [CrossRef]
23. Gallos, A.; Crowet, J.-M.; Michely, L.; Raghuwanshi, V.S.; Mention, M.; Langlois, V.; Dauchez, M.; Garnier, G.; Allais, F. Blending Ferulic Acid Derivatives and Polylactic Acid into Biobased and Transparent Elastomeric Materials with Shape Memory Properties. *Biomacromolecules* **2021**, *22*, 1568–1578. [CrossRef] [PubMed]
24. Jeong, H.; Yuk, J.; Lee, H.; Kang, S.; Park, H.; Park, S.; Jihoon, S. Lactide-derived ester oligomers for highly compatible poly(lactide) plasticizer produced through an eco-friendly process: Renewable resources, biodegradation, enhanced flexibility, and elastomeric performance. *Green Chem.* **2021**, *23*, 7549–7565. [CrossRef]
25. Jariyasakoolroj, P.; Rojanaton, N.; Jarupan, L. Crystallization behavior of plasticized poly(lactide) film by poly(l-lactic acid)-poly(ethylene glycol)-poly(l-lactic acid) triblock copolymer. *Polym. Bull.* **2020**, *77*, 2309–2323. [CrossRef]
26. Chaos, A.; Sangroniz, A.; Fernández, J.; Río, J.; Iriarte, M.; Sarasua, J.R.; Etxeberria, A. Plasticization of poly(lactide) with poly(ethylene glycol): Low weight plasticizer vs. triblock copolymers. Effect on free volume and barrier properties. *J. Appl. Polym. Sci.* **2019**, *137*, 48868. [CrossRef]
27. Koosomsuan, W.; Yamaguchi, M.; Phinyocheep, P.; Sirisinha, K. High-Strain Shape Memory Behavior of PLA-PEG Multiblock Copolymers and Its Microstructural Origin. *J. Polym. Sci. B Polym. Phys.* **2019**, *57*, 241–256. [CrossRef]
28. Guo, Y.; Ma, J.; Lv, Z.; Zhao, N.; Wang, L.; Li, Q. The effect of plasticizer on the shape memory properties of poly(lactide acid)/poly(ethylene glycol) blends. *J. Mater. Res.* **2018**, *33*, 4101–4112. [CrossRef]
29. Younes, H.; Cohn, D. Phase separation in poly(ethylene glycol)/poly(lactic acid) blends. *Eur. Polym. J.* **1988**, *24*, 765–773. [CrossRef]
30. Wang, B.; Hina, K.; Zou, H.; Zuo, D.; Yi, C. Thermal, crystallization, mechanical and decomposition properties of poly(lactic acid) plasticized with poly(ethylene glycol). *J. Vinyl Addit. Technol.* **2018**, *24*, E154–E163. [CrossRef]
31. Li, F.-J.; Zhang, S.-D.; Liang, J.-Z.; Wang, J.-Z. Effect of polyethylene glycol on the crystallization and impact properties of polylactide-based blends. *Polym. Adv. Technol.* **2015**, *26*, 465–475. [CrossRef]
32. Piontek, A.; Vernaez, O.; Kabasci, S. Compatibilization of Poly(Lactic Acid) (PLA) and Bio-Based Ethylene-Propylene-Diene-Rubber (EPDM) via Reactive Extrusion with Different Coagents. *Polymers* **2020**, *12*, 605. [CrossRef] [PubMed]
33. Luo, F.; Li, J.; Ji, F.; Weng, Y.-X.; Ren, J. Preparation of poly(lactic acid)-based shape memory polymers with low response temperature utilizing composite plasticizers. *Polym. Bull.* **2022**, *79*, 4761–4781. [CrossRef]
34. Raquez, J.-M.; Narayan, R.; Dubois, P. Recent Advances in Reactive Extrusion Processing of Biodegradable Polymer-Based Compositions. *Macromol. Mater. Eng.* **2008**, *293*, 447–470. [CrossRef]
35. Hwang, S.W.; Lee, S.B.; Lee, C.K.; Lee, J.Y.; Shim, J.K.; Selke, S.; Soto-Valdez, H.; Matuana, L.; Rubino, M.; Auras, R. Grafting of maleic anhydride on poly(L-lactic acid). Effects on physical and mechanical properties. *Polym. Test.* **2012**, *31*, 333–344. [CrossRef]
36. Hassouna, F.; Raquez, J.-M.; Addiego, F.; Dubois, P.; Toniazzo, V.; Ruch, D. New approach on the development of plasticized polylactide (PLA): Grafting of poly(ethylene glycol) (PEG) via reactive extrusion. *Eur. Polym. J.* **2011**, *47*, 2134–2144. [CrossRef]
37. Kim, S.K.; Jang, R.; Kim, W.N. Effects of compatibilizer on the mechanical, rheological, and shape memory behaviors of poly(lactic acid) and poly(MnBM) blends. *J. Appl. Polym. Sci.* **2019**, *137*, 48591. [CrossRef]
38. Davachi, S.M.; Kaffashi, B. Preparation and Characterization of Poly L-Lactide/Triclosan Nanoparticles for Specific Antibacterial and Medical Applications. *Int. J. Polym. Mater. Polym. Biomater.* **2015**, *64*, 497–508. [CrossRef]
39. Panda, P.K.; Yang, J.-M.; Chang, Y.-H. Water-induced shape memory behavior of poly(vinyl alcohol) and p-coumaric acid-modified water-soluble chitosan blended membrane. *Carbohydr. Polym.* **2021**, *257*, 117633. [CrossRef]
40. Tang, X.; Liu, C.; Keum, J.; Chen, J.; Dial, B.E.; Wang, Y.; Tsai, W.-Y.; Bras, W.; Saito, T.; Bowland, C.C.; et al. Upcycling of semicrystalline polymers by compatibilization: Mechanism and location of compatibilizers. *RSC Adv.* **2022**, *12*, 10886–10894. [CrossRef]
41. Liu, H.; Xie, T.; Zhang, Y.; Ou, Y.; Yang, G. Crystallization Behaviors of Polypropylene/Polyamide-6 Blends Modified by a Maleated Thermoplastic Elastomer. *Polym. J.* **2006**, *38*, 21–30. [CrossRef]
42. Athanasoulia, I.-G.; Tarantili, P.A. Preparation and characterization of polyethylene glycol/poly(L-lactic acid) blends. *Pure Appl. Chem.* **2017**, *89*, 141–152. [CrossRef]

43. Wang, W.; Jin, Y.; Ping, P.; Chen, X.; Jing, X.; Su, Z. Structure Evolution in Segmented Poly(ester urethane) in Shape-Memory Process. *Macromolecules* **2010**, *43*, 2942–2947. [CrossRef]
44. Tcharkhtchi, A.; Abdallah-Elhirtsi, S.; Ebrahimi, K.; Fitoussi, J.; Shirinbayan, M.; Farzaneh, S. Some New Concepts of Shape Memory Effect of Polymers. *Polymers* **2014**, *6*, 1144–1163. [CrossRef]
45. Kong, D.; Xiao, X. High Cycle-life Shape Memory Polymer at High Temperature. *Sci. Rep.* **2016**, *6*, 33610. [CrossRef] [PubMed]
46. Kallel, A.; Abdallah, A.B.; Gamaoun, F.; Farzaneh, S.; BenDaly, H.; Fitoussi, J.; Tcharkhtchi, A. Driving force for shape memory effect of polymers. *J. Polym. Rev.* **2021**, *28*, 308. [CrossRef]
47. Tian, Y.; Zhu, C.; Gong, J.; Yang, S.; Ma, J.; Xu, J. Lamellae break induced formation of shish-kebab during hot stretching of ultra-high molecular weight polyethylene precursor fibers investigated by in situ small angle X-ray scattering. *Polymer* **2014**, *55*, 4299–4306. [CrossRef]

BIOGRAPHY

Wasana Nonkrathok is pursuing a Master of Engineering degree in Materials Engineering at Suranaree University of Technology, Institute of Engineering, Thailand. In 2018, she received a Bachelor's degree in Polymer Engineering from Suranaree University of Technology, Thailand. Her primary areas of research interest are Polymer Blends, Polymer Composites, and Shape Memory Polymers. She has published two articles in International Conference Proceedings and one article in Polymer Journal.